arXiv:astro-ph/0310175v1 7 Oct 2003

Table 1. X-ray Properties of Nearby Abell Cluster Sample

Abell	z	EXP	RA	DEC	[1]Offset	[2]f_X	[3]L_X	$\frac{F_{500}}{F_{62.5}}$	$(\frac{C}{\sqrt{B}})_{500}$	$(\frac{C}{\sqrt{B}})_{max}$
A14	0.0655	285	00:15:13.9	-23:53:20	···	···	0.75 ± 0.17	···	6.8	···
	···	···	00:15:11.2	-23:51:57	103	1.01 ± 0.21	0.86 ± 0.18	8.1	8.2	9.7
A16	0.0843	509	00:16:46.2	06:44:40	···	···	1.10 ± 0.19	···	7.1	···
	···	···	00:16:43.7	06:47:02	208	0.77 ± 0.13	1.10 ± 0.19	10.1	11.3	12.0
A27	0.0542	262	00:24:49.1	-20:42:23	···	<0.42	<0.24	···	···	···
A71	0.0724	391	00:37:45.7	29:35:30	···	<0.25	<0.26	···	···	···
A74	0.0651	315	00:38:53.2	-22:18:31	···	<0.36	<0.30	···	···	···
A75	0.0626	194	00:39:50.0	21:15:28	···	···	0.76 ± 0.19	···	7.4	···
	···	···	00:39:39.9	21:15:02	156	1.05 ± 0.26	0.81 ± 0.20	4.4	7.5	13.8
*A76	0.0405	117	00:39:47.0	06:46:28	···	···	1.03 ± 0.18	···	14.1	···
	···	···	00:39:36.4	06:51:50	262	3.06 ± 0.56	0.98 ± 0.18	7.9	7.0	8.1
A77	0.0708	379	00:40:34.1	29:31:28	···	···	2.45 ± 0.26	···	16.2	···
	···	···	00:40:28.1	29:33:33	179	2.61 ± 0.26	2.60 ± 0.26	12.3	29.1	33.7
*A85	0.0555	342	00:41:37.8	-09:20:33	···	···	14.40 ± 0.48	···	106.1	···
	···	···	00:41:49.7	-09:18:25	213	24.72 ± 0.81	15.00 ± 0.49	8.6	190.0	255.6
A86	0.0634	328	00:42:28.9	-21:47:34	···	···	0.36 ± 0.13	···	4.6	···
	···	···	00:42:52.1	-21:48:22	360	0.55 ± 0.18	0.44 ± 0.14	7.1	4.3	6.8
A102	0.0653	341	00:48:40.0	01:22:21	···	<0.30	<0.25	···	···	···
A104	0.0821	124	00:49:46.1	24:31:20	···	···	1.92 ± 0.48	···	10.1	···
	···	···	00:49:52.7	24:26:22	431	2.23 ± 0.42	3.00 ± 0.56	15.3	12.3	16.3
A114	0.0587	327	00:53:39.7	-21:40:44	···	<0.43	<0.29	···	···	···
A116	0.0665	379	00:55:51.9	00:38:14	···	···	0.45 ± 0.13	···	4.9	···
	···	···	00:55:50.4	00:38:51	49	0.54 ± 0.15	0.47 ± 0.13	9.7	5.7	5.8
A117	0.0535	380	00:56:00.9	-10:01:46	···	···	0.27 ± 0.09	···	4.7	···
	···	···	00:56:02.4	-10:00:08	95	0.53 ± 0.16	0.30 ± 0.09	13.3	4.1	5.6
*A119	0.0442	324	00:56:21.3	-01:15:47	···	···	3.31 ± 0.19	···	36.4	···
	···	···	00:56:18.9	-01:14:37	62	8.63 ± 0.52	3.30 ± 0.20	22.5	59.3	59.8
A126	0.0546	328	00:59:47.4	-14:12:50	···	···	0.21 ± 0.08	···	4.0	···
	···	···	00:59:43.9	-14:15:28	160	0.36 ± 0.14	0.21 ± 0.08	8.8	4.3	7.2
*A133	0.0566	277	01:02:38.6	-21:47:54	···	···	4.23 ± 0.31	···	28.2	···
	···	···	01:02:42.7	-21:52:53	303	7.76 ± 0.52	4.90 ± 0.33	7.2	46.7	72.0
A134	0.0699	310	01:03:02.9	-02:31:54	···	···	0.34 ± 0.13	···	4.1	···
	···	···	01:02:40.4	-02:29:01	456	0.34 ± 0.13	0.33 ± 0.13	21.3	4.8	7.4

Table 1—Continued

Abell	z	EXP	RA	DEC	[1]Offset	[2]f_X	[3]L_X	$\frac{F_{500}}{F_{62.5}}$	$(\frac{C}{\sqrt{B}})_{500}$	$(\frac{C}{\sqrt{B}})_{\rm max}$
A147	0.0447	312	01:08:10.4	02:10:00	···	···	0.92 ± 0.11	···	14.4	···
	···	···	01:08:12.9	02:10:52	51	2.38 ± 0.28	0.93 ± 0.11	12.5	28.6	34.6
A150	0.0588	367	01:09:14.2	13:09:59	···	···	0.83 ± 0.13	···	8.7	···
	···	···	01:09:17.8	13:10:35	65	1.19 ± 0.19	0.81 ± 0.13	5.2	14.0	22.4
A151	0.0533	327	01:08:52.3	-15:25:01	···	···	2.04 ± 0.19	···	21.5	···
	···	···	01:08:49.7	-15:24:39	41	3.58 ± 0.34	2.00 ± 0.19	10.2	45.3	55.3
A154	0.0636	315	01:10:58.0	17:39:56	···	···	1.06 ± 0.18	···	9.1	···
	···	···	01:11:03.9	17:37:49	168	1.06 ± 0.20	0.85 ± 0.16	11.5	8.9	13.1
A158	0.0645	323	01:11:45.8	16:52:55	···	···	0.82 ± 0.15	···	7.9	···
	···	···	01:11:48.4	16:53:02	42	1.02 ± 0.18	0.84 ± 0.15	8.7	9.7	11.7
A160	0.0447	326	01:12:51.4	15:30:54	···	···	0.72 ± 0.10	···	10.3	···
	···	···	01:13:06.4	15:30:33	174	1.87 ± 0.26	0.73 ± 0.10	12.3	12.5	14.3
A168	0.0450	412	01:15:09.8	00:14:51	···	···	1.15 ± 0.11	···	14.3	···
	···	···	01:14:58.3	00:21:57	371	3.28 ± 0.30	1.30 ± 0.12	23.2	25.1	25.1
A171	0.0706	330	01:16:46.0	16:15:49	···	<0.30	<0.30	···	···	···
A179	0.0547	308	01:21:47.8	19:28:41	···	···	0.26 ± 0.09	···	4.5	···
	···	···	01:22:04.6	19:33:36	365	0.41 ± 0.14	0.24 ± 0.08	26.3	5.2	7.4
A193	0.0488	215	01:25:07.3	08:41:36	···	···	3.06 ± 0.25	···	35.6	···
	···	···	01:25:04.5	08:41:17	39	6.63 ± 0.56	3.10 ± 0.26	13.3	55.9	68.7
*A194	0.0180	428	01:25:33.0	-01:30:25	···	···	0.26 ± 0.02	···	13.9	···
	···	···	01:25:51.0	-01:22:39	182	4.63 ± 0.48	0.29 ± 0.03	10.8	16.3	21.5
A195	0.0430	357	01:26:54.0	19:10:00	···	<0.39	<0.14	···	···	···
A225	0.0687	411	01:38:55.1	18:53:13	···	<0.28	<0.26	···	···	···
A240	0.0612	411	01:41:55.5	07:37:07	···	···	0.53 ± 0.12	···	5.9	···
	···	···	01:42:14.1	07:38:44	313	0.61 ± 0.15	0.45 ± 0.11	6.5	6.2	7.8
A245	0.0790	377	01:44:06.9	06:23:03	···	<0.23	<0.29	···	···	···
A246	0.0700	328	01:44:42.6	05:48:02	···	···	0.76 ± 0.17	···	6.5	···
	···	···	01:44:45.2	05:48:39	64	0.78 ± 0.17	0.76 ± 0.17	6.2	8.5	11.2
A257	0.0703	244	01:48:59.2	13:58:54	···	···	0.86 ± 0.20	···	7.7	···
	···	···	01:48:36.9	14:01:13	427	0.97 ± 0.21	0.95 ± 0.21	6.4	14.6	19.4
	···	···	01:49:06.6	13:55:38	270	0.27 ± 0.13	0.26 ± 0.13	7.7	4.0	12.4
	···	···	01:49:05.0	14:03:55	378	0.59 ± 0.17	0.58 ± 0.17	6.4	9.1	14.7
	···	···	01:49:21.5	14:02:14	461	0.51 ± 0.16	0.50 ± 0.16	29.4	7.8	11.6

Table 1—Continued

Abell	z	EXP	RA	DEC	^{1}Offset	^{2}f$_X$	^{3}L$_X$	$\frac{F_{500}}{F_{62.5}}$	$(\frac{C}{\sqrt{B}})_{500}$	$(\frac{C}{\sqrt{B}})_{\max}$
*A262	0.0163	280	01:52:50.4	36:08:46	···	···	1.36 ± 0.05	···	41.5	···
	···	···	01:52:45.0	36:09:30	24	27.29 ± 0.97	1.40 ± 0.05	4.9	61.8	102.3
A272	0.0877	329	01:55:19.1	33:56:41	···	···	2.66 ± 0.38	···	10.5	···
	···	···	01:55:10.1	33:54:47	234	2.53 ± 0.29	3.90 ± 0.44	17.8	21.0	21.3
A278	0.0891	314	01:57:18.0	32:13:37	···	···	1.86 ± 0.34	···	8.1	···
	···	···	01:57:21.0	32:13:15	65	1.26 ± 0.22	2.00 ± 0.35	22.2	10.7	13.1
A279	0.0797	403	01:56:22.2	01:03:39	···	···	0.30 ± 0.15	···	3.4	···
	···	···	01:56:07.8	01:03:00	296	0.43 ± 0.13	0.54 ± 0.17	17.0	4.6	4.9
A281	0.0880	394	01:57:06.3	-05:50:23	···	···	1.12 ± 0.23	···	6.8	···
	···	···	01:57:07.3	-05:53:23	265	0.57 ± 0.13	0.88 ± 0.20	8.9	8.9	11.2
	···	···	01:56:53.8	-05:49:29	285	0.40 ± 0.12	0.62 ± 0.18	22.1	6.3	10.0
	···	···	01:57:33.9	-05:48:44	623	0.77 ± 0.15	1.20 ± 0.24	9.1	12.0	12.9
A358	0.0576	314	02:30:12.2	-13:11:42	···	···	0.67 ± 0.14	···	7.3	···
	···	···	02:29:53.3	-13:15:21	356	0.98 ± 0.20	0.64 ± 0.13	12.8	8.3	9.9
	···	···	02:30:28.6	-13:16:28	377	0.47 ± 0.17	0.31 ± 0.11	12.1	4.1	8.8
A376	0.0484	305	02:45:48.5	36:51:36	···	···	1.91 ± 0.17	···	25.5	···
	···	···	02:46:04.2	36:54:06	207	4.79 ± 0.39	2.20 ± 0.18	13.7	78.5	86.1
A415	0.0805	71	03:06:47.3	-12:02:29	···	···	1.15 ± 0.52	···	6.9	···
	···	···	03:06:51.0	-12:05:51	284	1.08 ± 0.43	1.40 ± 0.55	5.3	5.7	9.9
A419	0.0662	170	03:08:30.3	-23:38:35	···	···	1.06 ± 0.24	···	9.7	···
	···	···	03:08:18.0	-23:40:15	225	1.27 ± 0.29	1.10 ± 0.25	5.7	13.3	23.3
A423	0.0791	43	03:11:17.1	-12:06:43	···	<0.75	<0.93	···	···	···
A428	0.0669	110	03:15:58.2	-19:05:59	···	<0.52	<0.46	···	···	···
A437	0.0847	228	03:26:49.2	-02:43:35	···	···	0.46 ± 0.20	···	3.9	···
	···	···	03:27:03.7	-02:46:12	381	0.33 ± 0.15	0.48 ± 0.21	6.0	4.5	6.1
*A496	0.0329	248	04:33:37.1	-13:14:46	···	···	5.79 ± 0.21	···	82.9	···
	···	···	04:33:37.4	-13:15:21	21	27.52 ± 1.00	5.80 ± 0.21	5.8	120.4	198.7
*A500	0.0670	199	04:38:56.2	-22:06:09	···	···	1.93 ± 0.30	···	13.9	···
	···	···	04:38:55.7	-22:06:41	37	2.14 ± 0.33	1.90 ± 0.29	7.7	13.7	18.9
*A514	0.0713	472	04:47:40.0	-20:25:44	···	···	1.07 ± 0.17	···	7.6	···
	···	···	04:48:03.7	-20:27:11	421	1.88 ± 0.21	1.90 ± 0.21	34.4	22.0	24.2
	···	···	04:48:29.8	-20:27:12	864	1.98 ± 0.22	2.00 ± 0.22	17.2	25.3	23.8
A533	0.0467	427	05:01:30.8	-22:36:43	···	···	0.45 ± 0.08	···	7.1	···

Table 1—Continued

Abell	z	EXP	RA	DEC	[1]Offset	[2]f_X	[3]L_X	$\frac{F_{500}}{F_{62.5}}$	$(\frac{C}{\sqrt{B}})_{500}$	$(\frac{C}{\sqrt{B}})_{max}$
	···	···	05:01:42.5	-22:35:35	146	0.94 ± 0.19	0.40 ± 0.08	12.5	7.5	8.9
	···	···	05:01:07.3	-22:33:08	325	0.94 ± 0.19	0.40 ± 0.08	9.9	7.4	9.2
*A548	0.0416	328	05:47:01.7	-25:36:59	···	···	0.57 ± 0.08	···	11.3	···
	···	···	05:46:53.3	-25:38:43	115	1.68 ± 0.24	0.57 ± 0.08	9.8	32.9	32.9
	···	···	05:47:24.5	-25:35:44	238	2.13 ± 0.27	0.72 ± 0.09	39.5	33.8	64.5
A564	0.0778	377	07:00:42.0	69:48:49	···	···	0.04 ± 0.10	···	1.9	···
	···	···	07:01:32.1	69:53:25	500	0.11 ± 0.09	0.13 ± 0.11	6.2	1.6	3.6
A576	0.0389	248	07:21:24.2	55:44:20	···	···	2.39 ± 0.16	···	35.2	···
	···	···	07:21:23.1	55:47:06	117	8.12 ± 0.54	2.40 ± 0.16	11.3	51.2	63.5
*A578	0.0866	396	07:25:01.3	66:59:07	···	···	1.03 ± 0.22	···	6.3	···
	···	···	07:25:03.1	66:58:57	21	0.67 ± 0.14	1.00 ± 0.21	8.5	9.1	10.2
A592	0.0628	219	07:42:37.8	09:21:51	···	···	1.79 ± 0.26	···	13.1	···
	···	···	07:42:37.2	09:21:58	12	2.31 ± 0.35	1.80 ± 0.27	8.2	21.4	32.0
A595	0.0666	306	07:48:50.5	52:04:29	···	···	0.35 ± 0.12	···	4.4	···
	···	···	07:49:18.6	52:04:15	299	0.48 ± 0.15	0.42 ± 0.13	11.3	7.3	8.7
A600	0.0775	394	07:56:21.1	63:45:02	···	···	0.02 ± 0.09	···	1.7	···
	···	···	07:56:50.0	63:44:53	252	0.07 ± 0.09	0.08 ± 0.11	5.9	0.8	3.8
A602	0.0619	376	07:53:19.0	29:21:10	···	···	1.93 ± 0.20	···	17.3	···
	···	···	07:53:21.9	29:22:18	84	2.64 ± 0.26	2.00 ± 0.20	11.4	34.0	40.1
A612	0.0773	420	08:01:02.1	34:48:41	···	···	0.67 ± 0.16	···	5.4	···
	···	···	08:00:57.9	34:49:18	83	0.60 ± 0.13	0.71 ± 0.16	7.8	7.9	12.0
A623	0.0902	225	08:05:38.8	-00:56:38	···	···	1.82 ± 0.36	···	10.1	···
	···	···	08:05:38.4	-00:57:30	78	1.16 ± 0.23	1.90 ± 0.37	9.7	13.6	15.3
A628	0.0834	336	08:10:07.8	35:13:07	···	···	0.77 ± 0.20	···	5.6	···
	···	···	08:10:10.4	35:17:45	393	0.60 ± 0.14	0.83 ± 0.20	6.4	6.8	10.2
A634	0.0265	374	08:14:33.7	58:02:52	···	<0.59	<0.08	···	···	···
A671	0.0502	280	08:28:29.3	30:25:01	···	···	1.35 ± 0.16	···	16.1	···
	···	···	08:28:36.8	30:25:37	92	2.83 ± 0.32	1.40 ± 0.16	9.4	29.4	33.8
A690	0.0788	359	08:39:14.2	28:50:23	···	<0.29	<0.36	···	···	···
A692	0.0894	254	08:40:53.7	26:44:18	···	···	0.46 ± 0.23	···	3.6	···
	···	···	08:41:13.4	26:40:35	515	0.36 ± 0.15	0.57 ± 0.24	11.7	4.3	5.5
	···	···	08:40:36.8	26:41:04	444	0.26 ± 0.14	0.42 ± 0.23	6.1	3.1	7.2
A699	0.0851	267	08:44:36.5	27:47:05	···	···	0.84 ± 0.29	···	5.1	···

Table 1—Continued

Abell	z	EXP	RA	DEC	[1]Offset	[2]f_X	[3]L_X	$\frac{F_{500}}{F_{62.5}}$	$(\frac{C}{\sqrt{B}})_{500}$	$(\frac{C}{\sqrt{B}})_{max}$
	···	···	08:44:56.7	27:45:03	420	0.76 ± 0.21	1.10 ± 0.31	26.3	4.8	6.6
	···	···	08:44:28.4	27:42:55	388	0.38 ± 0.18	0.55 ± 0.26	5.1	2.4	5.0
*A744	0.0729	293	09:07:17.6	16:39:53	···	···	1.16 ± 0.02	···	9.3	···
	···	···	09:07:22.4	16:39:24	93	1.04 ± 0.19	1.10 ± 0.20	5.7	15.5	28.3
*A754	0.0542	374	09:08:50.1	-09:38:12	···	···	8.48 ± 0.34	···	68.8	···
	···	···	09:09:05.5	-09:40:03	242	17.29 ± 0.64	10.00 ± 0.37	47.6	152.2	152.2
A757	0.0517	291	09:12:47.3	47:42:38	···	···	0.85 ± 0.14	···	9.1	···
	···	···	09:13:06.6	47:42:15	179	2.66 ± 0.30	1.40 ± 0.16	10.6	31.1	32.1
	···	···	09:13:44.5	47:42:04	530	2.28 ± 0.30	1.20 ± 0.16	5.6	19.7	27.5
A763	0.0847	315	09:12:28.7	15:59:38	···	···	2.84 ± 0.36	···	15.5	···
	···	···	09:12:31.6	15:55:31	356	2.02 ± 0.26	2.90 ± 0.37	4.1	26.0	60.3
*A779	0.0229	403	09:19:50.8	33:46:17	···	···	0.29 ± 0.04	···	11.5	···
	···	···	09:19:45.5	33:45:53	29	2.85 ± 0.39	0.29 ± 0.04	5.1	10.7	18.9
*A780	0.0539	397	09:18:30.3	-12:15:40	···	···	1.23 ± 0.14	···	12.0	···
	···	···	09:18:23.1	-12:23:11	441	0.52 ± 0.16	0.30 ± 0.09	7.7	4.7	31.3
A819	0.0759	312	09:32:16.7	09:39:42	···	<0.31	<0.35	···	···	···
A834	0.0709	326	09:40:39.8	66:40:22	···	···	0.38 ± 0.13	···	4.2	···
	···	···	09:41:25.5	66:43:48	415	0.50 ± 0.14	0.50 ± 0.14	10.2	5.4	10.9
A838	0.0502	447	09:37:06.4	-05:00:31	···	<0.30	<0.15	···	···	···
A841	0.0696	446	09:38:37.0	-04:11:34	···	···	0.32 ± 0.11	···	3.9	···
	···	···	09:38:44.6	-04:21:27	723	0.44 ± 0.12	0.42 ± 0.12	6.6	5.4	7.7
	···	···	09:38:36.5	-04:08:57	188	0.27 ± 0.11	0.26 ± 0.11	7.9	3.4	5.6
	···	···	09:38:50.5	-04:12:26	249	0.23 ± 0.10	0.22 ± 0.10	18.3	2.9	6.4
A858	0.0863	290	09:43:25.7	05:53:14	···	···	0.86 ± 0.23	···	5.7	···
	···	···	09:43:23.2	05:54:20	109	0.66 ± 0.17	0.99 ± 0.25	16.2	10.4	13.2
A912	0.0446	427	10:01:09.7	-00:06:28	···	<0.36	<0.14	···	···	···
A930	0.0549	305	10:06:54.6	-05:37:40	···	···	0.21 ± 0.01	···	4.0	···
	···	···	10:06:52.8	-05:37:54	29	0.39 ± 0.13	0.23 ± 0.08	6.2	5.5	10.9
A957	0.0436	414	10:13:57.3	-00:54:54	···	···	1.31 ± 0.12	···	15.9	···
	···	···	10:13:40.9	-00:55:02	192	3.49 ± 0.32	1.30 ± 0.12	13.2	26.5	31.3
A970	0.0587	446	10:17:34.3	-10:42:02	···	···	2.53 ± 0.19	···	22.1	···
	···	···	10:17:20.9	-10:40:58	213	4.27 ± 0.31	2.90 ± 0.21	11.1	47.4	59.0
A971	0.0929	442	10:19:46.7	40:57:55	···	···	1.88 ± 0.29	···	9.1	···

Table 1—Continued

Abell	z	EXP	RA	DEC	[1]Offset	[2]f_X	[3]L_X	$\frac{F_{500}}{F_{62.5}}$	$(\frac{C}{\sqrt{B}})_{500}$	$(\frac{C}{\sqrt{B}})_{max}$
	···	···	10:19:59.3	40:59:33	266	1.04 ± 0.16	1.80 ± 0.27	12.4	16.7	22.1
A978	0.0544	423	10:20:30.5	-06:31:07	···	···	0.79 ± 0.11	···	9.1	···
	···	···	10:20:28.0	-06:31:29	41	1.37 ± 0.19	0.80 ± 0.11	21.5	13.9	16.0
A979	0.0535	405	10:20:23.9	-07:53:07	···	<0.32	<0.18	···	···	···
A991	0.0884	202	10:22:25.4	18:52:50	···	<0.35	<0.55	···	···	···
A993	0.0488	408	10:21:55.4	-04:57:10	···	···	0.22 ± 0.08	···	4.4	···
	···	···	10:21:56.0	-04:53:02	215	0.64 ± 0.19	0.30 ± 0.09	6.1	4.8	8.2
A1016	0.0322	114	10:27:03.0	10:58:41	···	<0.99	<0.20	···	···	···
A1020	0.0649	143	10:27:50.7	10:24:40	···	···	0.10 ± 0.10	···	1.3	···
	···	···	10:27:58.0	10:32:33	546	0.53 ± 0.23	0.44 ± 0.19	22.9	4.1	5.0
A1032	0.0794	231	10:30:17.6	04:00:36	···	···	0.15 ± 0.13	···	2.4	···
	···	···	10:30:01.2	03:53:41	648	0.31 ± 0.14	0.39 ± 0.17	11.2	5.0	8.7
	···	···	10:30:11.3	04:02:03	172	0.14 ± 0.10	0.17 ± 0.13	3.9	2.2	7.5
A1035	0.0684	428	10:32:07.3	40:12:33	···	···	1.79 ± 0.24	···	10.5	···
	···	···	10:32:13.8	40:16:12	273	1.40 ± 0.19	1.30 ± 0.18	8.3	16.9	20.3
	···	···	10:32:22.1	40:10:54	231	1.62 ± 0.20	1.50 ± 0.19	18.6	18.8	19.4
A1066	0.0699	187	10:39:23.9	05:10:21	···	···	1.89 ± 0.32	···	12.9	···
	···	···	10:39:38.6	05:10:28	264	1.44 ± 0.29	1.40 ± 0.28	16.3	8.8	9.9
	···	···	10:39:07.6	05:11:14	299	1.75 ± 0.31	1.70 ± 0.30	16.4	10.8	10.8
A1069	0.0650	313	10:39:54.3	-08:36:40	···	···	1.40 ± 0.19	···	12.0	···
	···	···	10:39:44.6	-08:41:02	337	2.27 ± 0.26	1.90 ± 0.22	9.6	31.3	33.8
A1100	0.0463	343	10:48:54.3	22:14:07	···	···	0.48 ± 0.09	···	7.5	···
	···	···	10:48:45.1	22:13:59	106	1.21 ± 0.21	0.51 ± 0.09	9.9	9.2	12.2
A1126	0.0846	282	10:53:57.6	16:51:01	···	···	2.40 ± 0.36	···	12.0	···
	···	···	10:53:50.6	16:50:58	142	1.61 ± 0.24	2.30 ± 0.35	4.9	16.9	27.0
*A1139	0.0398	414	10:58:04.2	01:29:56	···	···	0.35 ± 0.07	···	7.2	···
	···	···	10:58:26.8	01:34:47	321	1.68 ± 0.26	0.52 ± 0.08	7.3	10.6	12.3
A1142	0.0349	326	11:00:55.0	10:32:52	···	···	0.40 ± 0.07	···	8.5	···
	···	···	11:00:50.4	10:32:59	43	1.77 ± 0.29	0.42 ± 0.07	8.4	9.2	10.0
A1145	0.0677	254	11:01:33.0	16:43:52	···	<0.30	<0.27	···	···	···
A1149	0.0710	409	11:03:00.0	07:37:50	···	<0.30	<0.30	···	···	···
A1169	0.0586	379	11:08:06.6	43:56:45	···	···	0.47 ± 0.11	···	5.7	···
	···	···	11:07:52.1	43:57:02	161	0.63 ± 0.16	0.43 ± 0.11	15.2	5.7	10.7

Table 1—Continued

Abell	z	EXP	RA	DEC	^{1}Offset	^2f_X	^3L_X	$\frac{F_{500}}{F_{62.5}}$	$(\frac{C}{\sqrt{B}})_{500}$	$(\frac{C}{\sqrt{B}})_{max}$
A1171	0.0746	314	11:07:28.6	02:56:45	···	···	0.38 ± 0.13	···	4.2	···
	···	···	11:07:23.5	03:01:11	352	0.26 ± 0.11	0.29 ± 0.12	4.4	5.0	9.3
	···	···	11:07:16.2	02:55:53	245	0.28 ± 0.12	0.31 ± 0.13	8.2	5.1	5.2
A1185	0.0325	188	11:10:47.8	28:40:42	···	···	0.72 ± 0.09	···	16.2	···
	···	···	11:10:36.6	28:43:00	120	3.70 ± 0.44	0.76 ± 0.09	12.3	24.5	26.5
A1187	0.0749	298	11:11:39.7	39:34:41	···	···	0.16 ± 0.14	···	2.6	···
	···	···	11:11:40.7	39:34:36	16	0.18 ± 0.13	0.20 ± 0.14	7.5	1.8	3.0
A1190	0.0751	365	11:11:46.2	40:50:41	···	···	3.00 ± 0.32	···	16.2	···
	···	···	11:11:36.4	40:50:30	143	2.76 ± 0.29	3.10 ± 0.33	27.3	27.8	30.5
A1203	0.0751	324	11:13:57.4	40:17:39	···	<0.29	<0.33	···	···	···
A1213	0.0469	254	11:16:29.0	29:15:37	···	···	0.56 ± 0.11	···	8.1	···
	···	···	11:16:20.0	29:22:42	369	1.00 ± 0.23	0.43 ± 0.10	8.5	6.3	8.0
	···	···	11:16:10.0	29:16:52	217	1.04 ± 0.23	0.45 ± 0.10	18.4	6.8	7.3
	···	···	11:16:51.6	29:15:28	248	1.02 ± 0.23	0.44 ± 0.10	20.1	6.6	10.1
A1216	0.0524	385	11:17:44.8	-04:28:24	···	<0.35	<0.19	···	···	···
A1218	0.0779	376	11:18:49.4	51:42:35	···	···	0.23 ± 0.14	···	3.0	···
	···	···	11:19:00.9	51:45:02	240	0.17 ± 0.12	0.21 ± 0.14	5.2	1.9	4.4
	···	···	11:18:36.0	51:47:07	395	0.19 ± 0.12	0.23 ± 0.14	51.0	2.1	3.7
*A1228	0.0352	170	11:21:29.7	34:19:33	···	···	0.13 ± 0.07	···	4.9	···
	···	···	11:21:25.5	34:25:44	240	0.54 ± 0.25	0.13 ± 0.06	4.3	3.1	8.7
A1238	0.0733	388	11:22:58.0	01:05:32	···	···	0.68 ± 0.16	···	5.8	···
	···	···	11:22:50.6	01:05:38	139	0.72 ± 0.15	0.77 ± 0.16	7.0	8.4	9.4
*A1257	0.0344	239	11:26:05.0	35:19:30	···	<0.65	<0.15	···	···	···
A1267	0.0329	297	11:27:56.7	26:51:28	···	<0.57	<0.12	···	···	···
A1270	0.0692	402	11:29:28.6	54:03:27	···	···	0.31 ± 0.12	···	3.9	···
	···	···	11:29:27.9	54:02:34	63	0.31 ± 0.13	0.29 ± 0.12	5.9	3.3	5.3
A1275	0.0603	175	11:29:58.5	36:40:27	···	···	0.78 ± 0.18	···	9.1	···
	···	···	11:30:01.0	36:37:50	168	1.25 ± 0.28	0.90 ± 0.20	13.3	15.8	16.1
A1279	0.0553	632	11:31:12.8	67:13:27	···	<0.28	<0.17	···	···	···
A1291	0.0527	414	11:32:04.4	56:01:26	···	···	1.02 ± 0.13	···	10.3	···
	···	···	11:32:22.2	55:58:42	206	2.01 ± 0.24	1.10 ± 0.13	11.5	14.5	25.7
A1307	0.0832	354	11:32:47.9	14:31:26	···	···	5.34 ± 0.44	···	28.6	···
	···	···	11:32:51.8	14:28:26	264	4.19 ± 0.33	5.80 ± 0.46	13.1	62.5	66.9

Table 1—Continued

Abell	z	EXP	RA	DEC	^{1}Offset	^{2}f$_X$	^{3}L$_X$	$\frac{F_{500}}{F_{62.5}}$	$(\frac{C}{\sqrt{B}})_{500}$	$(\frac{C}{\sqrt{B}})_{max}$
A1308	0.0511	242	11:32:51.2	-03:58:35	···	<0.41	<0.21	···	···	···
A1314	0.0335	320	11:34:48.7	49:02:25	···	···	0.67 ± 0.08	···	12.6	···
	···	···	11:34:44.5	49:03:44	54	3.02 ± 0.37	0.66 ± 0.08	19.2	14.2	15.0
A1317	0.0705	221	11:35:07.9	-13:31:36	···	···	1.22 ± 0.25	···	8.9	···
	···	···	11:35:16.1	-13:32:22	155	1.42 ± 0.26	1.40 ± 0.26	15.4	13.9	14.3
	···	···	11:35:30.8	-13:28:40	457	1.62 ± 0.28	1.60 ± 0.28	6.4	15.4	19.2
A1318	0.0578	420	11:36:26.1	54:57:24	···	···	0.10 ± 0.08	···	3.4	···
	···	···	11:35:31.9	55:04:36	645	0.41 ± 0.15	0.27 ± 0.10	5.7	3.8	5.3
	···	···	11:36:39.2	55:09:12	727	0.46 ± 0.14	0.30 ± 0.09	9.1	4.2	4.8
A1334	0.0550	147	11:38:51.2	-04:18:38	···	<0.49	<0.29	···	···	···
A1337	0.0826	377	11:39:22.9	10:09:22	···	···	0.18 ± 0.13	···	2.5	···
	···	···	11:39:40.6	10:09:16	364	0.21 ± 0.10	0.28 ± 0.14	8.5	2.8	5.1
	···	···	11:39:26.3	10:12:23	261	0.23 ± 0.10	0.32 ± 0.14	13.6	3.3	3.5
A1344	0.0764	319	11:40:50.6	-10:43:38	···	<0.28	<0.33	···	···	···
A1365	0.0753	278	11:44:24.7	30:54:21	···	···	0.57 ± 0.17	···	5.1	···
	···	···	11:44:35.4	30:52:47	214	0.53 ± 0.16	0.60 ± 0.18	8.2	8.5	10.4
*A1367	0.0220	336	11:44:29.5	19:50:20	···	···	2.25 ± 0.08	···	60.9	···
	···	···	11:44:43.6	19:43:45	181	24.54 ± 0.85	2.30 ± 0.08	21.3	135.2	141.2
A1371	0.0687	387	11:45:29.0	15:32:20	···	···	1.08 ± 0.17	···	8.6	···
	···	···	11:45:09.0	15:28:24	442	1.28 ± 0.19	1.20 ± 0.18	22.1	14.7	17.6
*A1377	0.0514	447	11:46:57.9	55:44:20	···	···	0.66 ± 0.10	···	7.9	···
	···	···	11:47:31.9	55:45:35	270	1.17 ± 0.19	0.61 ± 0.10	13.9	10.0	12.5
A1383	0.0597	426	11:48:09.2	54:37:19	···	···	0.73 ± 0.13	···	7.2	···
	···	···	11:47:53.5	54:42:32	356	1.38 ± 0.20	0.97 ± 0.14	5.3	12.8	20.0
A1385	0.0831	385	11:48:04.5	11:33:19	···	<0.24	<0.33	···	···	···
A1390	0.0826	362	11:49:34.5	12:15:19	···	<0.25	<0.34	···	···	···
A1400	0.0778	436	11:51:25.9	55:06:19	···	···	0.13 ± 0.12	···	2.7	···
	···	···	11:51:11.7	55:09:04	271	0.20 ± 0.11	0.24 ± 0.13	5.2	2.1	3.4
A1412	0.0839	740	11:55:45.2	73:28:18	···	···	1.44 ± 0.18	···	7.8	···
	···	···	11:56:18.6	73:25:38	302	1.28 ± 0.14	1.80 ± 0.20	11.9	19.6	21.8
A1424	0.0768	406	11:57:33.8	05:02:18	···	···	1.22 ± 0.20	···	8.3	···
	···	···	11:57:26.7	05:07:12	408	1.02 ± 0.17	1.20 ± 0.20	14.2	13.7	13.9
A1436	0.0658	430	12:00:28.1	56:15:18	···	···	0.89 ± 0.15	···	7.5	···

Table 1—Continued

Abell	z	EXP	RA	DEC	[1]Offset	[2]f_X	[3]L_X	$\frac{F_{500}}{F_{62.5}}$	$(\frac{C}{\sqrt{B}})_{500}$	$(\frac{C}{\sqrt{B}})_{max}$
	···	···	12:00:22.7	56:13:53	109	1.17 ± 0.19	1.00 ± 0.16	27.6	12.5	12.9
A1452	0.0631	387	12:03:38.8	51:44:18	···	<0.30	<0.24	···	···	···
A1461	0.0537	223	12:04:38.8	42:31:18	···	···	0.23 ± 0.11	···	4.3	···
	···	···	12:05:23.0	42:31:15	464	0.63 ± 0.21	0.36 ± 0.12	5.1	5.5	9.8
A1468	0.0844	381	12:05:38.1	51:25:18	···	···	0.33 ± 0.16	···	3.3	···
	···	···	12:05:36.4	51:29:55	393	0.17 ± 0.11	0.24 ± 0.15	23.4	2.0	4.5
	···	···	12:05:27.0	51:21:21	367	0.08 ± 0.09	0.12 ± 0.13	4.8	1.0	3.4
A1474	0.0801	440	12:07:57.2	14:57:18	···	···	0.33 ± 0.13	···	3.4	···
	···	···	12:07:55.7	14:54:25	236	0.26 ± 0.10	0.33 ± 0.13	7.9	3.3	4.2
	···	···	12:08:12.0	14:58:27	305	0.24 ± 0.10	0.31 ± 0.13	6.2	3.1	5.7
A1480	0.0734	340	12:10:44.1	30:51:19	···	<0.21	<0.22	···	···	···
A1500	0.0720	645	12:13:50.4	74:23:19	···	<0.24	<0.25	···	···	···
A1507	0.0604	466	12:15:50.3	59:58:20	···	···	0.21 ± 0.09	···	3.7	···
	···	···	12:15:03.8	59:53:41	471	0.51 ± 0.14	0.37 ± 0.10	24.3	5.4	8.2
A1526	0.0799	162	12:22:08.2	13:44:22	···	···	0.58 ± 0.23	···	5.1	···
	···	···	12:22:08.9	13:44:19	14	0.50 ± 0.19	0.64 ± 0.24	5.7	6.8	9.7
	···	···	12:22:21.3	13:49:03	459	0.62 ± 0.20	0.79 ± 0.26	13.2	8.4	12.5
A1534	0.0702	440	12:24:03.4	61:30:23	···	···	0.21 ± 0.10	···	3.1	···
	···	···	12:24:32.9	61:29:47	258	0.21 ± 0.10	0.21 ± 0.10	4.1	2.9	6.3
*A1541	0.0893	380	12:27:26.5	08:50:24	···	···	1.70 ± 0.29	···	8.4	···
	···	···	12:27:27.5	08:49:30	83	1.13 ± 0.19	1.80 ± 0.30	16.4	15.0	16.4
*A1552	0.0858	160	12:29:50.0	11:44:26	···	···	2.04 ± 0.05	···	9.2	···
	···	···	12:30:01.7	11:48:20	417	1.76 ± 0.34	2.60 ± 0.50	11.3	9.6	10.2
	···	···	12:29:34.1	11:46:24	376	1.15 ± 0.29	1.70 ± 0.43	27.2	6.3	6.3
	···	···	12:30:03.7	11:42:58	316	1.49 ± 0.32	2.20 ± 0.47	12.6	8.1	8.4
A1564	0.0792	426	12:34:57.4	01:50:29	···	···	0.47 ± 0.15	···	4.1	···
	···	···	12:34:52.9	01:46:50	307	0.33 ± 0.12	0.41 ± 0.15	11.0	4.1	6.5
*A1569	0.0735	125	12:36:18.7	16:35:29	···	···	1.30 ± 0.39	···	7.8	···
	···	···	12:36:23.6	16:31:37	304	1.49 ± 0.40	1.60 ± 0.43	17.5	7.7	9.1
A1589	0.0725	376	12:41:35.8	18:35:33	···	···	1.94 ± 0.24	···	12.3	···
	···	···	12:41:17.3	18:33:54	349	2.49 ± 0.26	2.60 ± 0.27	21.0	27.1	28.1
A1609	0.0891	465	12:46:27.2	26:25:37	···	<0.20	<0.32	···	···	···
A1616	0.0833	442	12:47:38.4	55:02:38	···	···	0.45 ± 0.14	···	3.9	···

Table 1—Continued

Abell	z	EXP	RA	DEC	[1]Offset	[2]f_X	[3]L_X	$\frac{F_{500}}{F_{62.5}}$	$(\frac{C}{\sqrt{B}})_{500}$	$(\frac{C}{\sqrt{B}})_{max}$
	···	···	12:47:16.1	55:00:02	346	0.51 ± 0.12	0.71 ± 0.17	10.9	7.9	9.0
A1630	0.0648	167	12:51:44.5	04:33:42	···	···	0.14 ± 0.17	···	3.4	···
	···	···	12:51:46.2	04:35:49	145	0.35 ± 0.20	0.29 ± 0.17	6.4	2.3	4.5
A1631	0.0462	296	12:52:49.8	-15:26:17	···	···	0.70 ± 0.12	···	8.8	···
	···	···	12:52:51.5	-15:25:39	37	1.79 ± 0.31	0.75 ± 0.13	13.4	9.5	10.4
A1638	0.0620	456	12:54:40.4	18:59:45	···	···	0.38 ± 0.10	···	4.7	···
	···	···	12:54:27.2	18:56:35	288	0.33 ± 0.13	0.25 ± 0.10	9.7	3.5	5.0
A1644	0.0473	207	12:57:14.7	-17:21:13	···	···	4.53 ± 0.30	···	46.5	···
	···	···	12:57:16.7	-17:23:23	112	10.48 ± 0.68	4.60 ± 0.30	19.0	85.5	94.9
A1650	0.0845	292	12:58:46.2	-01:45:11	···	···	10.70 ± 0.70	···	42.0	···
	···	···	12:58:41.3	-01:45:51	118	7.70 ± 0.50	11.00 ± 0.72	11.3	70.4	87.6
*A1651	0.0844	282	12:59:22.9	-04:11:10	···	···	12.40 ± 0.77	···	50.3	···
	···	···	12:59:21.9	-04:11:52	63	9.12 ± 0.55	13.00 ± 0.78	13.3	82.2	95.2
*A1656	0.0231	483	12:59:48.7	27:58:50	···	···	9.18 ± 0.13	···	152.4	···
	···	···	12:59:45.4	27:55:37	85	89.97 ± 1.35	9.30 ± 0.14	17.4	327.3	373.6
A1668	0.0634	418	13:03:51.4	19:15:55	···	···	2.87 ± 0.24	···	21.5	···
	···	···	13:03:44.5	19:16:28	113	3.77 ± 0.30	3.00 ± 0.24	14.0	43.6	52.3
*A1691	0.0722	566	13:11:23.2	39:12:04	···	···	1.60 ± 0.18	···	10.8	···
	···	···	13:11:07.1	39:13:09	245	1.74 ± 0.18	1.80 ± 0.19	14.0	23.5	28.2
A1741	0.0745	715	13:24:04.2	71:28:23	···	<0.18	<0.20	···	···	···
A1749	0.0571	571	13:29:32.2	37:37:31	···	···	0.24 ± 0.09	···	4.2	···
	···	···	13:29:22.8	37:37:05	115	0.36 ± 0.14	0.23 ± 0.09	4.7	3.2	7.1
*A1750	0.0852	199	13:30:52.5	-01:50:27	···	···	3.03 ± 0.47	···	16.9	···
	···	···	13:30:50.1	-01:51:50	129	2.20 ± 0.33	3.20 ± 0.48	15.9	29.0	32.0
A1767	0.0702	518	13:36:00.3	59:12:43	···	···	4.35 ± 0.28	···	32.4	···
	···	···	13:36:05.7	59:12:15	60	4.60 ± 0.29	4.50 ± 0.28	13.7	89.2	101.7
A1773	0.0765	271	13:42:08.5	02:14:53	···	···	2.48 ± 0.34	···	13.6	···
	···	···	13:42:06.3	02:13:15	134	2.23 ± 0.29	2.60 ± 0.34	32.5	19.0	20.2
*A1775	0.0717	392	13:41:55.5	26:21:53	···	···	4.55 ± 0.34	···	27.9	···
	···	···	13:41:53.4	26:22:38	65	4.60 ± 0.34	4.70 ± 0.35	12.2	53.7	71.3
A1780	0.0786	212	13:44:38.2	02:52:58	···	···	0.46 ± 0.19	···	4.3	···
	···	···	13:44:35.7	02:52:03	88	0.37 ± 0.15	0.45 ± 0.19	7.0	4.8	9.1
	···	···	13:44:48.7	02:56:55	379	0.38 ± 0.15	0.47 ± 0.19	9.8	5.0	7.8

Table 1—Continued

Abell	z	EXP	RA	DEC	[1]Offset	[2]f_X	[3]L_X	$\frac{F_{500}}{F_{62.5}}$	$(\frac{C}{\sqrt{B}})_{500}$	$(\frac{C}{\sqrt{B}})_{max}$
A1781	0.0618	384	13:44:28.9	29:50:58	···	···	0.31 ± 0.11	···	4.1	···
	···	···	13:44:22.2	29:54:49	266	0.33 ± 0.15	0.25 ± 0.11	14.2	3.0	3.7
	···	···	13:44:09.9	29:49:31	282	0.34 ± 0.15	0.26 ± 0.11	5.2	3.0	4.6
	···	···	13:44:56.4	29:44:10	585	0.50 ± 0.16	0.38 ± 0.12	4.4	4.4	8.8
A1783	0.0690	545	13:43:21.4	55:35:56	···	···	0.39 ± 0.10	···	4.4	···
	···	···	13:43:23.4	55:37:34	118	0.51 ± 0.12	0.48 ± 0.11	10.2	6.7	7.7
A1793	0.0831	403	13:48:20.6	32:17:05	···	···	0.41 ± 0.16	···	3.6	···
	···	···	13:48:08.2	32:17:55	231	0.30 ± 0.12	0.41 ± 0.16	12.7	3.6	5.6
*A1795	0.0631	434	13:49:00.5	26:35:07	···	···	18.10 ± 0.54	···	116.5	···
	···	···	13:48:52.7	26:35:44	121	24.13 ± 0.70	19.00 ± 0.55	7.8	247.0	372.4
A1800	0.0755	415	13:49:41.4	28:04:08	···	···	3.03 ± 0.29	···	17.3	···
	···	···	13:49:21.8	28:06:14	371	3.53 ± 0.29	4.00 ± 0.33	13.5	39.5	44.0
A1809	0.0789	302	13:53:18.8	05:09:15	···	···	2.44 ± 0.32	···	14.8	···
	···	···	13:53:03.9	05:09:36	299	2.42 ± 0.28	3.00 ± 0.35	30.1	35.1	36.2
A1825	0.0595	428	13:57:57.4	20:39:25	···	···	0.47 ± 0.13	···	5.3	···
	···	···	13:58:04.3	20:38:17	123	0.76 ± 0.19	0.53 ± 0.13	11.4	5.4	7.1
A1827	0.0654	428	13:58:14.6	21:42:26	···	<0.37	<0.31	···	···	···
A1828	0.0623	404	13:58:22.8	18:23:26	···	<0.42	<0.32	···	···	···
A1831	0.0615	443	13:59:10.1	27:59:28	···	···	3.20 ± 0.23	···	21.4	···
	···	···	13:59:15.7	27:58:40	94	4.28 ± 0.31	3.20 ± 0.23	9.9	39.7	53.4
A1836	0.0363	323	14:01:40.5	-11:36:27	···	<0.62	<0.16	···	···	···
*A1837	0.0698	329	14:01:46.3	-11:09:27	···	···	1.90 ± 0.26	···	11.5	···
	···	···	14:01:37.3	-11:07:46	200	2.07 ± 0.27	2.00 ± 0.26	8.3	17.4	24.9
A1873	0.0776	470	14:11:44.3	28:08:56	···	···	0.29 ± 0.13	···	3.4	···
	···	···	14:11:34.7	28:10:17	198	0.27 ± 0.12	0.32 ± 0.14	16.8	3.0	5.7
A1890	0.0574	239	14:17:34.3	08:11:10	···	···	1.34 ± 0.20	···	11.8	···
	···	···	14:17:28.8	08:08:02	206	1.85 ± 0.29	1.20 ± 0.19	10.5	16.2	17.8
A1898	0.0774	312	14:20:33.7	25:09:18	···	···	0.36 ± 0.15	···	3.7	···
	···	···	14:20:35.4	25:07:42	129	0.27 ± 0.13	0.32 ± 0.15	6.7	4.0	6.8
A1899	0.0536	298	14:21:21.4	17:41:20	···	···	0.39 ± 0.13	···	5.7	···
	···	···	14:21:38.6	17:45:13	321	0.60 ± 0.21	0.34 ± 0.12	8.8	3.2	4.2
*A1904	0.0708	505	14:22:07.8	48:33:22	···	···	1.15 ± 0.17	···	7.8	···
	···	···	14:22:15.4	48:30:47	209	1.41 ± 0.19	1.40 ± 0.19	37.1	13.8	14.4

Table 1—Continued

Abell	z	EXP	RA	DEC	[1]Offset	[2]f_X	[3]L_X	$\frac{F_{500}}{F_{62.5}}$	$(\frac{C}{\sqrt{B}})_{500}$	$(\frac{C}{\sqrt{B}})_{max}$
A1913	0.0528	164	14:26:51.8	16:40:34	···	···	0.66 ± 0.18	···	7.5	···
	···	···	14:26:34.4	16:39:41	238	1.11 ± 0.33	0.61 ± 0.18	9.5	4.9	6.9
A1927	0.0947	371	14:31:02.1	25:39:45	···	···	3.90 ± 0.39	···	19.9	···
	···	···	14:31:08.0	25:38:11	193	2.38 ± 0.24	4.30 ± 0.44	7.2	53.2	73.1
A1939	0.0881	427	14:37:14.2	24:50:01	···	···	0.45 ± 0.17	···	3.6	···
	···	···	14:37:28.1	24:46:58	387	0.27 ± 0.10	0.42 ± 0.16	6.3	4.3	6.7
	···	···	14:37:09.6	24:45:28	412	0.30 ± 0.11	0.46 ± 0.17	8.2	4.7	6.4
A1983	0.0436	332	14:52:44.0	16:44:46	···	···	1.06 ± 0.13	···	12.0	···
	···	···	14:52:59.2	16:42:10	210	2.96 ± 0.35	1.10 ± 0.13	6.6	18.8	31.3
*A1991	0.0587	389	14:54:30.2	18:37:51	···	···	2.51 ± 0.22	···	16.0	···
	···	···	14:54:31.8	18:38:47	62	3.53 ± 0.32	2.40 ± 0.22	4.4	23.8	48.7
A2004	0.1365	331	14:58:35.9	24:56:04	···	···	0.31 ± 0.11	···	4.2	···
	···	···	14:58:27.3	24:54:59	283	0.34 ± 0.10	1.30 ± 0.40	13.8	8.7	8.7
A2018	0.0878	554	15:01:12.3	47:16:12	···	···	1.77 ± 0.23	···	10.0	···
	···	···	15:01:03.9	47:16:59	143	1.29 ± 0.16	2.00 ± 0.24	24.1	26.0	26.4
A2019	0.0807	442	15:02:57.2	27:11:17	···	···	0.32 ± 0.14	···	3.3	···
	···	···	15:03:24.8	27:09:27	524	0.35 ± 0.12	0.46 ± 0.15	8.3	4.3	7.0
	···	···	15:03:07.7	27:14:55	353	0.15 ± 0.10	0.20 ± 0.13	4.3	1.8	4.3
A2020	0.0578	230	15:03:45.0	07:55:19	···	<0.59	<0.39	···	···	···
A2022	0.0578	459	15:04:19.7	28:25:22	···	···	0.57 ± 0.11	···	6.5	···
	···	···	15:04:17.9	28:28:58	220	1.08 ± 0.18	0.71 ± 0.12	28.0	9.9	14.3
A2026	0.0876	404	15:08:33.9	-00:16:26	···	···	0.64 ± 0.22	···	4.4	···
	···	···	15:08:25.4	-00:16:03	189	0.46 ± 0.15	0.71 ± 0.23	7.8	4.3	5.4
A2028	0.0777	299	15:09:33.2	07:31:38	···	···	1.32 ± 0.29	···	7.1	···
	···	···	15:09:35.7	07:33:29	154	1.50 ± 0.27	1.80 ± 0.32	11.3	9.3	9.3
	···	···	15:09:19.9	07:38:00	568	1.91 ± 0.25	2.30 ± 0.30	12.9	20.7	20.7
*A2029	0.0773	391	15:10:58.7	05:45:42	···	···	26.00 ± 0.85	···	87.4	···
	···	···	15:10:55.9	05:44:34	104	22.68 ± 0.72	27.00 ± 0.86	10.5	168.8	214.4
A2033	0.0818	376	15:11:28.1	06:21:44	···	···	4.81 ± 0.43	···	16.7	···
	···	···	15:11:27.4	06:20:41	88	3.74 ± 0.33	5.00 ± 0.44	15.2	26.9	30.1
A2040	0.0460	364	15:12:45.2	07:25:48	···	···	0.59 ± 0.13	···	8.7	···
	···	···	15:12:50.7	07:25:54	67	1.30 ± 0.31	0.54 ± 0.13	5.5	5.1	8.6
*A2052	0.0350	403	15:16:45.5	07:00:01	···	···	4.46 ± 0.17	···	38.5	···

Table 1—Continued

Abell	z	EXP	RA	DEC	^{1}Offset	^{2}f$_X$	^{3}L$_X$	$\frac{F_{500}}{F_{62.5}}$	$(\frac{C}{\sqrt{B}})_{500}$	$(\frac{C}{\sqrt{B}})_{max}$
	···	···	15:16:44.4	07:01:21	52	18.85 ± 0.71	4.50 ± 0.17	4.3	64.9	133.8
A2055	0.0530	395	15:18:46.1	06:12:08	···	<0.65	<0.36	···	···	···
A2056	0.0846	294	15:19:12.3	28:16:10	···	···	0.17 ± 0.14	···	2.6	···
	···	···	15:19:13.9	28:22:20	527	0.14 ± 0.10	0.20 ± 0.15	14.9	2.2	5.7
*A2063	0.0353	184	15:23:01.8	08:38:22	···	···	4.28 ± 0.23	···	54.1	···
	···	···	15:23:06.7	08:36:30	85	17.70 ± 0.95	4.30 ± 0.23	9.3	127.8	178.7
A2065	0.0726	365	15:22:42.6	27:43:21	···	···	6.41 ± 0.42	···	33.8	···
	···	···	15:22:26.5	27:42:48	269	7.16 ± 0.43	7.50 ± 0.45	15.3	69.5	77.6
A2067	0.0748	259	15:23:14.7	30:54:23	···	···	0.92 ± 0.22	···	7.1	···
	···	···	15:23:07.3	30:52:13	205	0.90 ± 0.21	1.00 ± 0.23	11.2	11.9	15.0
A2079	0.0661	338	15:28:04.7	28:52:40	···	···	0.75 ± 0.17	···	6.4	···
	···	···	15:27:52.7	28:57:00	348	1.27 ± 0.22	1.10 ± 0.19	12.6	10.2	10.4
A2089	0.0732	250	15:32:41.3	28:00:56	···	<0.40	<0.43	···	···	···
*A2092	0.0669	247	15:33:19.3	31:08:58	···	···	1.18 ± 0.22	···	9.6	···
	···	···	15:33:23.5	31:08:51	62	1.35 ± 0.25	1.20 ± 0.22	12.3	15.7	19.9
*A2107	0.0411	357	15:39:47.9	21:46:21	···	···	2.12 ± 0.15	···	20.8	···
	···	···	15:39:38.6	21:46:40	97	6.36 ± 0.45	2.10 ± 0.15	8.0	30.3	42.2
^{4}A2122	0.0661	236	15:44:29.2	36:07:38	···	···	1.70 ± 0.25	···	12.9	···
	···	···	15:44:06.7	36:12:47	471	0.90 ± 0.22	0.78 ± 0.19	12.0	9.4	17.8
^{4}A2124	0.0661	255	15:44:59.3	36:03:40	···	···	2.14 ± 0.27	···	14.5	···
	···	···	15:45:03.1	36:07:02	237	2.43 ± 0.31	2.10 ± 0.27	6.7	20.2	27.1
*A2142	0.0909	538	15:58:16.1	27:13:28	···	···	26.80 ± 0.85	···	95.0	···
	···	···	15:58:21.7	27:13:25	113	16.88 ± 0.52	28.00 ± 0.87	16.1	222.6	242.4
*A2147	0.0350	542	16:02:17.1	15:53:43	···	···	2.60 ± 0.11	···	28.9	···
	···	···	16:02:18.2	15:57:40	151	12.56 ± 0.50	3.00 ± 0.12	29.6	66.2	71.2
A2148	0.0430	489	16:03:17.9	25:27:47	···	···	0.52 ± 0.06	···	9.5	···
	···	···	16:03:13.0	25:26:21	84	1.55 ± 0.19	0.56 ± 0.07	18.7	19.1	20.1
A2149	0.0679	723	16:01:38.0	53:52:43	···	···	1.59 ± 0.14	···	12.8	···
	···	···	16:01:24.0	53:54:22	185	1.86 ± 0.16	1.70 ± 0.15	16.4	40.0	43.7
*A2151	0.0366	573	16:05:14.9	17:44:55	···	···	1.58 ± 0.09	···	18.8	···
	···	···	16:04:39.5	17:43:21	342	6.12 ± 0.38	1.60 ± 0.10	7.6	33.9	49.2
A2152	0.0410	562	16:05:22.4	16:26:55	···	···	0.31 ± 0.07	···	8.0	···
	···	···	16:05:34.3	16:26:04	132	0.85 ± 0.21	0.28 ± 0.07	4.9	4.9	12.3

Table 1—Continued

Abell	z	EXP	RA	DEC	[1]Offset	[2]f_X	[3]L_X	$\frac{F_{500}}{F_{62.5}}$	$(\frac{C}{\sqrt{B}})_{500}$	$(\frac{C}{\sqrt{B}})_{max}$
A2162	0.0322	698	16:12:29.9	29:32:23	···	···	0.14 ± 0.03	···	6.1	···
	···	···	16:12:35.6	29:27:46	169	0.64 ± 0.15	0.13 ± 0.03	5.5	4.7	8.6
A2168	0.0626	907	16:13:05.0	54:09:27	···	<0.19	<0.15	···	···	···
A2169	0.0586	430	16:14:06.6	49:07:31	···	···	0.36 ± 0.10	···	5.0	···
	···	···	16:13:41.2	49:07:34	256	0.49 ± 0.15	0.33 ± 0.10	9.0	5.2	5.8
A2184	0.0562	420	16:21:02.8	50:11:58	···	···	0.02 ± 0.08	···	3.1	···
	···	···	16:21:04.2	50:09:35	142	0.59 ± 0.14	0.37 ± 0.09	8.4	6.8	6.8
*A2197	0.0308	864	16:28:10.4	40:54:26	···	···	0.34 ± 0.04	···	9.4	···
	···	···	16:27:40.5	40:54:55	192	1.73 ± 0.22	0.32 ± 0.04	4.5	11.8	20.6
	···	···	16:29:41.4	40:50:06	602	1.90 ± 0.22	0.35 ± 0.04	11.7	12.8	17.2
*A2199	0.0299	817	16:28:36.9	39:31:27	···	···	6.82 ± 0.12	···	97.1	···
	···	···	16:28:37.7	39:32:55	48	39.70 ± 0.69	6.90 ± 0.12	5.0	262.9	514.6
A2205	0.0876	232	16:32:31.5	12:52:42	···	<0.46	<0.71	···	···	···
*A2241	0.0635	663	16:59:40.5	32:32:35	···	···	1.43 ± 0.13	···	12.2	···
	···	···	16:59:42.8	32:36:58	292	2.01 ± 0.18	1.60 ± 0.14	6.4	35.3	54.0
A2245	0.0850	706	17:02:44.8	33:31:48	···	···	1.12 ± 0.16	···	6.8	···
	···	···	17:02:33.7	33:30:20	234	0.90 ± 0.12	1.30 ± 0.17	12.1	17.2	19.2
A2248	0.0646	1374	16:57:47.5	77:00:36	···	···	0.22 ± 0.06	···	3.5	···
	···	···	16:57:20.7	77:03:06	196	0.35 ± 0.07	0.29 ± 0.06	8.5	6.4	7.9
A2249	0.0816	766	17:09:43.0	34:27:18	···	···	4.35 ± 0.27	···	20.0	···
	···	···	17:09:47.2	34:26:49	82	3.38 ± 0.21	4.50 ± 0.28	22.3	48.3	50.5
A2250	0.0654	885	17:10:45.5	39:41:23	···	···	1.21 ± 0.12	···	9.3	···
	···	···	17:11:01.9	39:41:35	215	1.42 ± 0.14	1.20 ± 0.12	13.4	19.9	27.6
A2253	0.0891	827	17:15:05.3	38:39:41	···	···	0.32 ± 0.12	···	3.1	···
	···	···	17:15:03.5	38:37:33	192	0.15 ± 0.07	0.24 ± 0.11	9.4	2.6	3.7
	···	···	17:15:06.9	38:44:33	435	0.12 ± 0.07	0.19 ± 0.11	4.3	2.1	4.9
	···	···	17:15:32.8	38:39:07	481	0.17 ± 0.07	0.27 ± 0.11	12.1	3.0	4.5
*A2255	0.0806	3056	17:12:31.0	64:05:33	···	···	5.14 ± 0.14	···	27.1	···
	···	···	17:12:53.3	64:03:55	239	4.70 ± 0.12	6.10 ± 0.16	25.6	176.4	176.8
*A2256	0.0576	1463	17:03:43.4	78:43:02	···	···	8.37 ± 0.19	···	58.8	···
	···	···	17:04:11.2	78:38:35	282	15.28 ± 0.32	10.00 ± 0.21	23.8	246.7	267.9
A2271	0.0576	1715	17:17:17.4	78:01:00	···	···	0.72 ± 0.06	···	7.1	···
	···	···	17:18:12.6	78:01:14	174	1.19 ± 0.11	0.78 ± 0.07	10.1	18.3	24.6

Table 1—Continued

Abell	z	EXP	RA	DEC	[1]Offset	[2]f_X	[3]L_X	$\frac{F_{500}}{F_{62.5}}$	$(\frac{C}{\sqrt{B}})_{500}$	$(\frac{C}{\sqrt{B}})_{max}$
A2293	0.0689	2812	18:01:18.3	57:38:04	···	···	0.49 ± 0.05	···	4.8	···
	···	···	18:02:12.0	57:41:49	577	0.73 ± 0.06	0.69 ± 0.06	6.3	18.0	25.6
A2295	0.0823	7288	17:59:55.7	69:13:01	···	···	0.75 ± 0.04	···	6.1	···
	···	···	18:00:28.1	69:13:42	246	0.55 ± 0.03	0.74 ± 0.04	16.3	32.7	38.3
A2296	0.0611	2003	17:53:57.8	77:40:39	···	<0.16	<0.12	···	···	···
*A2304	0.0890	5489	18:19:35.1	68:55:26	···	···	0.84 ± 0.06	···	5.1	···
	···	···	18:20:11.4	68:57:17	334	0.69 ± 0.04	1.10 ± 0.07	19.4	30.6	38.3
A2308	0.0824	2317	18:33:33.8	71:01:28	···	···	0.75 ± 0.07	···	5.8	···
	···	···	18:34:22.7	70:58:05	435	0.81 ± 0.06	1.10 ± 0.08	12.9	35.8	37.6
A2309	0.0525	1446	18:42:03.3	77:42:08	···	<0.20	<0.11	···	···	···
A2311	0.0890	1991	18:49:43.1	70:22:37	···	···	1.06 ± 0.10	···	6.4	···
	···	···	18:50:12.8	70:22:13	225	0.69 ± 0.06	1.10 ± 0.10	25.2	29.0	32.5
A2331	0.0793	366	20:58:10.3	-07:45:21	···	···	1.24 ± 0.22	···	7.8	···
	···	···	20:58:02.8	-07:47:00	200	0.88 ± 0.18	1.10 ± 0.22	6.3	11.9	16.5
A2361	0.0608	234	21:39:07.7	-14:19:25	···	···	0.33 ± 0.13	···	4.6	···
	···	···	21:39:00.6	-14:20:20	124	0.45 ± 0.18	0.33 ± 0.13	9.1	4.6	6.6
	···	···	21:39:25.6	-14:18:26	283	0.49 ± 0.18	0.36 ± 0.13	18.9	5.0	6.4
A2366	0.0529	277	21:42:50.4	-0652:15	···	···	0.50 ± 0.12	···	6.4	···
	···	···	21:42:45.9	-0649:23	172	0.85 ± 0.22	0.47 ± 0.12	13.8	6.5	7.3
A2372	0.0583	261	21:45:17.4	-19:58:09	···	···	0.73 ± 0.15	···	8.3	···
	···	···	21:45:14.6	-19:59:55	115	1.12 ± 0.22	0.75 ± 0.15	14.2	13.8	14.5
A2377	0.0808	221	21:45:58.4	-10:02:08	···	···	2.36 ± 0.37	···	14.2	···
	···	···	21:45:56.0	-10:05:54	312	2.07 ± 0.31	2.70 ± 0.40	8.3	24.1	30.7
A2378	0.0829	230	21:47:17.2	-19:59:05	···	···	0.10 ± 0.14	···	2.1	···
	···	···	21:47:18.6	-19:58:46	38	0.08 ± 0.10	0.11 ± 0.14	4.0	1.1	3.9
*A2382	0.0618	262	21:52:01.8	-15:38:53	···	···	1.16 ± 0.21	···	9.1	···
	···	···	21:51:53.2	-15:42:45	283	1.59 ± 0.28	1.20 ± 0.21	13.8	9.7	10.4
	···	···	21:52:17.8	-15:43:24	384	1.72 ± 0.28	1.30 ± 0.21	20.2	10.5	10.6
A2388	0.0615	256	21:53:34.7	08:14:11	···	···	0.70 ± 0.16	···	7.4	···
	···	···	21:53:29.3	08:14:32	89	0.91 ± 0.21	0.68 ± 0.16	9.9	10.6	13.6
A2399	0.0579	253	21:57:32.5	-07:47:40	···	···	1.21 ± 0.19	···	10.5	···
	···	···	21:57:26.9	-07:47:26	85	1.81 ± 0.29	1.20 ± 0.19	23.2	14.2	15.3
	···	···	21:57:49.1	-07:53:33	437	1.03 ± 0.24	0.68 ± 0.16	4.4	7.8	14.5

Table 1—Continued

Abell	z	EXP	RA	DEC	[1]Offset	[2]f_X	[3]L_X	$\frac{F_{500}}{F_{62.5}}$	$(\frac{C}{\sqrt{B}})_{500}$	$(\frac{C}{\sqrt{B}})_{max}$
	···	···	21:56:58.5	-07:48:41	517	1.19 ± 0.26	0.79 ± 0.17	8.0	9.3	11.5
A2400	0.0882	323	21:57:46.7	-11:22:40	···	···	0.56 ± 0.21	···	4.1	···
	···	···	21:57:42.2	-11:23:47	138	0.36 ± 0.13	0.56 ± 0.21	8.4	3.9	6.9
A2401	0.0571	195	21:58:52.3	-20:05:38	···	···	0.53 ± 0.16	···	6.3	···
	···	···	21:58:18.8	-20:06:22	475	1.38 ± 0.30	0.89 ± 0.19	13.8	10.6	14.7
	···	···	21:58:51.9	-20:06:41	63	0.70 ± 0.23	0.45 ± 0.15	11.5	5.4	10.7
A2402	0.0809	315	21:58:39.7	-09:45:38	···	···	2.35 ± 0.32	···	12.1	···
	···	···	21:58:31.0	-09:48:16	278	2.07 ± 0.26	2.70 ± 0.34	11.0	19.8	25.0
A2410	0.0809	297	22:02:03.6	-09:53:30	···	···	1.40 ± 0.27	···	8.2	···
	···	···	22:02:21.3	-09:49:36	480	0.99 ± 0.20	1.30 ± 0.26	16.3	10.3	11.9
A2412	0.0781	239	22:04:10.6	-21:26:26	···	···	0.79 ± 0.22	···	6.1	···
	···	···	22:03:58.5	-21:30:36	400	0.71 ± 0.19	0.86 ± 0.23	7.7	6.6	7.9
A2415	0.0581	168	22:05:25.0	-05:35:23	···	···	2.75 ± 0.33	···	22.7	···
	···	···	22:05:40.6	-05:35:30	237	4.21 ± 0.51	2.80 ± 0.34	13.6	28.6	40.4
A2420	0.0846	281	22:10:22.5	-12:11:13	···	···	6.67 ± 0.56	···	28.7	···
	···	···	22:10:20.3	-12:10:19	89	4.75 ± 0.39	6.80 ± 0.56	19.0	52.8	54.5
A2428	0.0851	256	22:16:14.7	-09:21:01	···	···	4.35 ± 0.48	···	19.3	···
	···	···	22:16:15.5	-09:20:29	48	3.04 ± 0.34	4.40 ± 0.49	7.6	28.6	44.8
A2448	0.0823	124	22:31:43.6	-08:26:33	···	···	0.35 ± 0.22	···	3.6	···
	···	···	22:31:25.5	-08:24:53	397	0.30 ± 0.17	0.41 ± 0.23	7.5	4.5	8.1
A2457	0.0594	145	22:35:45.2	01:28:33	···	···	2.27 ± 0.33	···	18.0	···
	···	···	22:35:40.6	01:28:32	71	3.30 ± 0.47	2.30 ± 0.33	13.5	20.0	25.3
A2459	0.0736	142	22:36:34.5	-15:39:26	···	···	0.43 ± 0.24	···	4.2	···
	···	···	22:36:26.8	-15:34:24	405	0.47 ± 0.23	0.51 ± 0.25	4.1	2.8	6.5
	···	···	22:36:14.4	-15:43:48	492	0.58 ± 0.25	0.63 ± 0.27	4.0	3.4	7.9
	···	···	22:36:58.1	-15:31:16	751	0.54 ± 0.24	0.58 ± 0.26	8.4	3.1	4.1
*A2462	0.0733	121	22:39:05.1	-17:21:22	···	···	0.75 ± 0.29	···	6.2	···
	···	···	22:39:14.0	-17:19:59	190	0.82 ± 0.29	0.88 ± 0.31	5.8	4.4	7.5
A2492	0.0711	93	22:50:28.9	-19:15:05	···	···	0.53 ± 0.28	···	5.0	···
	···	···	22:50:24.7	-19:15:21	75	0.56 ± 0.29	0.56 ± 0.29	4.1	4.2	11.5
A2495	0.0775	297	22:50:23.9	10:53:55	···	···	4.37 ± 0.40	···	26.9	···
	···	···	22:50:20.3	10:54:19	76	3.76 ± 0.34	4.50 ± 0.41	11.3	49.1	68.9
A2511	0.0780	254	22:58:54.2	-07:36:55	···	···	0.27 ± 0.16	···	3.2	···

Table 1—Continued

Abell	z	EXP	RA	DEC	[1]Offset	[2]f_X	[3]L_X	$\frac{F_{500}}{F_{62.5}}$	$(\frac{C}{\sqrt{B}})_{500}$	$(\frac{C}{\sqrt{B}})_{max}$
	···	···	22:58:49.5	-07:35:19	157	0.39 ± 0.15	0.47 ± 0.18	14.3	4.3	4.5
A2524	0.0805	377	23:03:10.4	17:44:10	···	···	0.96 ± 0.20	···	6.5	···
	···	···	23:03:09.8	17:43:12	79	0.66 ± 0.15	0.85 ± 0.19	7.7	8.0	8.4
	···	···	23:02:54.6	17:45:22	322	0.85 ± 0.15	1.10 ± 0.19	12.1	12.9	13.0
A2525	0.0788	254	23:03:36.9	-10:34:49	···	<0.31	<0.39	···	···	···
A2538	0.0831	90	23:08:39.3	-19:52:44	···	···	1.11 ± 0.44	···	7.3	···
	···	···	23:08:42.4	-19:52:03	83	0.72 ± 0.30	1.00 ± 0.42	5.1	6.6	12.9
A2556	0.0865	66	23:13:03.3	-21:37:40	···	···	4.84 ± 1.02	···	24.9	···
	···	···	23:13:01.1	-21:37:57	50	3.34 ± 0.67	5.00 ± 1.00	5.6	25.7	51.8
A2559	0.0796	218	23:13:07.2	-13:41:40	···	···	0.41 ± 0.19	···	3.9	···
	···	···	23:13:05.6	-13:38:02	295	0.36 ± 0.15	0.45 ± 0.19	8.7	4.9	8.6
A2566	0.0821	133	23:15:56.6	-20:22:37	···	···	2.60 ± 0.53	···	12.9	···
	···	···	23:16:09.1	-20:27:12	452	3.04 ± 0.48	4.10 ± 0.65	9.6	16.0	32.8
*A2572	0.0403	341	23:18:23.5	18:44:25	···	···	1.23 ± 0.11	···	15.9	···
	···	···	23:18:30.5	18:42:55	97	3.78 ± 0.35	1.20 ± 0.11	9.8	23.0	33.8
*A2589	0.0414	0	23:24:00.5	16:49:29	···	<0.00	<0.00	···	···	···
A2593	0.0413	95	23:24:31.0	14:38:29	···	···	1.44 ± 0.23	···	18.6	···
	···	···	23:24:23.2	14:39:35	97	4.50 ± 0.72	1.50 ± 0.24	24.7	11.9	17.0
*A2597	0.0852	300	23:25:18.0	-12:06:30	···	···	11.70 ± 0.72	···	58.2	···
	···	···	23:25:19.4	-12:07:38	101	8.26 ± 0.50	12.00 ± 0.73	8.8	97.4	143.1
A2618	0.0705	411	23:33:48.4	23:00:35	···	···	0.42 ± 0.13	···	4.5	···
	···	···	23:34:06.6	22:57:31	377	0.43 ± 0.13	0.42 ± 0.13	6.0	4.6	8.5
	···	···	23:33:16.8	22:55:49	632	1.22 ± 0.18	1.20 ± 0.18	13.4	12.8	17.8
A2622	0.0620	364	23:34:53.8	27:25:36	···	···	1.51 ± 0.18	···	15.4	···
	···	···	23:34:59.2	27:22:15	230	2.11 ± 0.24	1.60 ± 0.18	12.1	37.3	45.7
A2625	0.0609	135	23:36:19.0	20:31:36	···	···	0.83 ± 0.22	···	8.7	···
	···	···	23:36:05.6	20:31:39	200	1.35 ± 0.33	0.99 ± 0.24	11.5	13.2	16.8
A2626	0.0553	230	23:36:31.0	21:09:36	···	···	3.07 ± 0.28	···	29.8	···
	···	···	23:36:31.1	21:08:57	38	5.15 ± 0.48	3.10 ± 0.29	6.7	63.1	95.2
A2630	0.0667	71	23:37:31.8	15:49:37	···	<0.48	<0.42	···	···	···
*A2634	0.0310	587	23:38:18.3	27:01:37	···	···	1.31 ± 0.07	···	22.0	···
	···	···	23:38:23.4	27:00:15	60	6.95 ± 0.37	1.30 ± 0.07	20.6	43.4	44.4
A2637	0.0702	343	23:39:07.2	21:27:38	···	···	2.24 ± 0.02	···	15.2	···

Table 1—Continued

Abell	z	EXP	RA	DEC	[1]Offset	[2]f_X	[3]L_X	$\frac{F_{500}}{F_{62.5}}$	$(\frac{C}{\sqrt{B}})_{500}$	$(\frac{C}{\sqrt{B}})_{max}$
	···	···	23:38:56.6	21:24:53	267	2.45 ± 0.28	2.40 ± 0.27	4.0	30.0	72.5
A2644	0.0693	356	23:41:09.7	00:05:38	···	···	0.21 ± 0.12	···	3.3	···
	···	···	23:41:06.1	00:04:45	90	0.23 ± 0.13	0.22 ± 0.12	8.4	2.3	4.3
A2656	0.0773	345	23:44:52.1	-04:06:20	···	<0.27	<0.32	···	···	···
A2660	0.0525	303	23:45:18.0	-25:58:20	···	···	0.18 ± 0.09	···	4.1	···
	···	···	23:45:18.3	-25:47:43	592	0.42 ± 0.17	0.23 ± 0.09	4.0	2.7	5.3
A2665	0.0556	296	23:50:45.4	06:06:41	···	···	2.58 ± 0.23	···	21.4	···
	···	···	23:50:51.7	06:09:51	207	3.94 ± 0.36	2.40 ± 0.22	7.2	25.0	39.3
A2666	0.0272	307	23:50:56.2	27:08:41	···	···	0.08 ± 0.04	···	6.4	···
	···	···	23:51:06.8	27:09:34	75	1.74 ± 0.28	0.25 ± 0.04	9.0	11.3	11.8
*A2670	0.0765	317	23:54:10.1	-10:24:18	···	···	3.95 ± 0.37	···	22.1	···
	···	···	23:54:13.5	-10:24:48	76	3.43 ± 0.33	4.00 ± 0.38	15.4	35.0	43.1
A2675	0.0713	431	23:55:33.4	11:25:42	···	···	1.27 ± 0.18	···	9.2	···
	···	···	23:55:39.1	11:20:04	426	1.88 ± 0.22	1.90 ± 0.22	14.9	22.0	24.9
A2678	0.0726	431	23:55:51.4	11:39:42	···	···	0.88 ± 0.16	···	6.9	···
	···	···	23:55:43.7	11:38:48	156	0.76 ± 0.15	0.80 ± 0.16	5.3	9.1	15.2
A2696	0.0844	387	00:03:21.7	00:53:42	···	···	0.19 ± 0.14	···	2.7	···
	···	···	00:03:12.2	00:53:34	202	0.18 ± 0.11	0.25 ± 0.15	5.1	2.1	4.2

*There is a pointed ROSAT PSPC observation (including serendipidous) $\leq 0.3°$of Abell's position.

[1] Offsets are in units of kpc, projected distance from Abell's position.

[2] Flux in units of $10^{-12} ergs\ cm^{-2}\ sec^{-1}$

[3] Luminosity in units of $10^{43}\ ergs\ sec^{-1}$with $H_0 = 75$and $q_0 = 0.5$.

[4] A2122 and A2124 form a bimodal cluster-pair at the same redshift

This figure "fig1.jpg" is available in "jpg" format from:

http://arXiv.org/ps/astro-ph/0310175v1

arXiv:astro-ph/0310175v1 7 Oct 2003

Table 2. X-ray Peaks and Optical ID's

Abell	RA(2000)$_X$	DEC(2000)$_X$	Offset (arcsec)	Peak Flux (10^{-4} c/sec/pix)	$\frac{F_{250}}{F_{62.5}}$	$(\frac{C}{\sqrt{B}})^{max}_{250}$	Note
A14	00:15:11.2	–23:51:57	91	1.05	3.7	9.7	C
···	00:15:31.6	–23:46:29	478	1.04	2.6	8.4	
···	00:14:29.7	–23:56:46	641	0.37	3.0	3.7	
···	00:14:55.1	–24:06:14	815	0.37	2.3	6.4	
A16	00:16:43.7	06:47:02	147	0.80	3.6	11.3	C
···	00:16:58.5	06:48:03	273	0.96	2.6	8.9	
···	00:16:39.1	06:38:51	365	0.54	8.6	5.0	
···	00:16:18.5	06:48:01	460	0.53	2.4	4.7	
A27	00:24:33.9	–20:40:30	241	0.73	2.7	9.6	
···	00:25:18.2	–20:51:08	665	1.81	3.4	18.8	
···	00:24:26.5	–20:27:32	946	0.37	3.7	6.9	
A71	00:38:29.9	29:29:37	677	0.26	51.3	3.6	
A74	00:39:07.8	–22:20:08	225	2.48	2.4	21.0	
···	00:38:19.4	–22:28:11	746	0.16	0.6	5.9	
A75	00:39:39.9	21:15:02	144	1.79	2.7	13.8	C
···	00:39:06.0	21:19:56	671	0.64	4.8	5.2	
A76	00:39:36.4	06:51:50	358	1.19	3.0	7.3	C
···	00:40:18.9	06:37:54	700	0.64	3.1	5.2	
···	00:40:31.9	06:54:48	835	1.15	7.7	6.9	
···	00:39:06.0	07:02:19	1129	0.42	2.2	3.3	
A77	00:40:28.1	29:33:33	148	3.68	6.9	32.7	C
···	00:39:56.0	29:22:45	722	0.18	1.2	5.2	
···	00:41:12.4	29:40:53	754	0.62	2.1	8.6	
A85	00:41:49.7	–09:18:25	219	25.09	5.7	255.6	C
···	00:42:09.7	–09:35:09	995	0.70	3.8	6.4	
A86	00:42:52.1	–21:48:22	327	0.89	4.1	6.8	C
A102	00:48:22.5	01:32:43	675	0.35	1.0	5.3	
···	00:49:22.5	01:27:58	721	0.32	2.8	3.6	
A104	00:49:52.7	24:26:22	312	3.89	10.1	16.3	C
A116	00:55:50.4	00:38:51	43	0.52	4.6	5.7	C
···	00:55:43.4	00:48:36	635	0.20	2.4	4.1	
···	00:55:15.4	00:44:21	659	0.07	0.9	5.8	

Table 2—Continued

Abell	RA(2000)$_X$	DEC(2000)$_X$	Offset (arcsec)	Peak Flux (10^{-4} c/sec/pix)	$\frac{F_{250}}{F_{62.5}}$	$(\frac{C}{\sqrt{B}})^{max}_{250}$	Note
···	00:56:46.4	00:35:36	833	0.28	1.2	4.1	
A117	00:56:02.4	–10:00:08	101	0.43	8.5	5.3	C
···	00:55:28.4	–09:56:14	584	0.36	2.1	4.5	
A119	00:56:18.9	–01:14:37	79	3.11	10.3	54.6	C
···	00:55:56.8	–01:34:54	1205	0.07	2.7	4.4	
···	00:56:20.9	–01:36:39	1252	0.20	5.3	4.0	
A126	00:59:43.9	–14:15:28	166	0.26	3.7	4.0	C
···	01:00:11.0	–14:22:05	652	0.27	4.0	6.3	
···	00:59:02.8	–14:01:19	948	0.32	2.8	6.6	
···	00:58:40.9	–14:14:49	974	0.30	2.3	5.5	
A133	01:02:42.7	–21:52:53	305	9.87	5.5	72.0	C
···	01:02:37.8	–21:36:31	683	0.36	2.5	3.5	
A134	01:02:40.4	–02:29:01	379	0.29	11.1	7.4	C
···	01:03:25.4	–02:33:21	350	0.46	2.4	4.3	
···	01:02:31.3	–02:38:28	616	0.27	3.2	3.4	
···	01:02:17.4	–02:31:10	684	0.42	3.6	4.0	
···	01:03:34.2	–02:21:44	769	0.29	3.1	4.9	
A147	01:08:12.9	02:10:52	64	1.50	7.6	34.6	C
···	01:08:56.7	02:23:42	1076	0.31	2.6	13.5	
···	01:07:16.6	02:22:50	1115	0.44	2.7	11.3	
A150	01:09:17.8	13:10:36	64	1.67	3.5	22.4	C
···	01:09:11.0	13:02:05	477	0.30	8.8	4.6	
···	01:10:03.0	13:11:26	717	0.42	4.6	7.0	
···	01:09:08.1	13:23:49	835	0.46	4.8	6.4	
A151	01:08:49.7	–15:24:39	44	3.57	6.1	55.3	C
···	01:08:56.5	–15:37:47	768	1.85	4.4	28.2	
···	01:09:50.7	–15:30:45	912	0.44	6.1	9.2	
A154	01:11:03.9	17:37:49	153	1.37	8.4	13.1	C
A158	01:11:48.4	16:53:02	38	1.41	4.4	11.7	C
···	01:11:12.6	16:59:42	627	0.22	17.9	3.2	
···	01:10:59.4	16:51:25	673	0.30	2.7	4.1	
···	01:12:11.4	17:02:26	680	0.55	1.3	6.7	

Table 2—Continued

Abell	RA(2000)$_X$	DEC(2000)$_X$	Offset (arcsec)	Peak Flux (10^{-4} c/sec/pix)	$\frac{F_{250}}{F_{62.5}}$	$(\frac{C}{\sqrt{B}})^{max}_{250}$	Note
···	01:11:00.9	16:42:40	892	0.20	4.0	3.1	
A160	01:13:06.4	15:30:33	219	1.07	6.6	13.4	C
···	01:13:46.5	15:44:38	1146	0.25	2.1	5.4	
A168	01:14:58.3	00:21:57	460	1.25	11.0	23.9	C
···	01:14:30.3	00:00:42	1035	0.55	1.5	10.3	
A171	01:17:04.2	16:13:56	286	0.27	2.5	3.2	
A179	01:22:04.6	19:33:36	378	0.23	9.8	4.0	C
···	01:21:44.4	19:21:34	430	0.26	8.6	4.8	
···	01:22:54.1	19:27:04	943	0.72	5.2	9.1	
···	01:20:56.5	19:18:16	958	0.13	0.6	7.3	
A193	01:25:04.5	08:41:17	46	5.32	8.0	68.7	C
···	01:24:56.8	08:53:01	703	0.36	4.6	5.6	
A194	01:25:51.0	–01:22:39	538	0.59	7.0	21.5	C
A195	01:27:32.7	19:10:42	549	6.78	2.0	124.8	
···	01:26:15.2	19:10:03	550	1.20	2.6	20.7	
···	01:27:57.2	18:59:43	1088	3.29	1.9	63.9	
A225	01:38:41.8	18:58:04	347	0.43	4.4	4.7	
···	01:38:15.6	18:51:01	577	0.29	0.0	7.6	
A240	01:42:14.1	07:38:44	294	0.39	2.3	7.8	C
···	01:42:08.1	07:31:29	387	0.17	1.2	4.6	
···	01:41:04.5	07:35:14	766	0.28	2.4	4.2	
A245	01:43:20.1	06:22:24	699	0.21	3.8	3.4	
A246	01:44:45.2	05:48:39	53	1.37	3.3	11.2	C
···	01:44:38.5	05:43:34	275	0.72	3.7	6.6	
···	01:44:36.0	05:57:54	600	0.32	1.2	4.6	
···	01:44:01.9	05:52:38	668	0.38	0.6	5.8	
A257	01:49:06.6	13:55:38	224	0.38	3.5	5.1	C?
···	01:49:05.0	14:03:55	312	0.74	2.3	11.3	C?
···	01:48:36.9	14:01:13	352	1.54	3.9	19.4	C?
···	01:49:21.5	14:02:14	382	0.57	14.3	7.8	C?
···	01:49:38.2	14:06:10	716	0.43	6.9	5.6	
···	01:49:24.9	13:48:40	719	0.38	2.3	6.0	

Table 2—Continued

Abell	RA(2000)$_X$	DEC(2000)$_X$	Offset (arcsec)	Peak Flux (10^{-4} c/sec/pix)	$\frac{F_{250}}{F_{62.5}}$	$(\frac{C}{\sqrt{B}})^{max}_{250}$	Note
A262	01:52:45.0	36:09:30	78	3.65	3.4	102.3	C
A272	01:55:10.1	33:54:47	160	3.75	8.6	20.4	C
···	01:54:48.1	33:52:55	446	4.00	3.1	20.4	
···	01:55:40.3	33:50:20	464	0.75	2.0	5.6	
A278	01:57:21.0	32:13:15	44	2.35	13.5	13.1	C
A279	01:56:07.8	01:02:60	220	0.62	6.5	4.9	C
···	01:55:50.8	01:05:60	492	0.35	3.1	3.8	
A281	01:57:33.9	–05:48:44	422	1.28	4.2	11.4	M
···	01:57:07.3	–05:53:23	181	1.22	4.3	11.2	M
···	01:56:53.8	–05:49:30	195	0.50	5.2	4.2	
A358	02:29:53.3	–13:15:21	352	1.01	7.0	9.9	C
···	02:30:28.6	–13:16:28	373	0.70	7.0	6.5	
A376	02:46:04.2	36:54:06	241	3.34	7.5	86.1	C
A415	03:06:51.0	–12:05:51	209	2.75	3.6	9.9	C
···	03:07:04.3	–12:02:37	249	1.19	3.7	3.9	
···	03:06:30.8	–12:09:17	475	1.13	1.3	10.3	
···	03:06:48.3	–12:13:35	666	0.91	1.6	5.6	
···	03:06:14.1	–12:12:26	766	1.31	3.1	5.6	
A419	03:08:18.0	–23:40:16	197	2.27	3.0	23.3	C
···	03:08:53.6	–23:41:34	367	0.44	1.5	5.6	
···	03:08:08.8	–23:34:42	375	0.81	9.9	7.1	
···	03:08:59.2	–23:33:38	496	0.50	1.4	12.5	
···	03:08:17.5	–23:48:36	626	0.73	3.4	6.4	
A428	03:15:58.2	–19:11:27	328	0.64	4.0	4.5	
···	03:16:40.0	–19:01:20	654	0.22	1.8	4.5	
···	03:16:21.5	–19:16:17	701	0.34	0.8	8.2	
A437	03:27:03.7	–02:46:12	269	0.47	2.8	6.1	C
···	03:26:35.2	–02:48:52	380	0.45	2.6	5.8	
···	03:27:30.5	–02:45:49	634	0.60	4.2	5.7	
A496	04:33:37.4	–13:15:21	35	13.98	4.4	198.7	C
···	04:34:29.4	–13:34:12	1394	0.49	3.2	7.0	
···	04:32:59.2	–13:39:57	1608	0.14	1.5	4.1	

Table 2—Continued

Abell	$\mathrm{RA(2000)}_X$	$\mathrm{DEC(2000)}_X$	Offset (arcsec)	Peak Flux (10^{-4} c/sec/pix)	$\frac{F_{250}}{F_{62.5}}$	$(\frac{C}{\sqrt{B}})^{max}_{250}$	Note
A500	04:38:55.7	–22:06:41	33	3.52	4.7	18.9	C
···	04:38:30.5	–22:12:03	503	1.17	9.6	8.2	
A514	04:48:03.7	–20:27:11	343	1.59	12.6	16.1	M
···	04:48:29.8	–20:27:12	704	1.59	5.5	17.8	M
···	04:47:44.2	–20:20:32	318	0.59	7.1	5.5	
···	04:47:18.5	–20:23:37	329	0.57	4.7	5.2	
···	04:47:06.6	–20:29:13	514	0.46	4.0	5.1	
A533	05:01:42.5	–22:35:35	176	0.63	4.8	8.9	M
···	05:01:07.3	–22:33:09	389	0.59	4.6	9.2	M
···	05:01:23.1	–22:45:06	515	0.25	21.9	4.3	
A548	05:46:54.2	–25:38:34	138	0.73	4.0	27.2	C
···	05:47:24.5	–25:35:44	316	0.60	10.8	18.9	
···	05:47:38.8	–25:19:02	1188	0.50	19.1	18.7	
A564	07:01:32.1	69:53:25	378	0.34	6.2	3.6	C
···	07:00:36.4	69:58:16	567	0.31	0.9	4.6	
···	06:58:40.6	69:47:05	637	0.07	2.3	5.1	
···	07:02:03.2	69:40:15	665	0.29	2.7	3.8	
A576	07:21:23.1	55:47:06	166	4.42	6.7	63.5	C
A578	07:25:03.1	66:58:57	15	1.42	4.5	10.3	C
···	07:25:16.6	66:54:52	271	0.99	3.6	7.2	
···	07:23:55.5	66:54:54	462	0.61	1.8	6.1	
···	07:24:03.7	67:04:40	474	0.44	5.6	3.6	
···	07:25:36.3	67:06:22	480	0.59	2.0	6.2	
A592	07:42:37.2	09:21:58	10	3.57	4.9	32.0	C
A595	07:49:18.6	52:05:15	263	0.57	6.1	8.7	C
···	07:48:18.9	52:08:31	379	0.23	1.9	6.4	
···	07:49:03.3	51:54:42	600	0.30	2.8	5.5	
···	07:47:39.1	52:00:35	699	0.29	1.6	7.9	
···	07:48:29.9	52:15:42	699	0.18	0.7	5.4	
···	07:49:37.1	52:14:06	719	0.29	1.7	5.4	
···	07:48:27.8	51:50:43	852	0.32	1.3	10.5	
A600	07:56:50.0	63:44:53	192	0.28	5.8	3.8	C

Table 2—Continued

Abell	RA(2000)$_X$	DEC(2000)$_X$	Offset (arcsec)	Peak Flux (10^{-4} c/sec/pix)	$\frac{F_{250}}{F_{62.5}}$	$(\frac{C}{\sqrt{B}})^{max}_{250}$	Note
···	07:56:15.1	63:56:10	670	0.49	7.7	5.2	
A602	07:53:21.9	29:22:18	77	3.25	6.5	39.6	C
···	07:52:18.9	29:19:41	790	0.29	1.9	6.9	
···	07:53:38.6	29:35:11	879	0.39	1.6	8.1	
···	07:52:30.3	29:31:58	908	0.54	3.8	7.6	
A612	08:00:57.9	34:49:18	64	1.09	4.0	12.0	C
···	08:01:19.1	34:49:18	212	0.86	2.5	8.1	
···	08:00:49.7	34:41:21	467	0.41	0.5	6.5	
···	08:01:17.7	34:41:20	482	0.26	70.0	4.0	
···	08:00:28.5	34:53:45	513	0.23	9.2	2.8	
A623	08:05:38.4	–00:57:30	54	2.55	5.0	13.7	C
···	08:05:42.9	–01:01:37	306	1.41	5.5	8.9	
···	08:05:14.3	–00:57:46	374	0.56	2.0	5.6	
···	08:05:15.4	–00:52:15	439	0.06	–0.5	5.6	
···	08:06:11.6	–00:55:35	496	0.44	0.8	8.2	
···	08:04:55.0	–00:57:56	661	0.53	1.5	6.0	
A628	08:10:10.4	35:17:45	280	1.13	4.6	10.2	C
···	08:09:46.7	35:08:40	372	0.43	1.8	6.5	
···	08:10:32.0	35:06:49	481	0.27	3.6	3.1	
A634	08:15:58.9	58:19:45	1217	0.43	2.7	13.7	
···	08:16:23.8	57:39:18	1665	0.53	1.4	19.8	
A671	08:28:36.8	30:25:37	104	2.08	5.2	32.9	C
A690	08:39:15.5	28:54:12	230	0.61	7.1	4.1	
···	08:39:36.5	28:52:28	320	0.58	2.1	4.3	
···	08:39:08.4	28:44:12	380	0.77	5.8	5.4	
···	08:38:42.8	28:49:39	414	0.55	2.9	3.5	
···	08:39:43.0	28:46:00	462	0.65	1.4	6.0	
···	08:38:44.0	28:56:31	542	0.55	2.0	3.5	
···	08:39:38.8	28:58:25	581	0.60	0.5	6.8	
···	08:39:58.1	28:49:25	581	0.69	1.4	5.8	
···	08:38:55.9	28:59:58	623	0.61	0.9	6.2	
A692	08:41:13.4	26:40:35	346	0.74	5.6	5.5	C

Table 2—Continued

Abell	RA(2000)$_X$	DEC(2000)$_X$	Offset (arcsec)	Peak Flux (10^{-4} c/sec/pix)	$\frac{F_{250}}{F_{62.5}}$	$(\frac{C}{\sqrt{B}})^{max}_{250}$	Note
···	08:40:36.8	26:41:03	298	0.97	5.1	6.2	
···	08:40:56.3	26:52:15	479	0.63	2.6	4.8	
···	08:41:41.7	26:44:38	644	0.91	2.5	5.4	
A699	08:44:56.7	27:45:03	295	1.65	15.9	6.6	C
···	08:44:28.4	27:42:55	273	0.58	2.0	4.0	
···	08:44:15.3	27:37:36	635	0.80	5.7	3.5	
A744	09:07:22.4	16:39:24	75	2.50	4.6	28.3	C
···	09:08:04.1	16:38:58	670	0.31	5.1	4.9	
···	09:06:30.7	16:45:51	762	2.11	2.6	50.1	
A754	09:09:05.5	–09:40:03	254	9.05	19.4	124.3	C
A757	09:13:06.5	47:42:13	197	1.59	3.7	24.1	M
···	09:13:44.5	47:42:04	579	1.71	2.6	27.5	M
A763	09:12:31.6	15:55:31	250	7.63	3.3	60.3	C
···	09:12:35.7	16:02:45	211	0.77	3.1	7.6	
A779	09:19:45.5	33:45:53	70	0.81	3.3	18.9	C
A780	09:18:06.4	–12:05:39	696	22.31	4.7	260.6	HydraA
···	09:18:05.0	–12:18:51	418	0.59	3.6	10.7	
···	09:18:23.1	–12:23:11	463	0.62	4.5	8.5	C
A819	09:32:18.3	09:41:19	99	0.69	2.2	5.8	
···	09:32:01.1	09:38:19	245	0.41	0.2	7.4	
A834	09:41:25.5	66:43:48	340	1.26	7.8	10.9	C
···	09:42:26.4	66:45:38	706	0.46	1.3	10.1	
A838	09:37:04.0	–05:02:53	147	0.19	1.7	3.8	
···	09:36:17.8	–04:56:23	767	0.86	3.0	11.9	
A841	09:38:44.6	–04:21:27	603	0.72	4.2	7.7	C
···	09:38:36.5	–04:08:57	157	0.22	2.5	3.7	
···	09:38:50.5	–04:12:26	209	0.26	6.8	4.8	
···	09:38:23.1	–04:15:24	311	0.49	4.1	3.6	
···	09:38:12.0	–04:12:28	377	0.47	1.7	5.2	
···	09:39:20.6	–04:10:40	655	0.16	1.8	8.8	
···	09:37:54.5	–04:15:59	689	0.31	1.7	8.7	
A858	09:43:23.2	05:54:20	76	1.46	9.5	13.2	C

Table 2—Continued

Abell	RA(2000)$_X$	DEC(2000)$_X$	Offset (arcsec)	Peak Flux (10^{-4} c/sec/pix)	$\frac{F_{250}}{F_{62.5}}$	$(\frac{C}{\sqrt{B}})^{max}_{250}$	Note
···	09:43:48.7	05:57:40	435	0.62	5.3	5.2	
···	09:43:16.1	05:46:15	443	0.56	2.4	5.8	
···	09:43:31.4	05:44:45	515	0.44	1.5	9.2	
···	09:44:02.0	05:51:01	558	0.53	2.5	8.2	
···	09:42:56.9	06:00:49	626	0.45	3.4	5.2	
A912	10:01:19.7	00:01:33	331	0.36	1.4	4.8	
···	10:01:20.8	–00:10:51	313	0.36	3.0	3.6	
···	10:01:19.8	–00:01:33	504	0.39	1.5	4.6	
A930	10:06:52.8	–05:37:54	31	0.29	3.0	10.9	C
···	10:07:41.7	–05:28:24	896	0.29	2.7	7.0	
···	10:06:44.1	–05:21:50	963	0.33	10.6	6.4	
···	10:07:53.0	–05:45:10	980	0.25	2.7	8.0	
A957	10:13:40.9	–00:55:02	247	2.45	7.5	31.3	C
···	10:13:20.9	–01:10:17	1072	0.26	1.6	5.4	
···	10:13:21.9	–00:38:32	1117	0.28	2.8	5.1	
A970	10:17:20.9	–10:40:58	207	5.02	6.9	59.0	C
A971	10:19:59.3	40:59:33	173	2.00	7.3	19.8	C
A978	10:20:28.0	–06:31:29	44	0.95	10.3	13.3	C
A979	10:20:00.1	–07:53:29	354	0.89	2.4	13.9	
A991	10:22:55.4	18:53:55	432	0.97	1.5	7.3	
···	10:22:56.8	18:47:40	543	1.43	2.0	8.3	
A993	10:21:56.0	–04:53:02	248	0.52	3.4	8.2	C
···	10:22:26.1	–05:02:47	570	0.34	0.7	8.1	
···	10:22:07.0	–04:42:02	924	0.24	6.7	4.2	
···	10:22:54.2	–05:03:47	965	0.23	1.6	4.2	
A1016	10:26:53.4	11:01:38	226	0.21	1.0	3.5	
···	10:27:29.1	10:46:36	821	0.21	1.4	6.1	
···	10:27:56.9	10:33:54	1686	0.30	3.2	3.4	
A1020	10:27:58.0	10:32:33	485	0.45	9.8	5.0	C
···	10:27:17.7	10:20:58	534	0.19	1.0	4.5	
···	10:26:58.8	10:29:12	812	0.32	2.0	4.1	
A1032	10:30:01.2	03:53:41	482	0.98	8.3	8.7	C

Table 2—Continued

Abell	$RA(2000)_X$	$DEC(2000)_X$	Offset (arcsec)	Peak Flux (10^{-4} c/sec/pix)	$\frac{F_{250}}{F_{62.5}}$	$(\frac{C}{\sqrt{B}})^{max}_{250}$	Note
···	10:30:11.3	04:02:03	128	0.30	1.2	6.4	
···	10:29:54.1	04:01:13	353	0.36	0.1	5.5	
···	10:30:26.0	04:08:48	508	0.59	1.9	8.3	
···	10:30:45.5	04:06:00	531	0.37	2.5	3.3	
···	10:29:44.2	04:06:01	597	0.50	1.5	7.1	
···	10:30:58.2	03:57:01	644	0.25	3.1	4.1	
A1035	10:32:13.8	40:16:12	232	3.04	4.6	24.6	C
···	10:32:22.1	40:10:54	196	1.00	3.2	9.2	
···	10:32:28.4	40:07:17	398	1.00	3.8	9.0	
···	10:32:57.9	40:19:13	704	0.24	1.5	4.1	
···	10:31:13.0	40:18:50	727	0.18	1.5	4.6	
A1066	10:39:38.6	05:10:28	220	1.51	7.9	8.8	M
···	10:38:42.1	05:13:59	661	0.95	5.0	7.0	M
···	10:39:07.6	05:11:14	251	1.63	5.2	7.2	
···	10:39:15.8	05:16:39	397	0.90	2.9	7.7	
···	10:39:41.6	05:18:58	581	0.69	1.3	7.0	
A1069	10:39:44.6	–08:41:02	299	3.00	4.9	33.8	C
A1100	10:48:45.1	22:13:59	128	0.95	5.8	12.2	C
···	10:49:45.5	22:09:59	754	0.29	4.6	5.0	
···	10:48:50.5	21:54:29	1179	0.23	1.7	5.7	
A1126	10:53:50.6	16:50:58	101	4.21	2.9	27.0	C
···	10:54:08.9	16:48:39	215	0.95	3.9	7.1	
···	10:54:12.5	16:52:21	227	0.94	2.5	6.9	
···	10:54:04.4	16:59:07	496	0.61	1.9	7.8	
···	10:53:19.5	16:55:31	610	0.55	1.5	8.4	
···	10:53:47.2	16:39:13	724	0.64	1.8	5.2	
A1139	10:58:26.8	01:34:47	446	0.82	3.7	12.3	C
A1142	11:00:50.4	10:32:59	68	0.45	3.2	9.0	C
···	11:00:33.7	10:24:20	601	0.37	4.8	5.6	
···	11:00:43.1	10:44:44	733	0.59	3.5	9.6	
···	11:01:56.7	10:17:47	1284	0.62	1.4	16.7	
A1145	11:01:39.6	16:45:09	122	0.44	1.0	4.7	

Table 2—Continued

Abell	RA(2000)$_X$	DEC(2000)$_X$	Offset (arcsec)	Peak Flux (10^{-4} c/sec/pix)	$\frac{F_{250}}{F_{62.5}}$	$(\frac{C}{\sqrt{B}})^{max}_{250}$	Note
···	11:01:24.6	16:42:59	130	0.29	1.3	4.7	
···	11:01:48.5	16:37:54	421	0.18	1.8	5.1	
···	11:02:12.6	16:52:06	754	0.17	0.3	4.8	
···	11:01:57.1	16:31:33	817	0.21	1.0	6.9	
A1149	11:03:04.6	07:34:42	200	0.41	2.5	4.6	
···	11:03:25.7	07:38:27	384	0.31	1.7	4.0	
···	11:02:30.2	07:42:42	531	0.41	3.3	4.2	
···	11:03:14.7	07:49:57	759	0.41	1.5	6.3	
A1169	11:07:52.1	43:57:02	158	0.87	13.6	10.2	C
···	11:08:55.0	44:04:36	703	0.24	3.5	3.4	
···	11:07:41.5	43:45:28	730	0.67	5.7	7.8	
A1171	11:07:23.5	03:01:11	278	0.55	2.2	8.8	C
···	11:07:16.2	02:55:53	193	0.30	4.2	4.8	
···	11:07:42.2	02:52:14	341	0.30	1.1	4.5	
···	11:08:06.9	02:52:60	617	0.24	3.1	5.3	
···	11:07:49.1	03:09:16	812	0.69	1.8	11.4	
A1185	11:10:36.6	28:42:60	202	1.24	6.5	26.1	C
···	11:09:10.2	28:40:30	1284	0.31	4.7	8.0	
···	11:11:11.3	28:18:42	1356	0.23	3.4	5.4	
A1187	11:11:35.1	39:34:42	53	0.53	4.3	3.0	C
···	11:12:21.9	39:38:14	532	0.64	3.8	5.4	
···	11:11:40.7	39:43:41	539	0.41	0.9	8.0	
A1190	11:11:36.4	40:50:30	111	2.98	13.4	27.3	C
···	11:11:26.9	40:41:32	591	0.58	4.3	4.0	
···	11:11:46.8	41:01:55	674	0.62	88.0	5.3	
···	11:10:41.1	40:49:31	742	0.31	0.5	10.3	
A1203	11:14:13.0	40:11:34	406	0.57	1.5	6.1	
···	11:13:05.6	40:17:50	593	0.34	2.1	3.5	
···	11:13:06.1	40:13:05	648	0.97	1.8	9.9	
A1213	11:16:10.0	29:16:52	260	0.51	7.1	5.3	C?
···	11:16:20.0	29:22:42	441	0.44	4.0	7.5	C?
···	11:16:51.6	29:15:28	295	0.30	3.1	4.3	

Table 2—Continued

Abell	RA(2000)$_X$	DEC(2000)$_X$	Offset (arcsec)	Peak Flux (10^{-4} c/sec/pix)	$\frac{F_{250}}{F_{62.5}}$	$(\frac{C}{\sqrt{B}})^{max}_{250}$	Note
· · ·	11:16:33.0	28:58:45	1014	0.14	0.8	5.4	
· · ·	11:17:50.8	29:18:13	1081	1.05	2.9	12.1	
A1216	11:17:21.1	–04:26:18	376	0.35	1.7	8.1	
A1218	11:19:00.9	51:45:02	182	0.34	2.4	4.1	C
· · ·	11:18:36.0	51:47:07	299	0.32	29.0	3.7	
· · ·	11:18:52.0	51:53:44	669	0.51	6.2	4.9	
· · ·	11:19:39.5	51:33:31	716	5.01	3.0	37.5	
A1228	11:21:25.9	34:25:44	374	0.22	2.2	8.7	C
· · ·	11:20:10.2	34:19:40	984	0.27	2.9	4.4	
· · ·	11:21:16.4	34:02:25	1041	0.40	2.6	7.0	
· · ·	11:22:51.7	34:07:43	1240	0.69	6.0	11.0	
A1238	11:22:50.6	01:05:38	111	0.88	3.5	9.4	C
· · ·	11:22:37.1	01:02:21	366	0.68	2.7	6.8	
· · ·	11:22:23.6	01:07:53	534	0.28	44.5	4.0	
A1270	11:29:27.9	54:02:34	54	0.44	3.5	5.3	C
· · ·	11:30:31.2	54:01:55	559	0.35	2.2	5.0	
· · ·	11:28:41.9	54:12:47	694	0.40	7.9	4.2	
· · ·	11:28:14.7	53:57:07	755	0.29	1.6	3.8	
· · ·	11:27:59.5	54:02:00	789	0.29	2.9	3.5	
A1275	11:30:01.0	36:37:50	160	0.87	6.7	16.1	C
· · ·	11:30:30.0	36:34:57	503	0.50	3.7	8.3	
· · ·	11:30:41.3	36:42:52	534	0.39	3.7	8.0	
· · ·	11:30:24.9	36:26:49	877	0.46	4.6	7.7	
A1279	11:31:52.2	67:15:40	265	0.21	1.4	6.1	
A1291	11:32:22.2	55:58:42	222	2.44	9.1	25.7	C
· · ·	11:31:40.3	56:09:37	531	0.23	2.6	3.6	
· · ·	11:33:00.8	56:10:45	731	0.27	3.1	3.4	
· · ·	11:30:03.3	56:05:16	1040	0.26	2.3	3.2	
A1307	11:32:51.8	14:28:26	188	6.02	6.9	65.5	C
· · ·	11:32:05.1	14:31:59	622	0.12	0.8	4.4	
A1308	11:33:58.9	–04:04:09	1067	0.29	3.6	6.3	
A1314	11:34:44.5	49:03:44	90	0.85	10.0	14.8	C

Table 2—Continued

Abell	RA(2000)$_X$	DEC(2000)$_X$	Offset (arcsec)	Peak Flux (10^{-4} c/sec/pix)	$\frac{F_{250}}{F_{62.5}}$	$(\frac{C}{\sqrt{B}})^{max}_{250}$	Note
···	11:34:18.1	48:38:02	1493	0.46	6.7	7.2	
A1317	11:35:16.1	–13:32:22	128	1.73	7.6	13.8	C
···	11:35:30.8	–13:28:40	377	1.75	2.9	19.2	
···	11:34:50.5	–13:23:13	563	0.37	1.8	5.7	
···	11:34:32.6	–13:36:59	608	0.34	1.7	5.0	
···	11:35:46.8	–13:40:32	780	0.29	2.8	4.6	
A1318	11:35:31.9	55:04:36	636	0.37	2.8	5.3	C
···	11:36:39.2	55:09:12	718	0.13	2.7	3.6	
···	11:37:23.4	55:08:45	840	0.28	1.5	5.3	
A1334	11:38:41.3	–04:17:50	156	0.29	0.9	5.0	
···	11:39:25.0	–04:19:42	510	0.76	1.2	11.2	
···	11:39:36.8	–04:11:41	799	0.46	0.5	5.6	
···	11:37:51.7	–04:13:25	944	0.32	0.6	11.6	
A1337	11:39:40.6	10:09:16	262	0.35	6.6	5.1	C
···	11:39:26.3	10:12:24	188	0.34	3.7	3.3	
···	11:39:35.2	10:17:31	521	0.32	3.8	4.0	
···	11:39:56.3	10:04:03	590	0.50	0.6	9.4	
···	11:39:42.0	09:58:46	696	0.22	0.4	3.8	
A1344	11:41:01.2	–10:41:00	223	0.31	0.4	4.1	
···	11:40:36.1	–10:51:02	493	0.39	1.9	3.7	
···	11:40:57.5	–10:34:59	530	0.51	0.6	4.2	
···	11:41:10.7	–10:50:59	531	0.43	0.9	5.5	
A1365	11:44:35.4	30:52:47	166	0.90	4.2	10.4	C
···	11:45:00.7	30:55:27	469	0.63	4.0	7.8	
···	11:44:34.0	30:43:16	675	0.68	4.7	10.4	
···	11:45:08.7	30:47:02	717	4.15	3.2	42.7	
A1367	11:44:51.9	19:40:50	651	2.99	10.5	132.8	C
···	11:47:58.3	20:12:58	3240	2.79	1.3	195.4	
A1371	11:45:09.0	15:28:24	374	1.52	13.3	17.6	C
A1377	11:47:31.9	55:45:35	297	0.94	8.7	12.5	C
···	11:46:40.4	55:36:12	510	0.20	3.0	4.1	
···	11:48:42.1	55:44:22	880	0.22	4.5	3.7	

Table 2—Continued

Abell	RA(2000)$_X$	DEC(2000)$_X$	Offset (arcsec)	Peak Flux (10^{-4} c/sec/pix)	$\frac{F_{250}}{F_{62.5}}$	$(\frac{C}{\sqrt{B}})^{max}_{250}$	Note
A1383	11:47:53.5	54:42:32	341	1.91	3.2	20.0	C
···	11:47:13.6	54:35:50	491	0.17	3.6	4.1	
···	11:48:00.9	54:28:04	560	0.53	13.6	6.3	
···	11:49:34.7	54:34:05	769	0.66	2.5	8.3	
A1385	11:48:04.1	11:35:11	112	0.59	1.8	8.0	C
···	11:48:47.5	11:33:27	632	0.33	1.5	4.2	
···	11:48:12.4	11:24:03	569	0.33	0.7	3.5	
A1390	11:49:07.6	12:12:18	434	0.42	5.4	3.7	
···	11:49:00.4	12:20:04	575	0.33	0.9	6.6	
···	11:49:15.5	12:21:01	441	0.23	0.9	3.4	
A1400	11:51:11.7	55:09:04	205	0.20	2.0	3.4	C
···	11:51:11.8	55:04:18	170	0.18	1.1	4.7	
···	11:50:38.7	55:04:03	427	0.35	6.2	3.9	
A1412	11:56:18.6	73:25:38	214	2.42	6.3	21.0	C
···	11:55:41.2	73:39:27	669	0.31	5.1	3.8	
A1424	11:57:26.7	05:07:12	312	1.30	6.6	12.7	C
···	11:57:05.3	04:59:10	465	0.96	2.9	15.1	
···	11:56:47.3	05:02:21	695	0.54	2.3	9.9	
A1436	12:00:22.7	56:13:53	96	1.20	12.3	11.4	C
···	11:58:58.9	56:17:20	753	0.35	2.2	4.7	
···	12:01:51.7	56:10:10	762	0.26	2.6	3.1	
···	11:59:41.0	56:03:39	802	1.49	3.5	18.0	
A1452	12:03:08.2	51:44:01	285	0.26	3.3	3.1	
···	12:03:12.4	51:39:51	363	0.27	2.6	6.0	
···	12:03:36.7	51:30:24	834	1.04	3.5	10.6	
A1468	12:05:36.4	51:29:55	277	0.47	19.2	4.5	C
···	12:05:00.2	51:26:43	365	0.30	5.6	3.0	
···	12:05:27.0	51:21:21	258	0.30	5.1	3.4	
A1474	12:07:55.7	14:54:25	175	0.08	2.1	3.7	C?
···	12:08:12.0	14:58:27	226	0.30	2.8	5.4	C?
···	12:07:59.3	15:06:11	533	0.42	5.8	5.3	
···	12:08:02.2	14:48:11	552	0.21	2.5	3.5	

Table 2—Continued

Abell	$RA(2000)_X$	$DEC(2000)_X$	Offset (arcsec)	Peak Flux (10^{-4} c/sec/pix)	$\frac{F_{250}}{F_{62.5}}$	$(\frac{C}{\sqrt{B}})_{250}^{max}$	Note
A1480	12:10:49.1	30:50:05	98	0.18	2.9	3.2	
···	12:10:32.8	30:58:18	443	0.34	2.5	3.6	
···	12:11:23.9	30:48:31	539	0.44	5.2	5.6	
···	12:09:56.1	30:46:32	680	0.32	9.5	5.4	
···	12:11:01.2	30:39:41	732	0.23	3.3	6.6	
A1500	12:11:35.5	74:15:56	703	0.42	2.8	4.6	
···	12:10:47.9	74:26:12	756	0.28	5.8	3.0	
···	12:16:30.1	74:31:29	807	0.33	2.0	3.6	
A1507	12:15:03.8	59:53:41	447	0.68	16.7	8.1	C
A1526	12:22:08.9	13:44:19	10	1.03	2.9	9.7	C
···	12:22:21.3	13:49:03	339	0.64	3.6	8.0	
···	12:22:07.8	13:37:59	383	0.57	2.4	8.2	
···	12:22:36.6	13:42:24	429	0.79	4.7	9.3	
···	12:21:50.9	13:53:12	587	0.49	2.9	9.7	
···	12:22:31.7	13:36:15	595	0.61	0.8	10.0	
···	12:21:47.2	13:33:56	697	0.72	1.9	15.4	
A1534	12:24:32.9	61:29:47	214	0.21	3.0	6.3	C
···	12:23:30.5	61:24:02	447	0.12	2.6	6.3	
···	12:24:57.3	61:36:41	540	0.27	5.3	3.6	
A1541	12:27:27.5	08:49:30	56	15.98	8.7	16.4	C
···	12:27:03.0	08:47:33	389	0.71	1.8	5.6	
···	12:27:56.1	08:50:27	439	0.65	4.5	4.5	
···	12:27:46.7	08:41:30	613	2.55	4.5	23.3	
A1552	12:29:34.1	11:46:24	262	1.74	10.0	5.8	C?
···	12:30:01.7	11:48:20	290	2.39	3.8	7.0	C?
···	12:30:03.7	11:42:58	220	1.51	2.3	5.6	
···	12:30:20.4	11:41:15	486	2.01	8.2	5.6	
···	12:29:09.2	11:42:33	609	2.26	2.6	8.5	
···	12:29:26.8	11:53:31	643	1.76	11.9	9.0	
A1564	12:34:52.9	01:46:50	229	0.42	4.4	4.5	C
···	12:34:23.9	01:52:05	511	0.36	1.5	5.3	
···	12:35:30.9	01:45:35	582	0.59	4.3	5.6	

Table 2—Continued

Abell	RA(2000)$_X$	DEC(2000)$_X$	Offset (arcsec)	Peak Flux (10^{-4} c/sec/pix)	$\frac{F_{250}}{F_{62.5}}$	$(\frac{C}{\sqrt{B}})^{max}_{250}$	Note
···	12:35:26.9	01:57:05	594	0.29	2.4	3.7	
A1569	12:36:23.6	16:31:37	243	1.83	10.3	9.1	C
···	12:36:32.6	16:40:38	368	0.51	0.9	5.3	
···	12:36:44.7	16:33:39	390	1.33	2.3	7.8	
···	12:35:56.4	16:30:17	449	1.27	2.7	5.8	
···	12:35:47.6	16:36:40	452	0.77	5.6	3.4	
A1589	12:41:17.3	18:33:54	280	3.16	10.7	27.5	C
···	12:42:10.0	18:39:28	540	0.40	2.5	5.4	
A1616	12:47:16.1	55:00:02	247	0.77	6.0	8.7	C
···	12:48:08.6	55:03:33	266	0.30	3.6	4.1	
···	12:47:39.0	54:54:50	468	0.52	2.9	8.6	
···	12:46:34.9	55:06:00	581	0.87	5.5	9.5	
A1630	12:51:46.2	04:35:49	129	0.84	3.7	4.5	C
···	12:51:26.9	04:47:18	857	1.22	3.5	7.5	
A1631	12:52:51.5	–15:25:39	45	0.59	5.1	7.6	C
···	12:51:32.7	–15:28:49	1125	0.21	2.2	4.4	
A1638	12:54:27.2	18:56:35	266	0.35	6.3	5.0	C
···	12:54:39.4	19:05:34	349	0.37	6.8	4.7	
···	12:55:21.9	19:03:43	635	0.28	2.1	4.3	
A1644	12:57:10.2	–17:24:03	181	5.07	9.6	86.6	C
···	12:57:52.9	–17:17:26	591	2.43	6.1	30.8	
A1650	12:58:41.3	–01:45:51	84	14.88	7.0	87.6	C
A1651	12:59:21.9	–04:11:52	44	15.20	7.6	95.2	C
···	12:59:41.6	–04:04:03	511	0.26	0.9	5.4	
···	13:00:00.4	–04:09:02	575	1.04	4.4	5.4	
A1656	12:59:45.4	27:55:37	198	13.75	9.8	368.6	C
A1668	13:03:44.5	19:16:28	103	4.59	8.4	52.3	C
···	13:04:07.4	19:03:40	769	0.56	5.5	7.2	
A1691	13:11:07.1	39:13:09	198	2.54	8.5	28.2	C
···	13:10:44.6	39:20:23	670	0.48	5.9	4.9	
···	13:12:23.9	39:18:02	791	0.40	2.8	5.0	
A1749	13:29:22.8	37:37:05	116	0.58	3.0	7.1	C

Table 2—Continued

Abell	RA(2000)$_X$	DEC(2000)$_X$	Offset (arcsec)	Peak Flux (10^{-4} c/sec/pix)	$\frac{\mathrm{F}_{250}}{\mathrm{F}_{62.5}}$	$(\frac{\mathrm{C}}{\sqrt{\mathrm{B}}})^{\mathrm{max}}_{250}$	Note
· · ·	13:28:53.7	37:28:11	724	0.26	1.2	4.3	
A1750	13:30:50.1	–01:51:50	91	4.01	8.5	31.1	C
· · ·	13:30:24.1	–01:51:34	431	0.58	1.3	7.3	
· · ·	13:31:06.1	–01:42:18	529	1.48	5.4	11.6	
· · ·	13:31:24.7	–01:46:49	530	1.11	3.9	11.1	
· · ·	13:31:05.8	–01:59:10	560	0.72	2.9	6.4	
A1767	13:36:05.7	59:12:15	50	4.83	7.6	98.6	C
· · ·	13:34:46.2	59:10:39	582	0.43	5.3	7.0	
A1773	13:42:06.3	02:13:15	104	2.18	14.0	16.5	C
· · ·	13:42:18.5	02:17:27	213	1.83	6.5	11.9	
· · ·	13:42:26.2	02:09:07	436	0.66	1.9	8.0	
· · ·	13:41:50.1	02:06:38	567	0.75	3.2	5.9	
· · ·	13:42:48.9	02:08:21	721	0.64	2.4	5.0	
A1775	13:41:53.4	26:22:38	54	7.43	8.0	71.3	C
· · ·	13:42:33.4	26:18:14	554	0.55	3.4	5.1	
A1780	13:44:35.7	02:52:03	67	0.85	4.3	8.4	C
· · ·	13:44:48.7	02:56:55	285	0.52	3.3	5.5	
· · ·	13:44:55.1	02:49:05	345	0.58	1.3	4.4	
· · ·	13:44:10.3	02:49:26	468	0.39	1.8	3.0	
· · ·	13:44:14.7	02:58:08	468	0.50	0.7	11.7	
· · ·	13:44:53.4	02:42:01	696	0.86	3.0	10.1	
· · ·	13:44:28.2	03:04:18	696	0.57	2.4	7.5	
· · ·	13:43:54.0	02:56:55	702	0.79	3.8	5.1	
· · ·	13:45:02.0	03:03:30	726	0.47	2.1	4.9	
A1781	13:44:22.2	29:54:49	247	0.30	6.5	3.3	C
· · ·	13:44:09.9	29:49:31	262	0.38	2.3	4.6	
· · ·	13:44:56.4	29:44:10	543	0.98	3.6	8.8	
· · ·	13:45:23.0	29:43:01	851	0.17	0.6	6.6	
A1783	13:43:23.4	55:37:34	99	0.52	5.2	7.7	C
· · ·	13:43:30.3	55:47:43	711	0.41	6.5	4.7	
· · ·	13:41:45.6	55:38:36	827	0.22	2.6	4.5	
A1793	13:48:08.2	32:17:55	165	0.40	6.2	5.6	C

Table 2—Continued

Abell	$\mathrm{RA}(2000)_X$	$\mathrm{DEC}(2000)_X$	Offset (arcsec)	Peak Flux (10^{-4} c/sec/pix)	$\frac{\mathrm{F}_{250}}{\mathrm{F}_{62.5}}$	$(\frac{\mathrm{C}}{\sqrt{\mathrm{B}}})^{\mathrm{max}}_{250}$	Note
···	13:48:32.9	32:21:47	322	0.51	4.4	4.5	
···	13:48:43.9	32:14:00	348	0.27	1.7	3.7	
···	13:47:53.6	32:24:53	580	0.70	1.8	7.1	
A1795	13:48:52.7	26:35:44	111	34.79	5.5	372.4	C
A1800	13:49:21.8	28:06:14	288	4.98	7.3	43.5	C
···	13:49:58.5	27:54:52	600	0.89	2.5	8.5	
···	13:49:58.8	28:13:31	609	0.30	2.3	4.3	
A1809	13:52:58.8	05:09:41	300	3.10	13.7	32.0	C
···	13:53:37.5	05:05:38	354	0.34	14.0	6.0	
···	13:53:32.3	05:15:16	413	1.01	5.1	9.7	
A1825	13:58:04.3	20:38:17	119	0.94	7.3	7.1	C
···	13:58:01.1	20:50:32	669	0.30	8.4	3.1	
···	13:57:08.7	20:47:47	847	0.54	2.1	6.3	
A1827	13:58:33.5	21:48:02	427	0.43	3.2	4.2	
A1828	13:58:45.5	18:25:20	342	0.33	3.6	3.0	
A1831	13:59:15.7	27:58:40	87	5.48	6.7	53.4	C
A1836	14:01:54.4	–11:36:50	205	0.29	2.7	5.4	
A1837	14:01:37.3	–11:07:46	166	3.66	5.9	24.9	C
···	14:02:12.9	–11:17:34	625	0.31	3.7	4.9	
A1873	14:11:34.7	28:10:17	151	0.48	11.9	5.7	C
···	14:11:43.8	28:14:09	313	0.56	1.6	5.8	
A1890	14:17:28.8	08:08:02	205	1.04	4.4	14.2	C
···	14:16:48.9	08:10:27	674	0.59	1.8	8.8	
···	14:18:01.2	08:22:39	797	0.44	5.2	6.6	
A1898	14:20:35.4	25:07:42	99	0.53	3.5	5.5	C
···	14:20:48.2	25:14:17	358	0.49	5.4	4.5	
···	14:20:13.7	25:18:28	614	0.62	5.9	4.4	
···	14:20:44.4	24:58:35	659	0.63	4.3	8.4	
A1899	14:21:38.6	17:45:13	339	0.53	5.2	4.2	C
···	14:21:10.7	17:41:19	156	0.67	4.0	5.6	
···	14:20:41.9	17:47:08	664	0.32	3.2	3.2	
A1904	14:22:15.4	48:30:47	172	1.01	16.6	12.3	C

Table 2—Continued

Abell	RA(2000)$_X$	DEC(2000)$_X$	Offset (arcsec)	Peak Flux (10^{-4} c/sec/pix)	$\frac{F_{250}}{F_{62.5}}$	$(\frac{C}{\sqrt{B}})_{250}^{max}$	Note
A1913	14:26:34.4	16:39:41	254	0.86	3.7	5.2	C
···	14:26:38.2	16:47:40	469	0.62	2.6	5.3	
···	14:27:30.2	16:49:48	781	1.06	8.0	5.5	
···	14:26:09.4	16:32:12	789	1.15	5.0	9.5	
···	14:27:58.8	16:36:42	992	0.70	2.4	6.1	
···	14:26:36.7	16:23:22	1054	1.10	2.6	8.2	
···	14:27:40.3	16:54:35	1092	1.56	6.8	12.6	
···	14:25:52.7	16:29:01	1096	1.16	2.0	7.7	
A1927	14:31:08.0	25:38:11	123	5.41	4.6	74.8	C
···	14:30:21.9	25:47:24	711	0.53	1.4	10.1	
···	14:31:02.7	25:51:47	722	0.46	3.6	7.2	
···	14:32:01.5	25:42:47	824	0.45	2.8	5.3	
A1939	14:37:28.1	24:46:58	264	0.67	2.7	6.7	C?
···	14:37:09.6	24:45:28	280	0.49	2.5	6.4	C?
···	14:37:45.6	24:52:03	444	0.61	3.1	6.3	
···	14:36:40.6	24:50:47	460	0.77	2.2	11.9	
A1983	14:52:59.2	16:42:10	269	2.69	4.7	31.3	C
A1991	14:54:31.8	18:38:47	61	6.47	3.5	48.7	C
···	14:54:25.0	18:30:22	455	1.16	1.7	11.5	
···	14:54:56.7	18:24:47	870	0.34	7.7	3.2	
A2004	14:58:27.3	24:54:59	134	1.09	6.1	7.7	C
···	14:58:15.8	24:53:08	324	1.00	4.4	5.1	
A2018	15:01:03.9	47:16:59	97	1.50	9.1	19.6	C
A2019	15:03:24.8	27:09:27	384	0.84	5.2	7.0	C
···	15:03:07.7	27:14:55	259	0.41	2.8	4.3	
···	15:02:41.1	27:05:07	428	0.33	1.3	4.8	
A2020	15:03:46.0	08:04:25	546	0.66	3.3	3.9	
···	15:04:36.0	07:47:58	877	0.99	13.5	6.7	
···	15:02:37.2	07:56:47	1011	0.77	6.2	4.6	
A2022	15:04:17.9	28:28:58	218	1.20	19.2	14.3	C
···	15:03:21.0	28:29:40	815	0.20	2.5	3.8	
A2026	15:08:25.4	–00:16:03	129	1.05	4.9	5.4	C

Table 2—Continued

Abell	RA(2000)$_X$	DEC(2000)$_X$	Offset (arcsec)	Peak Flux (10^{-4} c/sec/pix)	$\frac{F_{250}}{F_{62.5}}$	$(\frac{C}{\sqrt{B}})^{max}_{250}$	Note
· · ·	15:08:49.4	–00:11:03	397	0.90	2.0	6.5	
A2028	15:09:35.7	07:33:29	118	1.62	4.4	8.0	M
· · ·	15:09:19.9	07:37:60	430	1.68	3.1	7.1	M
A2029	15:10:55.9	05:44:34	80	38.07	6.7	214.4	C
· · ·	15:11:32.0	05:45:46	497	2.38	4.1	12.3	
A2033	15:11:27.4	06:20:41	64	5.36	8.5	30.1	C
· · ·	15:12:01.8	06:16:05	605	0.61	6.4	3.2	
A2040	15:12:50.7	07:25:54	83	1.34	4.2	8.6	C
A2052	15:16:44.4	07:01:21	82	13.60	3.6	133.8	C
A2055	15:18:44.7	06:13:52	107	6.41	2.9	42.5	
· · ·	15:19:33.8	06:19:30	837	0.96	5.5	4.1	
· · ·	15:19:30.8	06:01:23	929	0.96	1.7	5.9	
A2056	15:19:13.9	28:22:20	371	0.53	13.9	5.7	C
· · ·	15:19:55.5	28:10:47	656	0.34	4.9	6.4	
A2063	15:23:06.7	08:36:31	133	7.92	6.1	178.7	C
· · ·	15:21:55.0	08:28:24	1157	1.52	5.1	30.2	
· · ·	15:22:39.2	09:01:01	1400	0.90	6.9	19.6	
A2065	15:22:26.5	27:42:45	216	8.13	8.0	72.5	C
· · ·	15:21:52.3	27:36:32	783	0.90	2.9	7.9	
A2067	15:23:07.3	30:52:13	161	1.07	6.1	13.1	C
· · ·	15:23:07.8	30:59:25	315	0.56	8.7	6.0	
· · ·	15:22:37.4	31:00:22	599	0.14	0.3	6.4	
· · ·	15:24:09.2	30:55:10	703	0.30	1.9	4.4	
A2079	15:27:52.7	28:57:00	304	0.76	5.3	8.7	C
· · ·	15:28:22.6	28:52:27	236	0.47	2.5	6.4	
· · ·	15:27:47.1	28:47:18	396	0.34	1.0	3.9	
· · ·	15:27:32.2	28:52:36	426	0.76	3.2	6.1	
· · ·	15:28:22.7	28:44:32	542	0.44	1.6	5.5	
· · ·	15:27:50.4	29:02:36	625	0.97	10.1	8.0	
· · ·	15:27:33.6	28:41:41	775	0.34	1.5	6.9	
A2089	15:32:28.3	27:58:46	215	0.74	3.2	4.3	
· · ·	15:32:57.6	28:09:18	547	0.47	7.8	3.9	

Table 2—Continued

Abell	RA(2000)$_X$	DEC(2000)$_X$	Offset (arcsec)	Peak Flux (10^{-4} c/sec/pix)	$\frac{F_{250}}{F_{62.5}}$	$(\frac{C}{\sqrt{B}})^{max}_{250}$	Note
A2092	15:33:23.5	31:08:51	54	1.61	7.4	19.9	C
· · ·	15:32:29.4	31:11:09	654	0.70	3.2	7.7	
A2107	15:39:38.6	21:46:40	131	4.57	5.5	41.6	C
A2122	15:45:02.2	36:06:58	402	4.19	3.9	31.4	M
· · ·	15:44:06.7	36:12:47	412	1.17	7.5	10.5	M
· · ·	15:45:00.6	35:57:19	726	0.97	3.2	10.7	
A2124	15:45:03.1	36:07:02	208	4.10	4.1	29.5	M
· · ·	15:44:06.5	36:12:44	839	1.15	7.0	9.5	M
· · ·	15:44:59.9	35:57:12	388	0.94	3.1	10.6	
A2142	15:58:21.7	27:13:25	75	28.23	8.4	232.6	C
A2147	16:02:18.2	15:57:38	235	2.62	11.4	50.9	C
· · ·	16:03:37.6	15:53:54	1161	3.14	2.6	51.6	
A2148	16:03:13.0	25:26:21	110	0.54	6.0	12.2	C
· · ·	16:02:48.2	25:20:17	605	1.51	2.2	44.1	
A2149	16:01:24.0	53:54:22	159	1.65	7.3	35.6	C
· · ·	16:02:53.9	53:52:34	671	0.24	5.5	4.8	
· · ·	16:00:26.3	53:48:13	690	0.43	2.8	9.2	
A2151	16:04:39.5	17:43:21	515	3.68	4.7	49.2	C
· · ·	16:06:40.4	17:46:41	1226	0.44	2.3	7.3	
A2152	16:05:34.3	16:26:04	179	1.00	5.1	12.3	C
A2162	16:12:35.6	29:27:46	286	0.33	3.8	8.6	C
· · ·	16:11:18.5	29:18:24	1255	0.10	1.3	6.1	
A2168	16:14:10.1	54:04:52	635	0.27	1.4	5.7	
· · ·	16:11:35.1	54:16:35	898	0.73	2.6	12.2	
A2169	16:13:41.2	49:07:34	249	0.66	4.3	5.6	C
· · ·	16:14:13.4	49:12:19	295	0.61	6.1	9.9	
· · ·	16:15:27.3	49:08:28	794	0.31	3.0	4.4	
A2184	16:21:04.2	50:09:35	143	0.56	3.5	6.4	C
· · ·	16:21:01.6	50:00:34	684	0.46	6.3	4.6	
· · ·	16:20:55.3	50:27:48	953	1.31	3.0	13.9	
A2197	16:27:40.5	40:54:55	340	0.80	2.7	20.6	C
· · ·	16:29:41.4	40:50:06	1064	0.59	6.1	14.3	

Table 2—Continued

Abell	RA(2000)$_X$	DEC(2000)$_X$	Offset (arcsec)	Peak Flux (10^{-4} c/sec/pix)	$\frac{F_{250}}{F_{62.5}}$	$(\frac{C}{\sqrt{B}})^{max}_{250}$	Note
···	16:30:07.5	40:36:41	1704	0.20	3.5	5.8	
A2199	16:28:37.7	39:32:55	88	19.03	4.0	514.6	C
A2205	16:32:40.2	12:53:40	139	0.93	0.7	6.4	
···	16:32:18.5	12:50:17	239	0.58	0.9	3.4	
···	16:32:12.5	12:54:18	293	0.73	0.1	6.7	
A2241	16:59:42.8	32:36:58	264	3.56	4.7	54.0	C
···	16:59:01.5	32:36:57	559	0.45	1.2	14.5	
···	16:58:59.1	32:28:39	575	0.38	5.7	6.7	
···	17:00:31.7	32:35:34	672	0.14	3.0	4.1	
A2245	17:02:33.7	33:30:20	164	1.70	6.5	18.5	C
···	17:03:13.7	33:27:15	453	0.48	3.4	5.7	
···	17:02:40.6	33:42:12	625	0.44	5.9	5.9	
A2248	16:57:20.7	77:03:06	175	0.48	3.8	7.9	C
···	16:56:15.3	76:50:44	669	0.34	2.6	7.2	
A2249	17:09:47.2	34:26:49	60	3.56	9.4	40.7	C
A2250	17:11:01.9	39:41:36	189	2.07	9.1	27.6	C
···	17:10:36.6	39:50:56	582	0.43	2.7	9.6	
A2253	17:15:03.5	38:37:33	130	0.33	4.5	3.7	C?
···	17:15:06.9	38:44:33	293	0.36	2.7	4.3	C?
···	17:15:32.8	38:39:07	325	0.35	4.9	4.0	C?
···	17:14:38.5	38:36:04	383	0.46	3.9	5.4	
···	17:15:54.6	38:40:25	579	0.46	2.0	5.4	
A2255	17:12:53.3	64:03:55	176	4.45	10.3	141.9	C
A2256	17:04:11.2	78:38:35	280	10.78	12.0	250.2	C
A2271	17:18:12.6	78:01:14	173	1.51	6.7	24.6	C
···	17:21:04.6	78:09:49	881	0.58	2.8	10.5	
A2293	18:02:12.0	57:41:49	486	1.39	4.3	25.6	C
A2295	18:00:28.1	69:13:42	177	3.30	9.5	38.3	C
A2304	18:20:11.4	68:57:17	225	1.53	12.1	38.3	C
A2308	18:34:22.7	70:58:06	313	1.39	6.7	37.3	C
A2311	18:50:12.8	70:22:13	152	0.68	8.2	19.0	C
···	18:49:28.9	70:25:43	199	0.58	7.0	12.9	

Table 2—Continued

Abell	RA(2000)$_X$	DEC(2000)$_X$	Offset (arcsec)	Peak Flux (10^{-4} c/sec/pix)	$\frac{F_{250}}{F_{62.5}}$	$(\frac{C}{\sqrt{B}})^{max}_{250}$	Note
· · ·	18:51:06.8	70:28:15	539	0.60	14.8	20.4	
A2331	20:58:02.8	–07:46:60	149	1.97	3.4	16.5	C
· · ·	20:58:20.6	–07:42:46	218	0.91	3.2	9.5	
· · ·	20:57:39.8	–07:40:25	542	0.51	2.0	9.7	
· · ·	20:58:10.8	–07:57:15	714	0.36	1.9	4.0	
A2361	21:39:00.6	–14:20:20	117	0.20	0.7	5.5	C?
· · ·	21:39:25.6	–14:18:26	266	0.44	4.7	5.3	C?
· · ·	21:39:29.2	–14:23:60	416	0.48	2.6	5.8	
· · ·	21:39:13.6	–14:27:02	465	0.41	3.7	8.7	
· · ·	21:38:35.1	–14:23:02	521	0.30	4.9	5.2	
A2366	21:42:45.9	–06:49:23	184	0.47	6.6	7.3	C
· · ·	21:43:10.1	–07:02:20	673	0.36	4.3	3.7	
· · ·	21:42:34.8	–07:05:06	804	0.37	1.2	8.0	
· · ·	21:42:31.0	–06:36:07	1010	0.57	1.6	7.2	
A2372	21:45:14.6	–19:59:55	113	0.79	5.3	10.3	C
· · ·	21:44:46.3	–19:51:24	598	0.42	4.7	5.0	
· · ·	21:45:44.2	–19:45:17	860	0.40	2.6	9.9	
· · ·	21:46:05.2	–20:07:59	895	0.27	2.3	9.6	
· · ·	21:44:11.0	–19:56:54	939	0.79	3.3	15.4	
A2377	21:45:56.0	–10:05:54	229	4.44	4.8	30.7	C
· · ·	21:46:18.6	–09:57:26	411	0.55	2.4	6.8	
· · ·	21:46:32.7	–10:01:34	507	0.68	1.0	10.3	
· · ·	21:45:30.6	–10:08:55	578	0.97	5.9	8.0	
· · ·	21:46:32.2	–10:07:17	587	0.76	6.8	5.3	
A2378	21:47:18.6	–19:58:46	27	0.41	4.5	3.9	C
· · ·	21:47:12.4	–19:53:27	345	0.47	24.7	3.8	
· · ·	21:47:48.7	–19:58:25	445	1.09	1.5	13.2	
· · ·	21:47:45.7	–20:05:25	552	0.32	2.8	4.4	
A2382	21:51:53.2	–15:42:45	264	1.45	6.7	9.7	C
· · ·	21:52:17.8	–15:43:24	356	1.07	5.8	6.9	
· · ·	21:52:18.7	–15:49:21	674	0.61	2.0	7.4	
· · ·	21:52:43.3	–15:44:58	701	0.70	3.9	7.3	

Table 2—Continued

Abell	RA(2000)$_X$	DEC(2000)$_X$	Offset (arcsec)	Peak Flux (10^{-4} c/sec/pix)	$\frac{F_{250}}{F_{62.5}}$	$(\frac{C}{\sqrt{B}})^{max}_{250}$	Note
A2388	21:53:29.3	08:14:32	83	1.08	5.9	13.6	C
···	21:53:00.8	08:19:56	610	0.29	2.1	7.3	
···	21:53:17.1	08:01:44	791	0.29	7.1	4.9	
···	21:54:05.2	08:00:52	919	0.37	1.3	7.1	
···	21:54:23.8	08:23:48	930	0.52	3.7	8.7	
A2399	21:57:26.9	–07:47:26	84	0.98	7.1	8.7	C
···	21:57:49.1	–07:53:33	430	1.11	2.6	14.5	
···	21:56:58.5	–07:48:41	509	1.20	2.6	11.5	
···	21:58:28.4	–07:50:03	843	0.26	4.5	4.4	
A2400	21:57:42.2	–11:23:47	94	1.12	6.6	6.9	C
···	21:58:11.8	–11:20:02	402	0.80	7.0	5.3	
···	21:58:04.7	–11:29:02	465	0.73	8.5	5.2	
···	21:57:22.8	–11:29:17	530	0.57	0.8	7.2	
A2401	21:58:18.8	–20:06:22	473	1.62	8.1	14.7	C
···	21:58:51.9	–20:06:41	64	0.54	3.4	4.9	
···	21:58:37.7	–19:56:49	567	0.33	3.3	4.9	
···	21:58:07.1	–19:59:46	727	0.91	3.3	9.2	
A2402	21:58:31.0	–09:48:16	203	4.40	6.8	25.0	C
···	21:59:08.1	–09:47:42	440	0.77	1.4	6.0	
···	21:58:20.9	–09:56:31	709	0.33	2.3	3.6	
A2410	22:02:21.3	–09:49:36	351	1.32	8.2	10.3	C
···	22:01:51.2	–09:56:19	248	1.05	3.5	7.5	
···	22:01:25.5	–09:54:20	565	0.95	4.9	5.5	
···	22:01:34.0	–09:45:23	655	0.74	1.6	7.6	
···	22:02:40.4	–09:45:32	725	1.14	3.4	8.8	
A2412	22:03:58.5	–21:30:36	302	1.16	4.5	7.8	C
···	22:04:21.7	–21:23:56	215	0.55	2.0	5.5	
···	22:03:21.9	–21:32:20	767	0.79	35.2	4.4	
A2415	22:05:40.6	–05:35:30	234	5.26	8.9	40.4	C
···	22:04:59.2	–05:31:04	463	0.98	2.6	9.5	
···	22:05:31.3	–05:50:39	920	0.91	4.2	11.5	
A2420	22:10:20.3	–12:10:19	63	6.35	11.6	45.2	C

Table 2—Continued

Abell	RA(2000)$_X$	DEC(2000)$_X$	Offset (arcsec)	Peak Flux (10^{-4} c/sec/pix)	$\frac{F_{250}}{F_{62.5}}$	$(\frac{C}{\sqrt{B}})^{max}_{250}$	Note
···	22:11:03.1	–12:13:00	604	0.67	2.4	4.1	
···	22:10:42.8	–12:20:33	634	0.46	3.9	4.6	
A2428	22:16:15.5	–09:20:29	34	8.24	5.9	44.8	C
A2448	22:31:25.5	–08:24:53	285	0.67	3.8	8.1	C
···	22:31:35.9	–08:18:32	495	0.69	3.5	8.2	
···	22:32:17.4	–08:30:22	552	0.36	6.1	7.4	
A2457	22:35:40.6	01:28:32	68	3.69	8.1	24.0	C
···	22:36:16.8	01:33:37	564	0.62	3.0	6.5	
···	22:35:40.0	01:39:30	661	2.29	2.3	17.9	
···	22:35:00.6	01:31:58	699	0.68	4.9	4.5	
A2459	22:36:26.8	–15:34:24	322	0.82	2.5	6.5	C?
···	22:36:58.1	–15:31:16	596	0.98	4.9	4.1	C?
···	22:36:14.4	–15:43:48	392	0.71	0.5	7.9	
···	22:36:44.5	–15:45:47	408	1.43	2.3	13.3	
···	22:35:46.3	–15:38:05	702	1.25	3.9	6.9	
A2462	22:39:14.0	–17:19:59	152	1.69	4.0	7.5	C
···	22:38:34.2	–17:27:30	576	1.10	12.4	5.4	
···	22:38:34.1	–17:12:15	704	0.96	1.3	6.6	
···	22:40:00.1	–17:22:56	793	0.97	2.2	5.1	
···	22:39:45.5	–17:30:57	816	0.90	1.5	6.0	
A2492	22:50:24.7	–19:15:21	61	0.65	0.8	11.5	C
···	22:50:29.0	–19:09:17	349	0.67	2.0	8.5	
···	22:50:09.4	–19:19:02	363	0.36	1.0	7.9	
···	22:49:47.3	–19:18:29	623	0.48	1.5	7.4	
···	22:49:51.8	–19:07:36	693	0.96	2.1	5.0	
···	22:50:21.1	–19:29:21	862	0.84	4.8	7.7	
A2495	22:50:20.3	10:54:19	58	7.12	7.7	68.9	C
···	22:49:38.9	10:59:46	750	4.05	3.1	39.7	
···	22:49:50.1	10:44:33	750	0.47	2.6	4.9	
A2511	22:58:49.5	–07:35:19	118	0.38	2.1	4.3	C
···	22:59:05.7	–07:36:59	171	0.49	1.4	5.6	
···	22:58:51.2	–07:40:39	228	0.57	3.9	3.7	

Table 2—Continued

Abell	RA(2000)$_X$	DEC(2000)$_X$	Offset (arcsec)	Peak Flux (10^{-4} c/sec/pix)	$\frac{F_{250}}{F_{62.5}}$	$(\frac{C}{\sqrt{B}})^{max}_{250}$	Note
···	22:58:25.3	–07:37:04	429	0.46	1.2	5.7	
···	22:58:40.5	–07:27:48	584	0.23	3.5	5.6	
···	22:58:28.7	–07:46:22	682	0.40	1.1	5.8	
···	22:58:06.6	–07:33:57	730	0.57	1.5	9.5	
A2524	23:03:09.8	17:43:12	59	0.83	2.4	8.2	M
···	23:02:54.6	17:45:22	236	1.05	3.8	8.7	M
···	23:03:05.6	17:48:32	270	0.75	6.5	8.1	
···	23:02:58.3	17:36:02	518	0.21	0.9	4.2	
···	23:02:36.2	17:40:17	542	0.31	0.6	5.4	
···	23:02:21.5	17:45:02	701	0.25	12.0	3.9	
A2525	23:03:19.0	–10:35:41	268	0.51	0.8	5.9	
···	23:04:04.4	–10:44:33	711	0.92	2.5	8.7	
A2538	23:08:42.4	–19:52:03	60	1.05	1.5	12.9	C
···	23:08:54.8	–19:54:32	244	1.12	3.0	9.9	
···	23:09:10.4	–20:01:22	679	1.07	1.1	10.3	
···	23:07:51.2	–19:57:57	746	0.75	3.3	8.0	
A2556	23:13:01.1	–21:37:57	34	11.81	4.7	51.8	C
···	23:13:38.0	–21:32:05	589	1.93	3.7	9.8	
···	23:13:44.1	–21:42:06	628	0.92	3.8	6.6	
A2559	23:13:05.6	–13:38:02	219	0.47	5.3	8.6	C
···	23:13:17.7	–13:42:09	157	0.39	2.4	5.7	
···	23:13:11.5	–13:45:37	245	0.50	1.3	11.8	
···	23:12:50.2	–13:46:47	395	0.43	2.6	5.7	
···	23:12:30.7	–13:43:46	546	0.55	3.3	5.9	
···	23:12:55.7	–13:29:56	723	0.52	3.9	5.7	
A2566	23:16:09.1	–20:27:12	325	9.46	8.0	32.8	C
···	23:15:37.1	–20:22:18	276	0.51	0.9	5.6	
···	23:15:31.3	–20:29:40	553	1.03	1.2	7.5	
···	23:15:51.5	–20:33:30	657	0.03	0.2	9.8	
···	23:15:13.0	–20:27:47	687	1.29	2.3	5.8	
A2572	23:18:30.5	18:42:55	133	2.50	6.5	31.3	C
···	23:17:12.4	18:42:07	1020	2.39	4.8	36.8	

Table 2—Continued

Abell	$\mathrm{RA(2000)}_X$	$\mathrm{DEC(2000)}_X$	Offset (arcsec)	Peak Flux (10^{-4} c/sec/pix)	$\frac{\mathrm{F}_{250}}{\mathrm{F}_{62.5}}$	$(\frac{\mathrm{C}}{\sqrt{\mathrm{B}}})^{\mathrm{max}}_{250}$	Note
A2593	23:24:23.2	14:39:35	130	2.70	13.6	17.0	C
· · ·	23:24:17.8	14:30:56	492	0.78	7.4	4.5	
· · ·	23:23:30.2	14:23:27	1262	0.47	4.7	3.5	
A2597	23:25:19.4	–12:07:38	71	20.13	6.5	143.1	C
A2618	23:33:16.8	22:55:49	521	2.06	8.8	17.8	C?
· · ·	23:34:06.6	22:57:31	312	1.00	4.8	8.5	C?
· · ·	23:34:34.7	23:00:37	640	0.30	3.2	3.5	
· · ·	23:33:36.1	23:13:09	772	0.48	2.4	6.1	
A2622	23:34:59.2	27:22:15	213	2.77	7.1	45.7	C
· · ·	23:34:55.5	27:35:24	589	0.30	3.2	8.9	
A2625	23:36:05.6	20:31:39	189	1.45	7.2	16.5	C
· · ·	23:36:55.0	20:30:58	506	0.28	2.2	6.8	
· · ·	23:36:19.9	20:21:25	612	0.33	1.4	4.7	
· · ·	23:36:56.7	20:25:46	635	0.22	1.4	7.8	
· · ·	23:36:56.0	20:39:48	715	0.44	2.4	10.0	
· · ·	23:36:03.9	20:46:05	894	0.24	3.0	5.1	
· · ·	23:35:33.7	20:20:20	930	0.36	0.7	13.0	
A2626	23:36:31.1	21:08:57	39	5.84	4.6	95.2	C
· · ·	23:35:45.9	21:20:42	916	0.36	3.0	6.8	
A2630	23:36:51.7	15:49:05	579	0.38	0.9	26.5	
· · ·	23:38:15.0	15:45:37	669	0.19	0.7	13.6	
A2634	23:38:23.4	27:00:15	106	1.74	9.0	37.9	C
A2637	23:38:56.6	21:24:53	222	6.89	2.9	72.5	C
· · ·	23:38:17.6	21:24:02	726	0.31	2.3	5.5	
· · ·	23:38:34.2	21:17:06	782	0.31	1.8	5.0	
A2644	23:41:06.1	00:04:45	76	0.39	5.2	4.3	C
· · ·	23:41:18.1	–00:02:44	519	0.44	2.6	4.6	
· · ·	23:41:07.1	00:18:45	788	2.92	2.8	24.5	
A2656	23:44:53.5	–04:00:57	324	0.48	4.2	4.1	
· · ·	23:45:14.6	–03:58:26	581	0.42	1.2	5.6	
· · ·	23:45:21.8	–04:13:41	626	0.25	1.0	4.7	
A2660	23:45:18.3	–25:47:43	637	0.49	2.5	5.3	C

Table 2—Continued

Abell	RA(2000)$_X$	DEC(2000)$_X$	Offset (arcsec)	Peak Flux (10^{-4} c/sec/pix)	$\frac{F_{250}}{F_{62.5}}$	$(\frac{C}{\sqrt{B}})^{max}_{250}$	Note
···	23:45:34.8	–25:41:27	1039	0.27	1.6	3.8	
A2665	23:50:51.7	06:09:51	212	5.32	4.9	39.3	C
···	23:50:44.9	06:23:18	997	0.21	1.2	4.8	
A2666	23:51:06.8	27:09:34	152	0.26	2.6	5.5	C
···	23:50:03.3	26:58:11	947	0.25	1.5	6.2	
···	23:49:57.7	27:20:55	1071	0.35	2.1	7.5	
···	23:49:06.6	27:04:16	1487	0.16	0.9	4.6	
A2670	23:54:13.5	–10:24:48	58	6.06	9.0	43.1	C
···	23:54:29.0	–10:15:27	601	0.75	2.6	6.4	
···	23:54:49.6	–10:20:43	622	0.57	1.0	11.0	
···	23:53:29.8	–10:18:15	698	0.13	0.3	8.9	
A2675	23:55:39.1	11:20:04	348	2.34	8.4	24.9	C
···	23:55:24.6	11:31:03	347	0.41	3.3	4.9	
···	23:56:07.5	11:24:43	506	0.74	3.0	7.0	
···	23:56:23.7	11:29:31	775	0.57	5.1	7.1	
A2678	23:55:43.7	11:38:48	125	1.67	3.3	15.2	C
···	23:56:01.7	11:36:37	239	0.73	4.0	6.7	
···	23:55:42.8	11:43:12	245	0.72	3.8	6.9	
···	23:55:24.7	11:31:02	652	0.41	3.7	5.6	
···	23:56:32.5	11:46:08	717	0.26	0.8	4.6	
···	23:56:23.7	11:29:37	769	0.43	6.9	5.7	
A2696	00:03:12.2	00:53:34	143	0.40	1.8	4.2	C
···	00:03:15.2	00:48:19	338	0.45	1.0	4.7	
···	00:03:55.2	00:55:19	511	0.30	1.4	5.7	

This figure "fig2a.jpg" is available in "jpg" format from:

http://arXiv.org/ps/astro-ph/0310175v1

This figure "fig2b.jpg" is available in "jpg" format from:

http://arXiv.org/ps/astro-ph/0310175v1

This figure "fig2c.jpg" is available in "jpg" format from:

http://arXiv.org/ps/astro-ph/0310175v1

arXiv:astro-ph/0310175v1 7 Oct 2003

Table 3. X-ray Dectection Statistics

Optical Type	# Detected	$^1 < L_X >$	$< N_{Abell} >$
BM *I*	16/18 (88.9)	6.1±2.1	62±6
BM *I-II*	21/22 (95.4)	3.2±0.8	63±6
BM *II*	43/47 (91.5)	2.6±0.7	58±3
BM *II-III*	40/50 (80.0)	1.6±0.3	56±3
BM *III*	84/103 (81.5)	1.3±0.2	52±2
cD	51/56 (91.1)	4.1±0.7	53±3
B	22/22 (100.0)	3.7±0.3	57±4
C	54/67 (80.6)	1.4±0.2	51±2
L	24/27 (88.9)	1.2±0.3	48±2
F	37/47 (78.7)	1.2±0.2	55±3
I	51/67 (76.1)	0.8±0.1	48±2

[1] Luminosities in units of $10^{43}\ h_{75}^{-2}\ ergs\ sec^{-1}$.

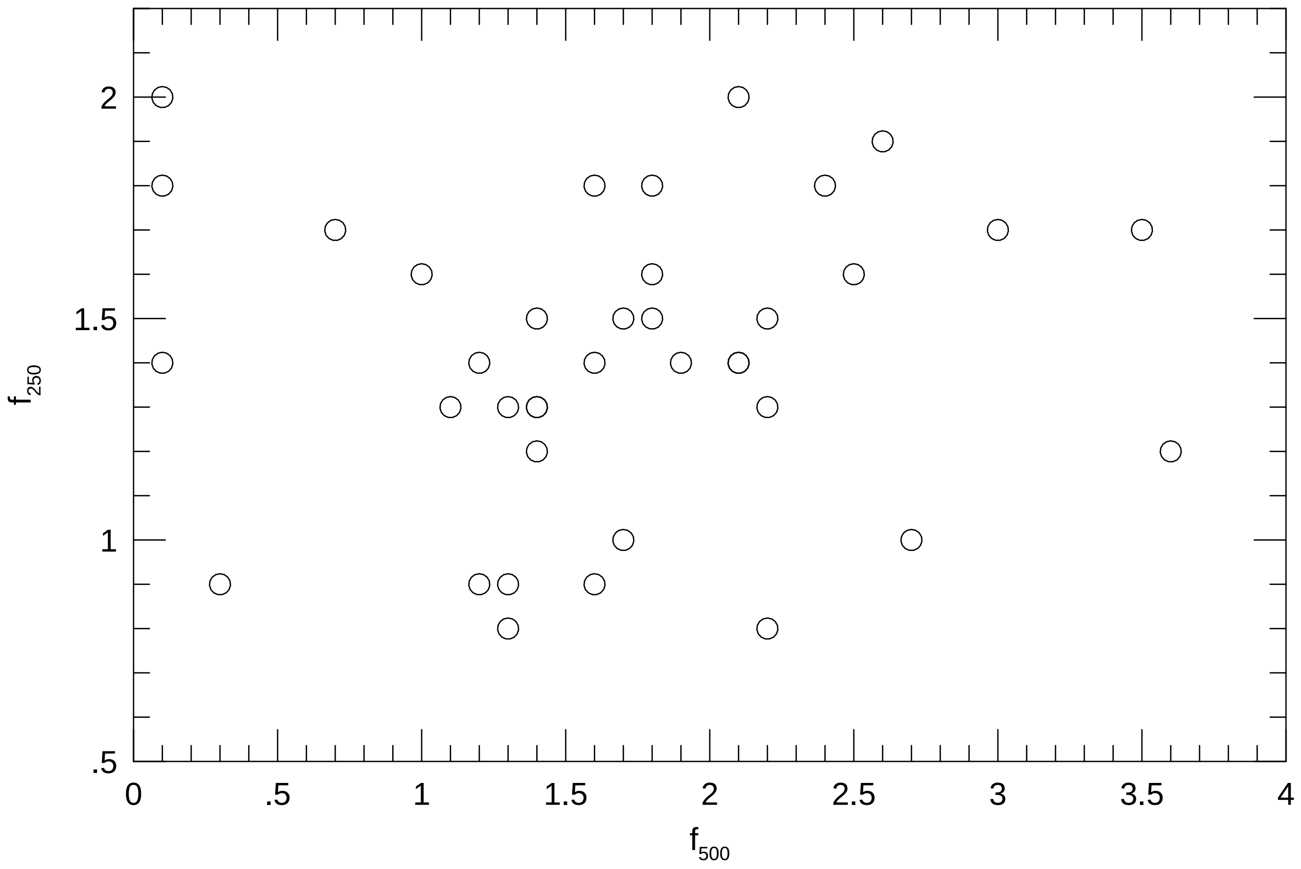
f_{250}
2
1.5
1
.5
0
.5
1
1.5
2
2.5
3
3.5
4
f_{500}

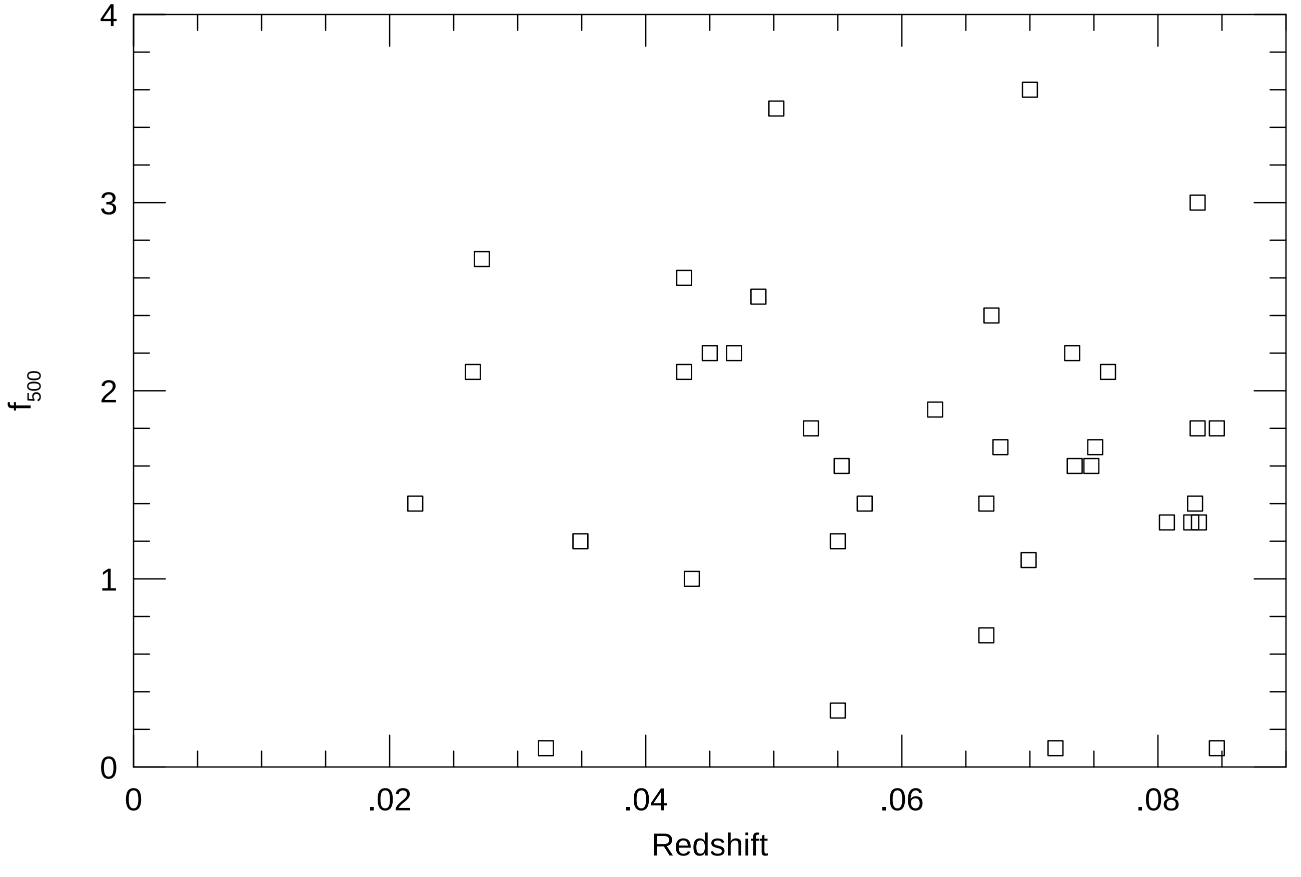
f_{500}
4
3
2
1
0
0
.02
.04
.06
.08
Redshift

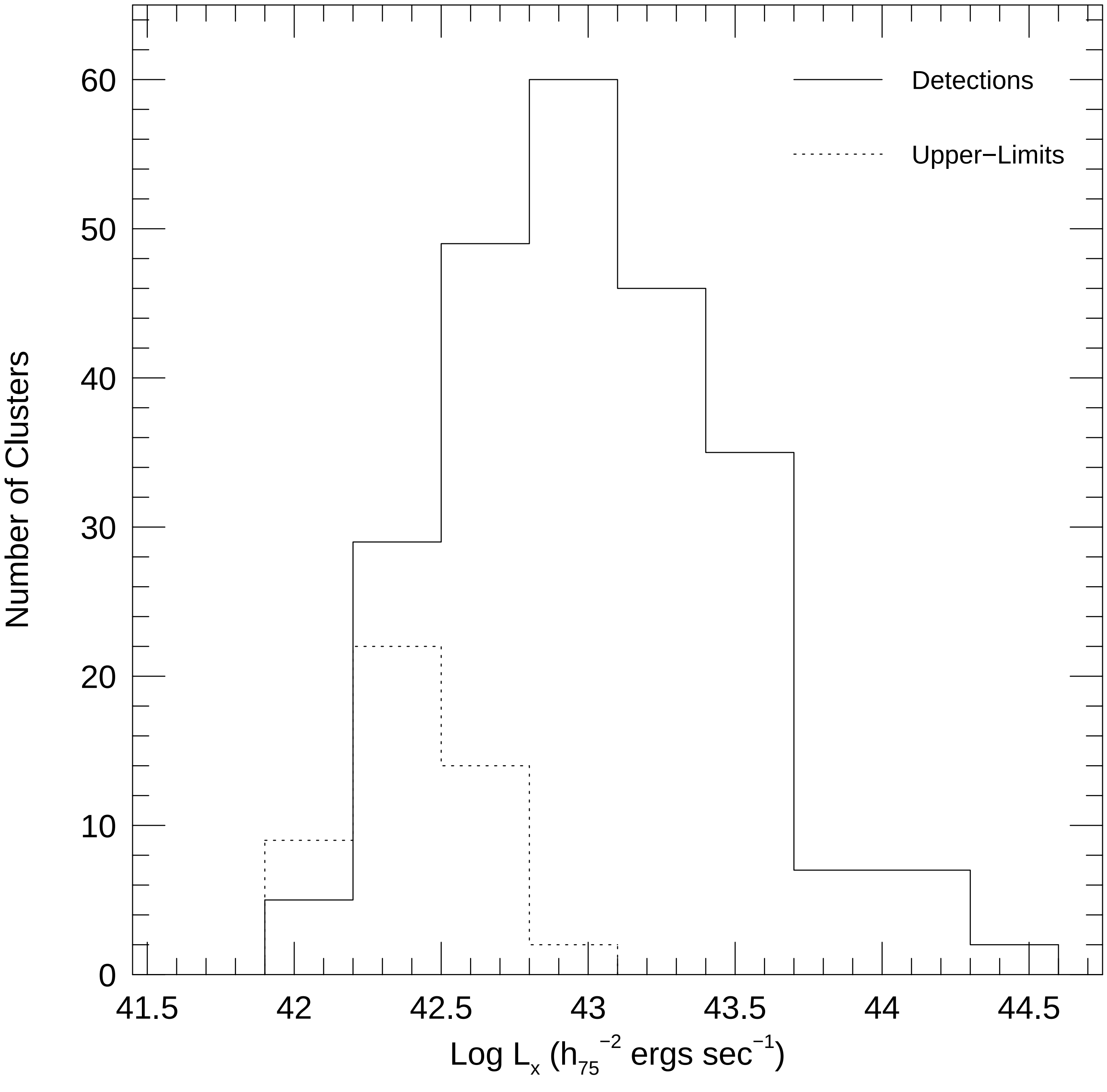

Detections
Upper−Limits
Number of Clusters
0
10
20
30
40
50
60
41.5
42
42.5
43
43.5
44
44.5
Log L_x (h_{75}^{-2} ergs sec^{-1})

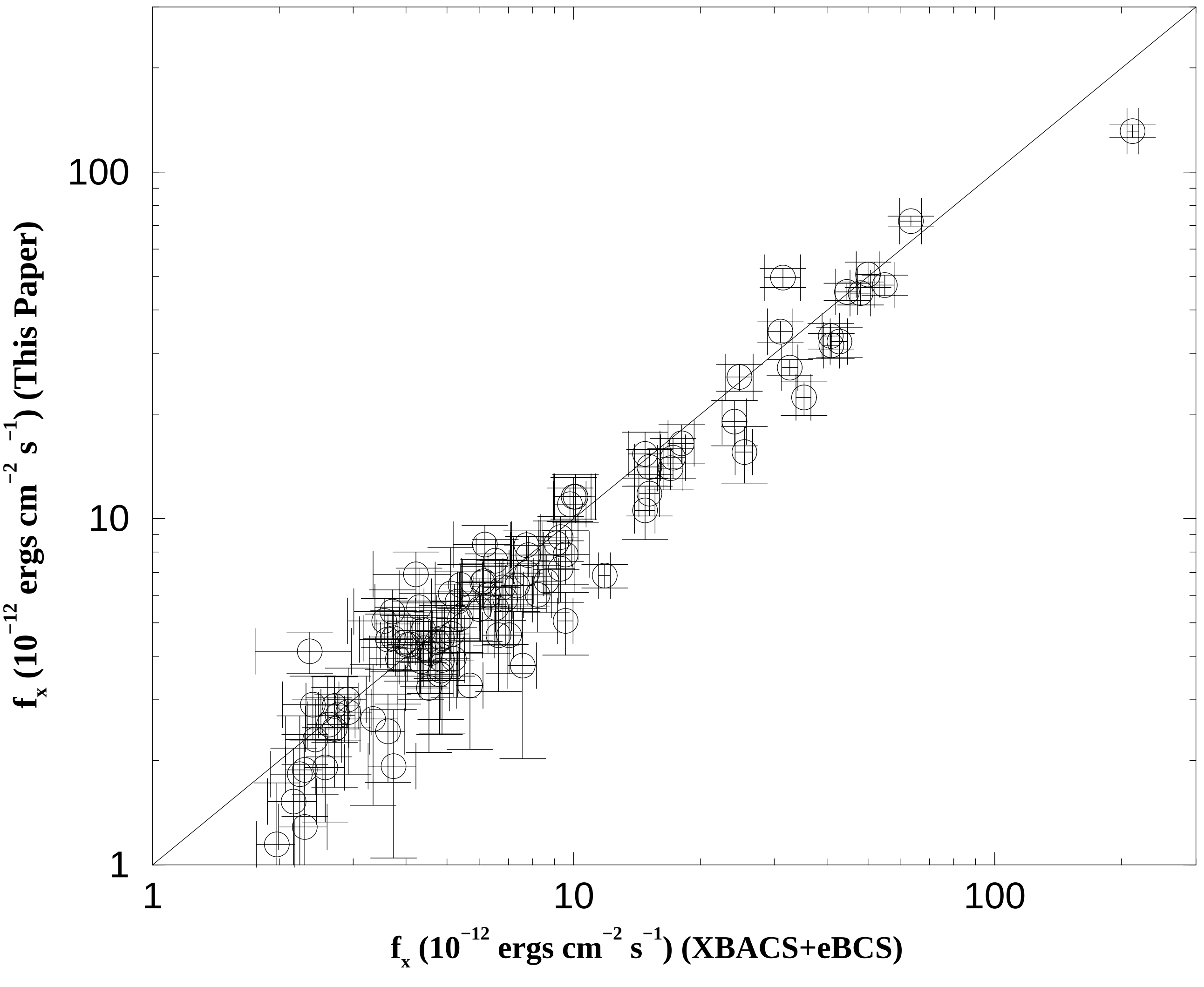

f_x (10^{-12} ergs cm^{-2} s^{-1}) (This Paper)
f_x (10^{-12} ergs cm^{-2} s^{-1}) (XBACS+eBCS)
1
10
100
1
10
100

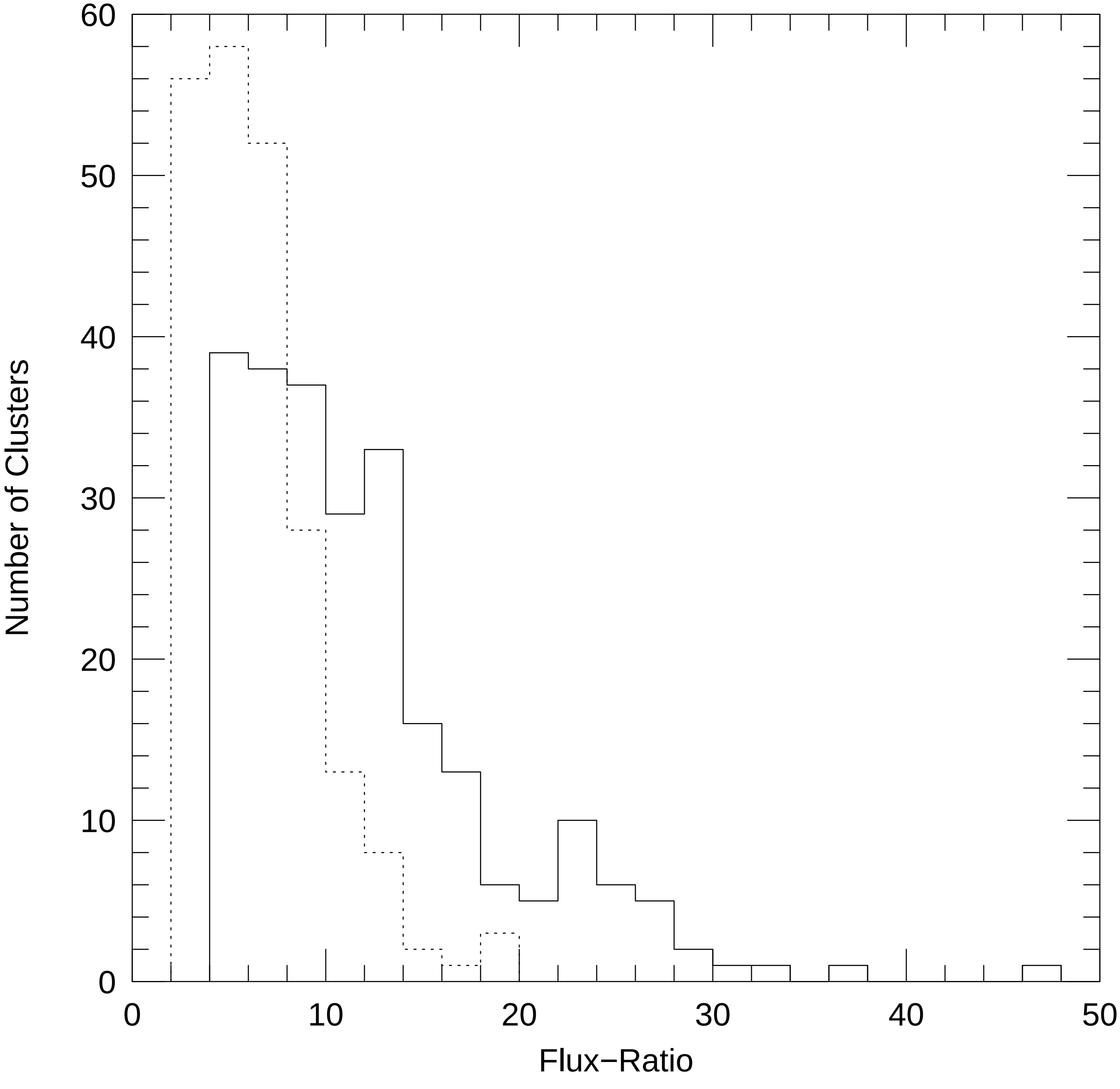

Number of Clusters
Flux−Ratio
0
10
20
30
40
50
60
0
10
20
30
40
50

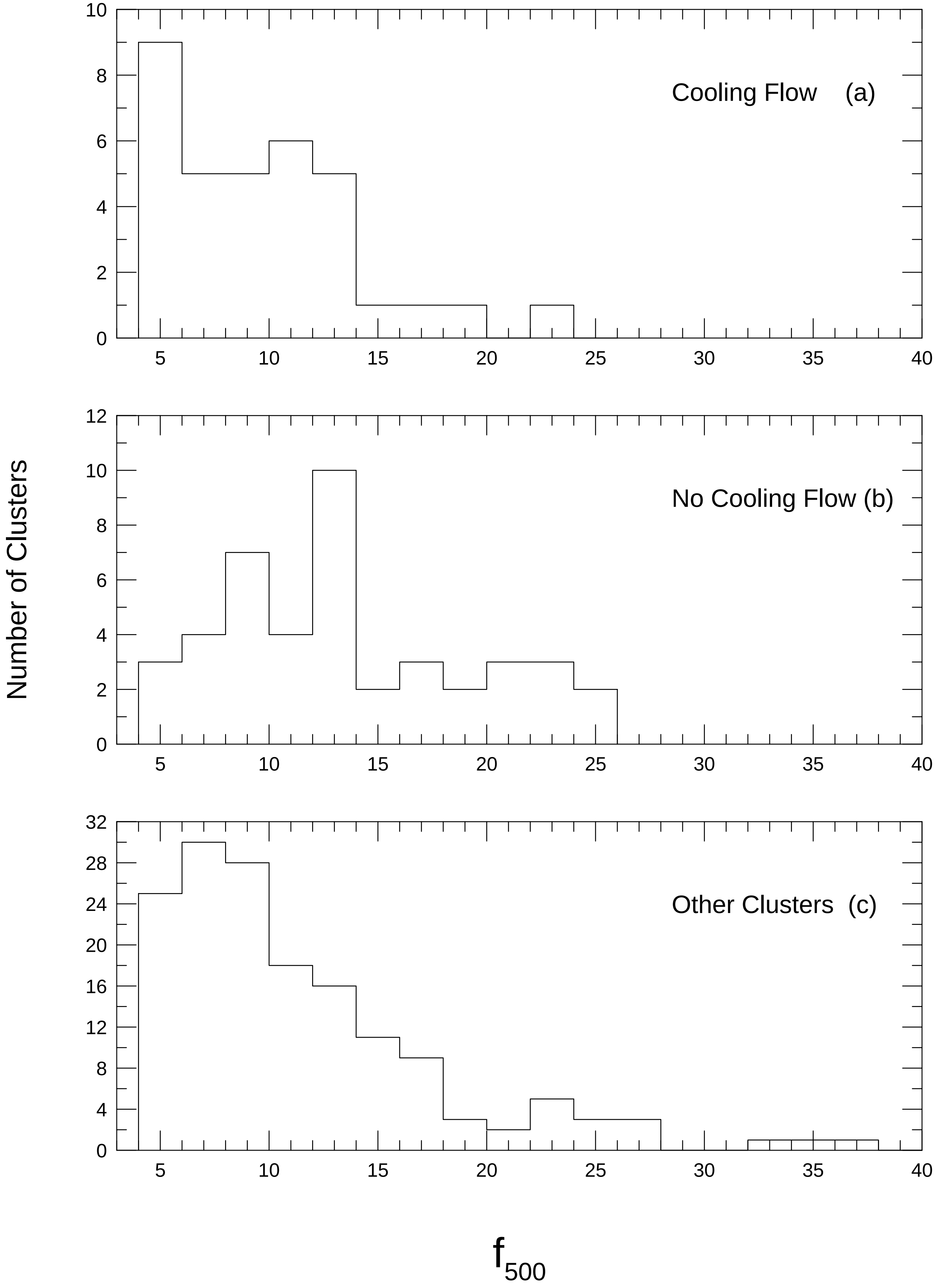
Cooling Flow (a)
No Cooling Flow (b)
Other Clusters (c)
Number of Clusters
f_{500}
0
2
4
6
8
10
12
0
4
8
12
16
20
24
28
32
5
10
15
20
25
30
35
40

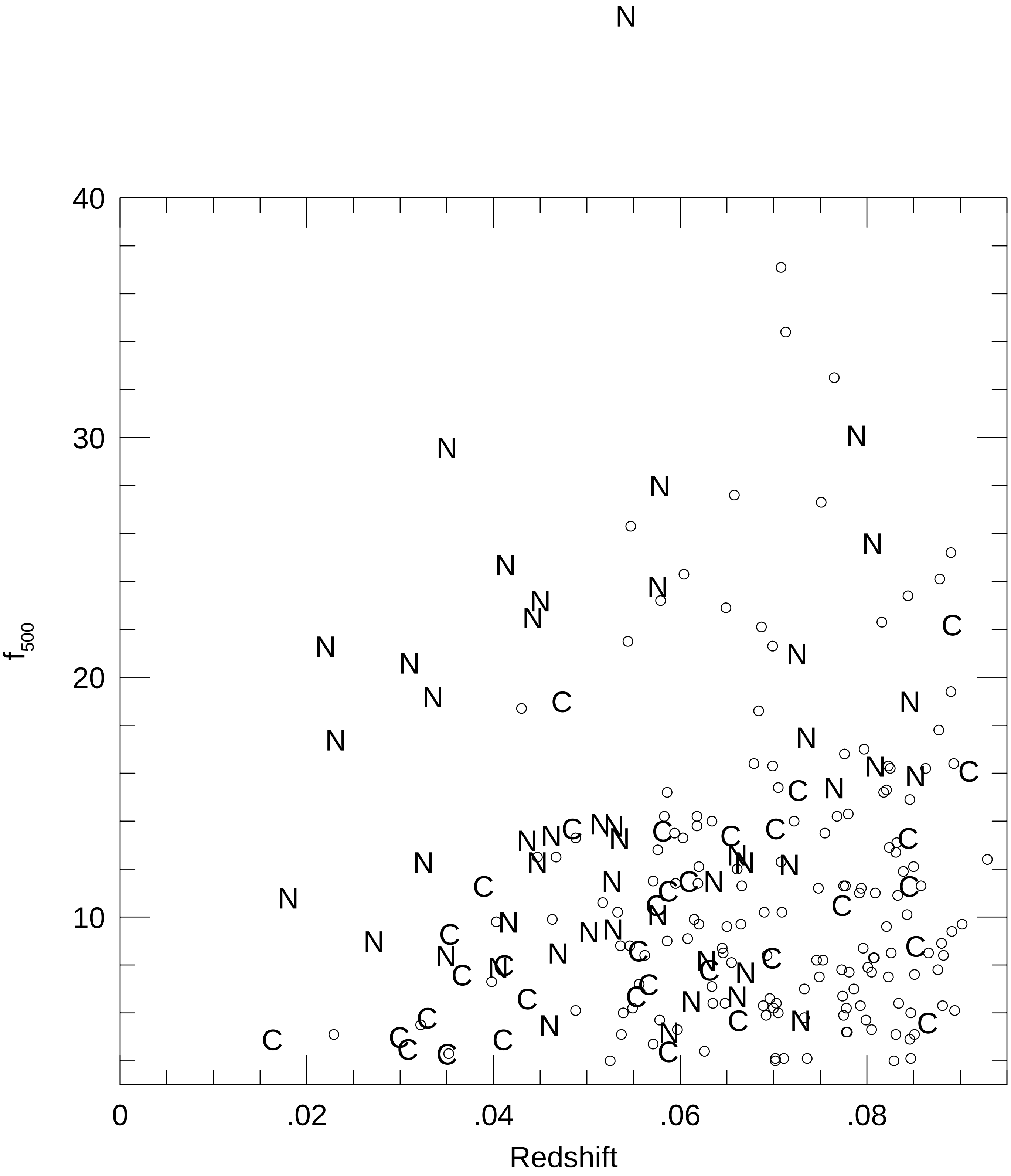

40
30
20
10
0
.02
.04
.06
.08
f$_{500}$
Redshift
N
C

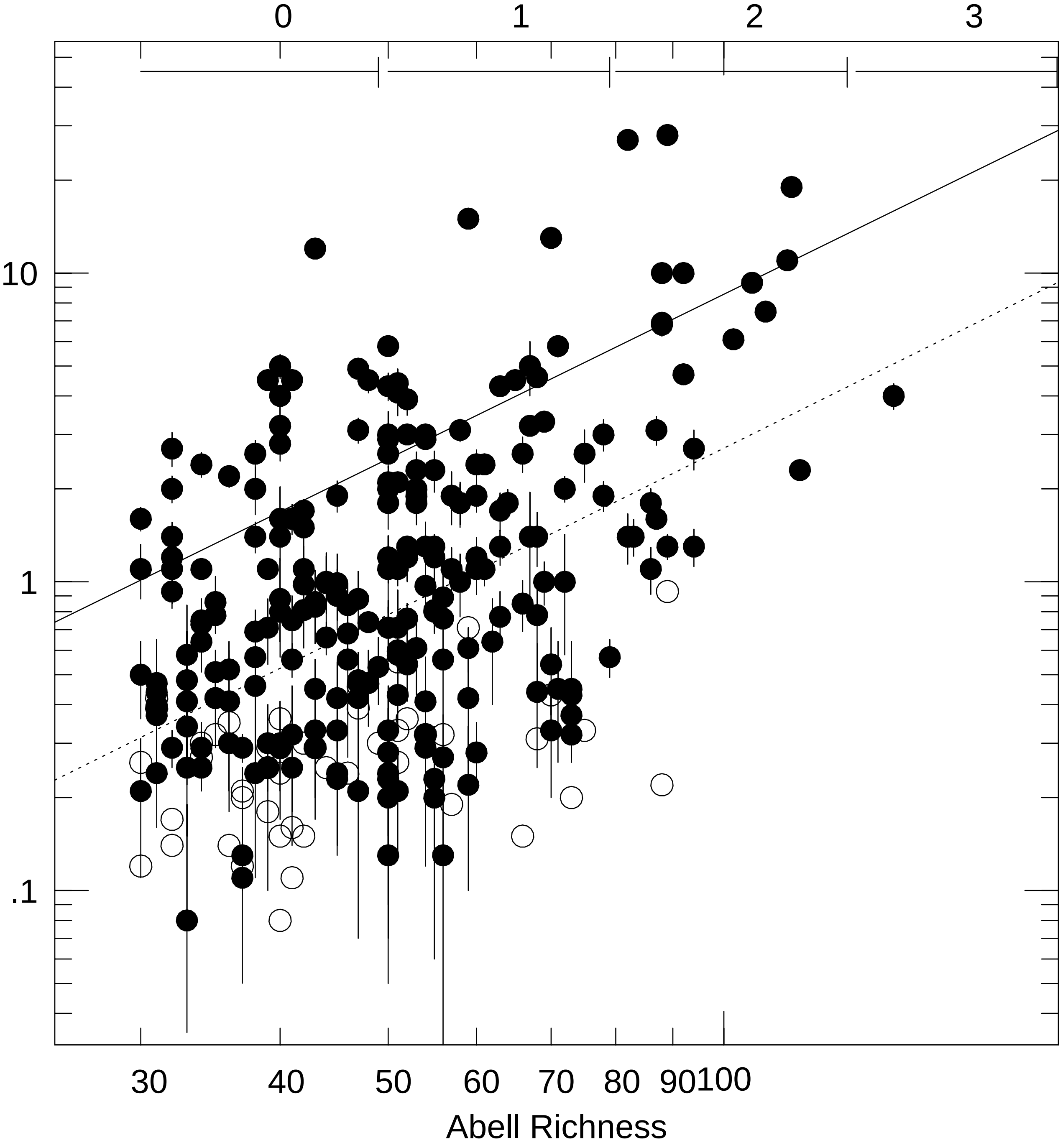

0
1
2
3
10
1
.1
L_X (h_{75}^{-2} 10^{43} ergs sec^{-1})
30
40
50
60
70
80
90
100
Abell Richness

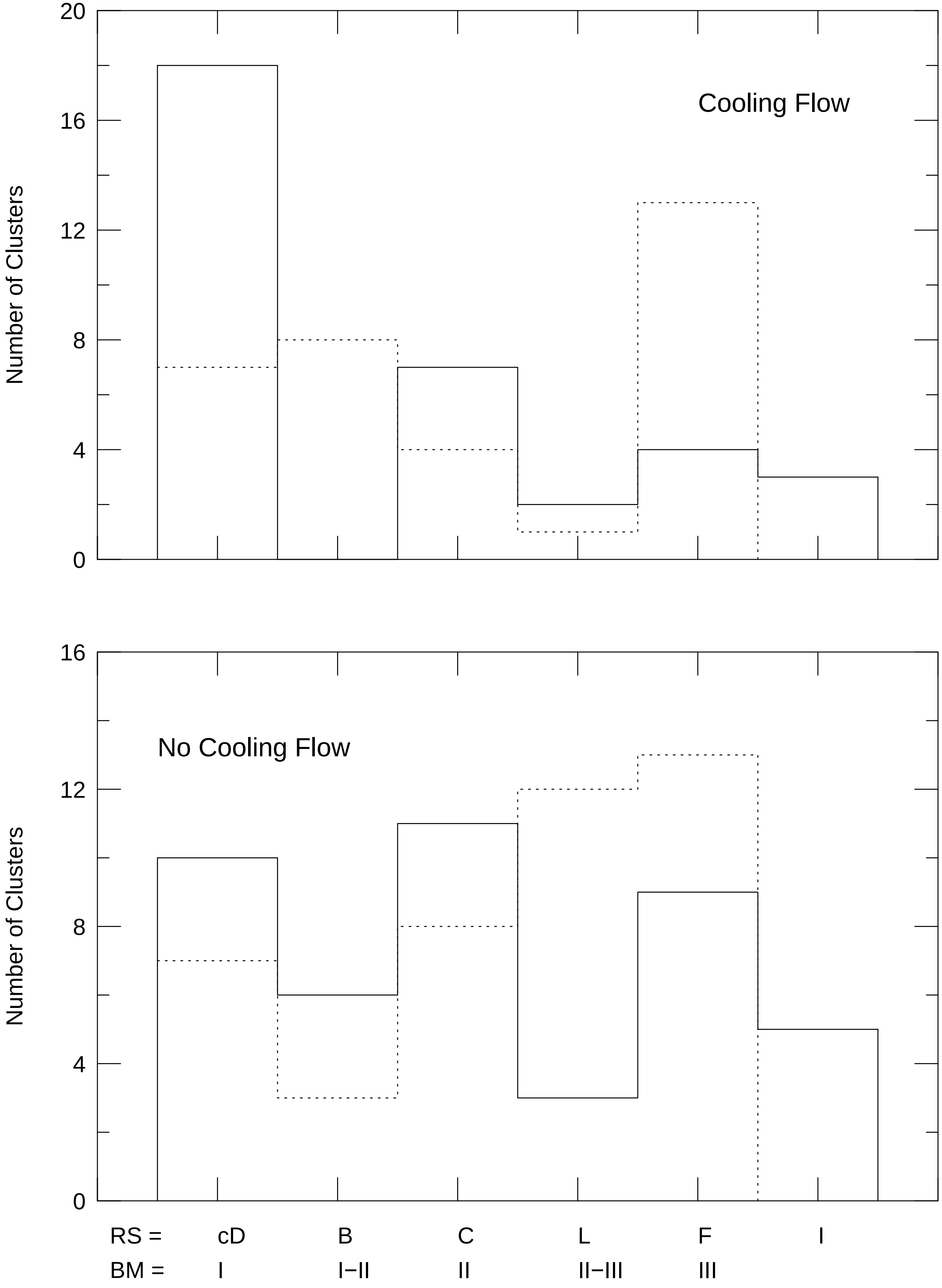
Cooling Flow
No Cooling Flow
Number of Clusters
Number of Clusters
0
4
8
12
16
20
0
4
8
12
16
RS = cD B C L F I
BM = I I−II II II−III III

arXiv:astro-ph/0310175v1 7 Oct 2003

The X-ray Properties of Nearby Abell Clusters from the ROSAT All-Sky Survey: The Sample and Correlations with Optical Properties

Michael J. Ledlow
Gemini Observatory, Southern Operations Center, AURA, Casilla 603, La Serena, Chile

Wolfgang Voges
Max-Planck-Institut für Extraterrestrische Physik, Postfach 1312, D-85740,
Garching bei München, Germany

Frazer N. Owen
National Radio Astronomy Observatory[1]*, Socorro, NM 87801*

Jack O. Burns
Department of Astrophysical & Planetary Sciences, University of Colorado, Boudler, CO 80309

ABSTRACT

We present an analysis of the X-ray emission for a complete sample of 288 Abell clusters spanning the redshift range $0.016 \leq z \leq 0.09$ from the *ROSAT* All-Sky Survey. This sample is based on our 20cm VLA survey of nearby Abell clusters. We find an X-ray detection rate of 83%. We report cluster X-ray fluxes and luminosities and two different flux ratios indicative of the concentration and extent of the emission. We examine correlations between the X-ray luminosity, Abell Richness, and Bautz-Morgan and Rood-Sastry cluster morphologies. We find a strong correlation between L_X and cluster richness coupled to a dependence on the optical morphological type. These results are consistent with the observed scatter between X-ray luminosity and temperature and a large fraction of cooling flows. For each cluster field we also report the positions, peak X-ray fluxes, and flux-ratios of **all** X-ray peaks above 3σ significance within a box of 2×2 h_{75}^{-1} Mpc centered on Abell's position.

1. Introduction

Rich clusters of galaxies are potentially powerful testbeds for cosmological models. They are rare, $\approx 10\sigma$ fluctuations in the mass spectrum and, thus, are sensitive to the underlying cosmology. Also, clusters are now commonly believed to have formed recently (Evrard et al. 1993; Bryan et al. 1994), so we can observe their evolution at relatively modest redshifts. Finally, rich clusters are luminous at optical, X-ray, and radio wavelengths making them bright observational targets out to $z \approx 1$.

Our view of clusters of galaxies has changed dramatically over the past decade. We no longer see clusters as simple spherical, isolated structures in virial and hydrostatic equilibrium. Rather, they are dynamic, evolving, and young systems that are strongly influenced by their connections to the large-scale structures in which they have formed (Chambers, Melott, & Miller 2000). Their evolution is driven by the accretion of dark matter, galaxies, and gas along filaments and via cluster-

---

[1] The National Radio Astronomy Observatory is operated by Associated Universities, Inc., under contract with the National Science Foundation.

cluster mergers (Bekki 2001; Burns 1998; Roettiger, Burns, & Loken 1996; Navarro & White 1994; Cen & Ostriker 1994). Evidence for the on-going accretion of subsystems, and thus relative youth, is found in the abundant substructure observed in both optical (Kolokotronis et al. 2001; Pinkney et al. 1996; Bird 1994) and X-ray (Sanders, Fabian, & Allen 2000; Jones & Forman 1999; Mohr, Fabrican, & Geller 1993) imaging of clusters. Even very rich nearby clusters such as Coma, once presumed to be relaxed and virialized, show evidence of recent merger activity (Watanabe et al. 1999; Burns et al. 1994; White, Briel, & Henry 1993). Extended radio sources in clusters have also been shown to be useful probes of cluster-cluster mergers (Burns 1998). Correlations between central X-ray substructure and bent radio sources, such as wide-angle tailed (Gómez et al. 1997), narrow-angle tailed (Bliton et al. 1998) radio galaxies, and cluster-wide radio haloes (Giovannini 2000) reveal strong evidence of recent mergers. These radio sources, when combined with numerical models (Loken et al. 1995) can be used as the only currently available probe of cluster gas dynamics.

Much of what we know about rich clusters at X-ray and radio wavelengths has come from incomplete samples observed with a wide variety of sensitivities and resolutions. However, with our VLA 20-cm survey of nearby Abell clusters (Ledlow & Owen 1995a; Owen & Ledlow 1997) and the *ROSAT* all-sky X-ray survey (RASS) (Voges et al. 1999), we have an opportunity to formulate and study statistical and uniform samples of rich clusters in the radio and the X-ray for the first time. In Ledlow et al. (1999) we presented the X-ray luminosity function (XLF) for this sample, and have used the observed local cluster abundance to constrain cosmological models, at least weakly.

The usefulness of the RASS for examining the X-ray properties of rich clusters has been previously demonstrated by several studies. Ebeling et al. (1993) performed a cross-correlation of the RASS with the entire ACO catalog (Abell, Corwin, & Olowin 1989) using an early release of the RASS with uniform exposure time (∼400 sec) to a flux limit of $\approx 7 \times 10^{-13}$ erg cm^{-2}s^{-1} (0.1-2.4 keV). Using a newly developed detection algorithm (VTP), Ebeling et al. (1996), compiled an X-ray flux-limited sample of the 242 X-ray Brightest Abell Clusters (XBACS) to a flux limit of $\approx 5 \times 10^{-12}$ erg cm^{-2} s^{-1} (0.1-2.4 keV). Briel & Henry (1993) measured X-ray fluxes and upper limits for a complete subsample of 145 Abell clusters with measured redshifts. They detected 46% of the clusters to 4.2×10^{-13} erg cm^{-2} s^{-1} (0.5-2.5 keV). Ebeling et al. (1998) compiled a completely X-ray selected sample of the 201 brightest clusters (BCS) with $z \leq 0.3$ and a flux-limit of 4.4×10^{-12} erg cm^{-2} s^{-1} (0.1-2.4 keV). Ebeling et al. (2000) extended the BCS (eBCS) to a flux-limit of 2.8×10^{-12} ergs cm^{-2} s^{-1} and the addition of 99 more clusters with z<0.3 (8 more with z>0.3). Similarly, de Grandi et al. (1999) identified clusters in the Southern hemisphere down to $3 - 4 \times 10^{-12}$ erg cm^{-2} s^{-1} (0.5-2.0 keV). They identified 130 clusters to this limit, 101 being Abell/ACO clusters. The work in the southern hemisphere was followed up by Cruddace et al. (2002) and Böhringer et al. (2001) (REFLEX: The ROSAT-ESO flux- limited X-ray Galaxy Cluster Survey). The former concentrating on an ≈ 1 steradian region around the south galactic pole, the latter making use of the 2nd reprocessing of the RASS and optical identifications from the COSMOS digital catalogue and a followup redshift survey. They identified 452 clusters to a limit of 3×10^{-12} erg cm^{-2} s^{-1} (0.1-2.4 keV). Gioia et al. (2001) compiled a sample of 64 clusters (nearly a third at $z > 0.3$) taking advantage of the deepest portion of the RASS at the north ecliptic pole (limit of $f_x \sim 7.8 \times 10^{-14}$ ergs cm^{-2} s^{-1} (0.5-2.0 keV)). Reiprich & Böhringer (2002); Ebeling, Edge, & Henry (2001) have concentrated on the most distant (z≥0.3) and most massive clusters detected by the RASS. See Edge (2003) for a complete summary of X-ray Surveys of low-redshift clusters.

In this paper, we use the RASS to examine the X-ray properties of a statistically complete sample of 288 northern Abell clusters with z≤0.09. Thus our sample is based on optically selected clusters, similar to the XBACs sample but includes clusters more than 10 times fainter (our average flux limit is 3.1×10^{-13} ergs cm^{-2} s^{-1} (0.5-2.0 keV)). Despite the optical-selection, the XLF agrees very well with X-ray selected cluster samples for $L_X \geq 10^{43} h_{50}^{-2}$ ergs/sec (Ledlow et al. 1999). The usefulness of our sample compared to previous compilations is the abundance of preexisting data (our VLA 20cm survey), complete redshift information, and its large size. Our sample is $\approx 50\%$ larger than the BCS within a volume that is nearly 10 times smaller in size by virtue of the lower flux limit.

In §2, we describe the construction of the Abell cluster sample used in this study. In §3, we discuss the basic properties of the RASS. In §4, we describe the methods used for finding and characterizing the X-ray emission, descriminating between extended and point-source emission, and measuring X-ray luminosities. In §5, we summarize the results with two extended tables. Table 1 includes detection statistics for the clusters, while Table 2 lists **all** significant X-ray peaks found in the fields. Also in §5, we look at the properties of known cooling flow clusters in our sample and examine correlations of the X-ray properties with cluster richness and optical morphology. We summarize our conclusions in § 6. We have used a Friedmann-Walker cosmology with H_o =75 km/sec/Mpc and q_o=0.5 throughout.

2. Description of the Sample

The sample studied in this paper was initially constructed as part of a VLA 20cm survey of rich clusters (Zhao, Burns, & Owen 1989; Owen, White, & Burns 1992; Owen, White, & Ge 1993). A detailed analysis of the optical and radio properties of these clusters is presented in Ledlow & Owen (1995a,b, 1996), and Owen & Ledlow (1997). In short, this sample includes all northern Abell clusters with measured redshifts ≤ 0.09. Clusters with high galactic extinction (> 0.1 magnitudes at R-band, corresponding to $\log N_H > 20.73$ and roughly to $|b| \lesssim 25°$) were excluded. In addition, clusters which were very discrepant in their $m_{10} - z$ relationship (~ 20 clusters) were also excluded (Ledlow & Owen 1995a). In most cases, these clusters are more distant than predicted by the $m_{10} - z$ relationship because of foreground galaxy contamination, which biased Abell's estimate. These selection criteria result in a sample of 288 Abell clusters with confirmed redshifts $0.016 \leq z \leq 0.09$, and forms a complete sample of nearby, optically-selected rich clusters useful for statistical studies.

Redshifts for each cluster were checked with NED and the most recent compilation of Struble & Rood (1999)(SR). The redshifts for eight clusters changed significantly as tabulated by SR from the time that we began this project. The changes in redshift from those listed in Ledlow & Owen (1995a) from which this sample is based are: A912 (z_{old}=0.08, z_{new}=0.0446), A971 (z_{old}=0.06, z_{new}=0.0929), A1035 (z_{old}=0.0799, z_{new}=0.0684), A1927 (z_{old}=0.0908, z_{new}=0.0947), A2004 (z_{old}=0.0640, z_{new}=0.1365), and A2295 (z_{old}=0.0540, z_{new}=0.0823). While exceeding our $z \leq 0.09$ cutoff, we have left A1927 (also in BCS), A971, and A2004 in the tables as these are the first measurements of cluster emission for all but A1927. There has been inconsistency in the literature for A1423. The cluster is catalogued at z=0.0761 in SR (based on 3 measurements) and they make note that Crawford et al. (1995) lists a galaxy at z=0.213 for the cluster redshift. More recently, Dahle et al. (2002) have found evidence from the color magnitude sequence to support the higher z=0.21 estimate. We have also eliminated A1461 (z_{old}=0.0537), listed as unreliable in SR at distance class = 5 and A2638 (z=0.0825 in SR), which is more likely at the redshift of a central radio galaxy with z=0.216 (Owen, Ledlow, & Keel 1995). Additionally, recent work by Blakeslee et al. (2001) suggests that the X-ray emission in A2152 is associated with a concentration of background galaxies (z=0.13) based on a detailed velocity and lensing analysis. Finally, A2589 ($z = 0.0414$) while part of the 288 clusters in the statistical sample, had essentially zero exposure time in the RASS and so no analysis was possible.

We derived the selection-function for our sample based on the criteria listed above. Using the *HI* map of Dickey & Lockman (1995), we first excluded all regions with $\log N_H > 20.73$ (based on a fit to E(B-V) vs. $\log N_H$)(Burstein & Heiles 1982). Second, we excluded regions (and clusters) of the sky judged to be statistically incomplete by Abell (1958). Third, we restricted the sky-coverage to declination $> -27°$ for Abell's northern catalog. A plot in galactic coordinates showing the survey area is given in Figure 1a. The solid-line is the $\delta = -27°$ limit. Solid dots denote regions of the sky which meet the selection criteria. In Figure 1b, we show the distribution of our sample on the same coordinate grid for comparison. We calculate a survey area of 4.31 steradians (14,155 deg^2) or 34% of the sky. Within the volume defined by this survey region and the redshift limits of $0.016 \leq z \leq 0.09$, we find the number density of clusters to be constant as a function of richness class and redshift interval suggesting that our sample is complete and volume-limited within the limits of Abell's selection criteria. These results are in agreement with Briel & Henry (1993) and Mazure et al. (1996) who found Abell's catalog to be complete for all richness classes over this range in redshift. However, we expect some incompleteness at the faint-end of the XLF because of our optical selection. Our sample is not flux-limited in the X-ray, and optically poorer clusters with L_X in the range of Richness-class 0 Abell clusters will be missed in our sample (Ledlow et al. 1999).

3. The ROSAT All-Sky Survey

The ROSAT All-Sky Survey (RASS) was conducted mainly during the first half year of the ROSAT mission in 1990 and 1991 (Trümper 1983). The ROSAT mirror system (Aschenbach 1988) and the Position Sensitive Proportional Counter (PSPC) (Pfeffermann et al. 1988) operating in the soft X-ray regime (0.1-2.4 keV) provided optimal conditions for the studies of celestial objects with low surface brightness. In particular, due to the unlimited field of view of the RASS and the low background of the PSPC, the properties of nearby clusters of galaxies can be ideally investigated.

During the survey phase, ROSAT scanned the sky in great circles whose planes were oriented roughly perpendicular to the solar direction. This resulted in an exposure time varying between about 400 sec and 40,000 sec at the ecliptic equator and poles, respectively. During the passages through the auroral zones and the South Atlantic Anomaly the PSPC had to be switched off, leading to a decrease of exposure over parts of the sky. In addition, some portions of the sky received less exposure where not enough guide stars for the automatic measuring and control system (AMCS) of the satellite were available. As a consequence of these various facts, the exposure map is not always homogenous; in some small regions of the sky (0.4%) the exposure time can be less than 50 seconds (Voges et al. 1999). We find an average exposure time of 473 seconds for our sample. Only one cluster (A2589) was effectively missed completely in the survey, and therefore no estimation of a detection threshold is possible.

For studying nearby clusters of galaxies, we extracted from the RASS all hard photons (0.5-2.0 keV) in a 2° box centered at the optical position of the Abell cluster to generate the photon event image. We then calculated the vignetting corrected exposure map to construct the exposure-corrected X-ray images.

In Figures 2a,b,c we show optical/X-ray overlays for six average-luminosity clusters from our sample ($L_X \approx h_{75}^{-2} 10^{43}$ *ergs sec*$^{-1}$). The X-ray images were smoothed to $250h_{75}^{-1}$ *kpc* resolution at the redshift of each cluster. The lowest contour shown is twice the estimated X-ray background (see next section). The optical images were obtained from the Digitized Sky Survey (POSS I). The field-of-view of each plot is $\approx 2.5h_{75}^{-1}$ *Mpc*. Overlays for the entire sample are available over the WWW at http://put.the.rightaddress.here.

4. Image Analysis

4.1. Methods for Finding the X-ray Peaks

In order to initially assess the quality and properties of the RASS data for this sample, we examined each cluster individually within the NRAO Astronomical Image Processing System (AIPS). First, we convolved the images to an effective spatial resolution of 250 and $500h_{75}^{-1}$ kpc at the redshift of the cluster using a Gaussian smoothing function to facilitate the identification of the X-ray peaks. We then visually identified peaks within a 2 Mpc diameter box centered on Abell's optical center position. For each peak, a surface brightness profile was measured using the AIPS task *IRING*. The procedure was to measure the mean and cumulative count rates in 32 equally-spaced circular annuli out to $1h_{75}^{-1}$ Mpc in radius centered on the identified X-ray peaks (the annuli were separated by $31.25h_{75}^{-1}$ kpc in radius, ≈2 pixels at the mean redshift of the sample). The surface brightness profiles were measured from minimally-smoothed (25″ FWHM) exposure-corrected images. From the surface-brightness profiles, some idea of the extent and brightness of the identified peaks could be determined.

We used these visually identified X-ray peaks only as a first-pass to get a *feel* for the data. In order to produce a more statistical catalog of

X-ray identifications within the cluster fields, we adopted the peak-finding program *SAD* (Search and Destroy) in the AIPS package. The *SAD* program finds all sources within some subimage whose peak is brighter than a given level. We specified the minimum level to be 3σ above the error in the background (see below). Once all the possible peaks are identified, *SAD* uses a least-squares method to fit an elliptical Gaussian to each peak. We used these peak locations for the coordinate positions of the identifications. We ran SAD in an automated mode on all 250 and $500 h_{75}^{-1}$ kpc smoothed images. Given the (X,Y) centroids of the significant peaks, we then processed the entire data set (*i.e.*measured surface-brightness profiles) in an automated batch-mode using a custom-written AIPS procedure. Additional stand-alone C and FORTRAN programs were then used to extract and analyze the intensity profiles and to calculate the X-ray luminosities. We only used the peaks identified from the $250 h_{75}^{-1}$ kpc smoothed images in the final analysis.

We checked the identifications from SAD with our visual ones, and computed surface-brightness profiles for any which appeared to have been missed. From the cumulative intensity profile we then checked these peaks against our $S/N \geq 3$ criteria over the $500 h_{75}^{-1}$ kpc aperture. Only a very few (<5%) of these additional visual-selected peaks survived, mostly being confused by a low peak imbedded in more diffuse emission and a few cases of overestimation in the background level. We thus judge our completeness level to be >95% for X-ray peaks in the cluster fields. For detecting the extended cluster emission we believe that our method is 100% complete within the sensitivity limits of the RASS.

4.2. X-ray Luminosities

In order to estimate the X-ray background on each image, we extracted strips from each edge of the frame (excluding a 5-pixel border). Each of these strips was smoothed with the $250 h_{75}^{-1}$ kpc Gaussian function. The four strips were then median-filtered using a sigma-clipping algorithm to reject deviant pixels. The median and 1σ deviation were then determined for each frame from the statistics of the coadded strips. We found an average background count-rate of $1.95 \pm 0.50 \times 10^{-5}$ counts/sec/pixel (pixels were $15'' \times 15''$), or a mean surface brightness of 3.12×10^{-4} counts sec^{-1} arcmin^{-2}.

For each X-ray peak, we calculated the detection threshold for each annulus of the intensity profile (as well as the cumulative profile) as the total background-subtracted counts from the source divided by the square-root of the background counts ($\frac{C}{\sqrt{B}}$). We also computed a total S/N including the Poisson error from the source (added in quadrature), in order to estimate the error on the integrated luminosity.

Conversion from count-rate to flux was accomplished using energy conversion factors (ECFs) derived for each cluster. The ECFs were determined using XSPEC, assuming an absorbed Raymond-Smith plasma with 0.3 solar abundance, a constant temperature of 5 keV, and convolved with the response matrix of the PSPC-C detector. The galactic N_H column densities were taken from the *HI* map of Lockman (Lockman & Dickey 1990; Dickey & Lockman 1995). Because of the soft-energy response of the PSPC these factors are not particularly sensitive to the assumed temperature. The difference in ECFs for $T = 3$ and $7\ keV$ results in less than a 3% difference in the calculated flux. As the clusters are limited to a narrow range in galactic absorption the ECFs only vary from $8.52 - 8.66 \times 10^{-12}$, with an average value of $8.61 \pm 0.03 \times 10^{-12}$ ergs cm^{-2} count^{-1}. The X-ray luminosity was then calculated in the usual way from the Luminosity distance of the cluster.

4.3. Extended and Point-Source Discrimination - Finding the Clusters

From the intensity profiles we have defined two different *flux-ratios* in order to parameterize the extent and concentration of the X-ray emission for each peak. Because the *IRING* data are binned into circular annuli of separation $31.25 h_{75}^{-1}$ kpc, we have chosen a minimal aperture of 2 bins or $62.5 h_{75}^{-1}$ kpc. The flux contained within this aperture is compared to that enclosed within apertures of both 250 and $500 h_{75}^{-1}$ kpc in size ($f_{250} = \frac{F_{250}}{F_{62.5}}$ and $f_{500} = \frac{F_{500}}{F_{62.5}}$).

We empirically determined the expected flux-ratios for a point source based on inspection of isolated X-ray peaks in a number of cluster fields. In Figure 3 we plot f_{250} versus f_{500} and f_{500} vs. redshift for these peaks. We verify that there is no dependence of f_{500} or f_{250} with redshift for point sources. While the aperture size increases with redshift, as we chose isolated peaks, the ratio is independent of aperture size as long as there is no significant contamination. We conservatively set limits of $f_{500} \geq 4$ and $f_{250} \geq 2$ in order to classify a peak as extended.

As a first pass in associating the catalogued peaks with the clusters we applied a positional constraint such that the expected X-ray centroid should be within $750 h_{75}^{-1}$ kpc of Abell's catalogued cluster position. At the median redshift of the sample this corresponds to 10.8 arcminutes, which is conservative enough to avoid missing any clusters in the first round of processing. After producing a list of candidate X-ray sources which met both the flux-ratio cutoffs for being extended and this positional constraint, we visually inspected the optical/X-ray overlays (see Figures 2a,b,c) to confirm a positional coincidence with a cluster. From the final tabulated list of X-ray cluster peaks, we find a median optical/X-ray offset of $188 h_{75}^{-1}$ kpc, which at the median redshift corresponds to an offset of just 2.6 arcminutes.

We also measured for each cluster the X-ray luminosity in a $500 h_{75}^{-1}$ kpc aperture centered on Abell's optical position, regardless of whether there was an actual X-ray peak at that location. For clusters with no significant X-ray peaks (or only those associated with point sources), upper-limits were calculated based on 3σ times the error in the background integrated over the $500 h_{75}^{-1}$ kpc aperture.

5. Results

The results of the X-ray analysis for each cluster is listed in Tables 1 and 2. For Table 1, the first line for each cluster includes the (1) cluster name, (2) redshift, (3) mean RASS exposure time in seconds, (4,5) optical position (RA,DEC) of the cluster center ((Abell, Corwin, & Olowin 1989)) in J2000 coordinates, (8) the X-ray luminosity and error measured within $500 h_{75}^{-1}$ kpc centered on Abell's position or an upper-limit if no significant X-ray peaks were detected, and (10) the total S/N within this aperture. Subsequent lines for each cluster list (4,5) the X-ray position (RA,DEC) of the peak(s) in J2000 coordinates (6) the projected positional offset from Abell's cluster position in h_{75}^{-1}kpc, (7) the flux and error within a $500 h_{75}^{-1}$ kpc aperture, (8) the X-ray luminosity and error calculated from the flux, (9) the flux ratio (f_{500}) measured from the surface-brightness profile (see definition above), (10) the significance (S/N) of the detection integrated over the $500 h_{75}^{-1}$ kpc aperture, and (10) the maximum S/N within this aperture in any of the 16 annular bins. The order of these subsequent lines for each cluster is first the most likely identification of the cluster emission followed by any other candidates in order of increasing distance from Abell's position. In some cases there is an ambiguity between multiple X-ray peaks of similar brightness. We list all such peaks in these cases. All peaks listed in Table 1 meet the criteria discussed in the previous section regarding offsets from Abell's positions and the measured flux-ratios, which insures that the peaks are resolved and possible candidates for the cluster emission.

In Table 2 we list all significant X-ray peaks found in the direction of all clusters within the $2 \times 2 h_{75}^{-1}$ Mpc search box. In columns 1-3 we list the Abell number of the field and RA, DEC of the X-ray peak. In the remaining columns we list (4) the offset in arcsec between the X-ray peak and the optical position of the cluster center, (5) the peak flux in *counts/sec/pixel*, (6) the flux-ratio f_{250} (see definition in the previous section), (7) the significance of the detection ($(\frac{C}{\sqrt{B}})_{250}^{max}$), and (8) a code if applicable identifying the peak with the cluster emission (C). Multiple peaks are labeled (M) if the cluster emission appears bimodal or multimodal.

Based on these classification criteria, we find a cluster detection rate of 83%. In Figure 4 we show a histogram of the X-ray luminosities and separately, the upper limits. We find an average and median L_X of 2.04 ± 0.22 and 0.99 ± 0.23 $h_{75}^{-2} 10^{43}$ ergs sec^{-1}, respectively. The precipitous decline in the number of clusters for $L_X < h_{75}^{-2} 10^{43}$ ergs sec^{-1} was shown (Ledlow et al. 1999) to be a result of incompleteness due to the optical selection of our sample (our sample is not X-ray flux-limited). While Abell's catalog is complete in an optical sense over these redshifts, there are a large number of optically poorer clusters with X-ray luminosities in the range of Richness class=0 Abell clusters.

We compare our measured fluxes to those

from previous work in Figure 5. We have cross-correlated our sample with the XBACS (Ebeling et al. 1996) and BCS+eBCS (Ebeling et al. 1998, 2000). A number of conversions are needed in order to directly compare the fluxes. These other samples report fluxes over the energy band (0.1-2.4 keV) and have applied statistical corrections for missing low-surface-brightness emission and for point-source contamination. For the comparison we adjust our fluxes (measured within a $500h_{75}^{-1}$ kpc radius aperture to a total flux following Briel & Henry (1993) and as described in Ledlow et al. (1999) assuming a core radius of 250 kpc for all clusters. This results in a count-rate correction factor of ~ 1.8, very close to that derived for the BCS (see fig 11 in Ebeling et al. (1998)) with a similar source extent (with a large scatter). We convert the BCS+eBCS and XBACS fluxes to 0.5-2.04 keV using the individual cluster temperatures given in their tables. In general the agreement is quite good; the dispersion increases with increasing flux as one would expect if the scatter is primarily due to differences in the correction for missing flux.

5.1. Flux-Ratios and Cooling Flows

In Figure 6, we plot both f_{500} (solid-histogram) and f_{250} (dashed-histogram) for all detected clusters using the selected cluster peak as listed in Tables 1 and 2. For the entire sample, we find $< f_{500} >= 12.1 \pm 6.9$ and $< f_{250} >= 6.3 \pm 3.4$. Thus, the vast majority of the clusters are significantly extended as compared to a point-source model ($f_{500} < 4$, $f_{250} < 2.0$).

As one of the observational signatures of a cooling flow is a central X-ray excess, these flux-ratios may be useful in finding clusters with compact cores. We have cross-correlated our sample with the Cooling-Flow cluster lists of Arnaud (1988), Jones & Forman (1999), White, Jones, & Forman (1997), and Peres et al. (1998). From these lists, we include a cluster as a cooling-flow if the derived $\dot{M}$ was > 0 and the cooling time was less than a Hubble time, as tabulated in these papers. For clusters with both *Einstein* and *ROSAT* measurements, we preferentially choose the *ROSAT* numbers. Similarly, we adopt the values determined from the *ROSAT* PSPC over the HRI if both are available. In Figure 7, we plot histograms of f_{500} for (a) clusters with cooling-flows, (b) no cooling-flow clusters, and (c) all other detected clusters in our sample for which no deprojections have been performed. Those clusters classified as *no cooling-flow* are labeled as such because the deprojection analysis of these clusters indicates a cooling time greater than a Hubble time. We find that f_{500} is biased towards smaller values for the cooling-flow clusters. The 75th, 50th, and 25th percentile values are for Cooling Flow Clusters: 5.8, 8.6, and 12.4, respectively, with a mean of 9.7±0.7. For Non Cooling Flows these are 9.3, 12.9, and 19.6 with a mean value of 15.3±1.2. We also ran several two-sample tests to compare the f_{500} distributions (Log-Rank, Gehan Wilcoxon, KS, etc.). All tests consistently find the two samples different at the >99% level. We find no correlation between $\dot{M}$ and f_{500}.

We plot f_{500} vs. redshift in Figure 8 with different symbols to indicate cooling flows (C), non cooling flows (N), and other clusters (small O). No significant correlations are found. The effective resolution in the RASS is $\approx 45''$. The smaller 62.5kpc aperture used in our flux ratios corresponds to $42''$ at z=0.09 and hence is a good match to the PSF. We therefore don't expect distance-related biases in our analysis.

While the f_{500} distributions for clusters with and without cooling flows are statistically different, the range of values overlap significantly making it difficult to use f_{500} alone as an indicator for a cooling flow.

5.2. Detection Statistics and Optical Cluster Properties

For the full sample we find an X-ray detection rate of 83%. As a function of Abell Richness Class we find detection rates of: RC0=76.6% (105/137), RC1=89.6% (111/124), RC2=91.6% (22/24), and RC3=100% (1/1). The higher detection rates for richer clusters are consistent with increasing gas mass and a deeper gravitational potential in richer systems. Thus, we might expect to find a correlation between L_X and cluster richness. This relationship has been examined by David, Forman, & Jones (1999)(DFJ99), Briel & Henry (1993), Johnson et al. (1983), and Bahcall (1977) among others, with varying results depending on the sample size and selection. Most, but not all of these previous studies preferentially selected the most X-ray luminous or richest clusters. Most recently, Yee &

Ellingson (2003) show that the richness (parameterized by B$_{gc}$; the galaxy cluster center correlation amplitude) is a key defining characteristic, tightly correlated with the velocity dispersion and X-ray temperature. We expect that the observed scatter between L_x and richness is directly related to the known scatter between L_x and temperature, and more fundamentally on the cluster mass.

In Figure 9 we show the relationship between L_X and Abell's richness for our sample. Statistical tests on these data indicate a positive correlation. Both the Spearman-ρ (rank-correlation) and Kendall-τ statistics derive a probability of $< 1 \times 10^{-4}$ that L_X and Richness are uncorrelated ($\rho = 0.544, \tau = 0.715$). We also show in Figure 9 the results of fitting the data. The solid-line is the result when the upper-limits are not used and the data points are weighted inversely by their standard deviations ($L_X(h_{75}^{-2} 10^{43}) = 0.002 \pm 0.0002 \times R^{1.77 \pm 0.01}$). The dashed-line is the result of a linear-regression fit (Buckley-James method)) which includes the censored data points ($L_X(h_{75}^{-2} 10^{43}) = 0.0007^{+0.0011}_{-0.0004} \times R^{1.79 \pm 0.19}$). The two fits agree within the estimated errors. Our derived slope is nearly identical to that of Briel & Henry (1993) when the difference in H_0 is taken into account.

There are wide-spread disagreements amongst previous studies as to the true correlation between L_X and cluster morphology, as it is difficult to disentangle the dominant factors given that morphology and richness are also correlated (at least weakly). Conclusions range from the cluster morphology having equal importance (DFJ99; Bahcall (1977)) in determining L_X to only a very weak dependence (Johnson et al. 1983; Jones & Forman 1978). In common to these studies, however, is the finding that the early-type cluster morphologies (BM type *I,I-II* and RS type *cD,B*) may have an independent influence on the luminosity, presumably due to the presence of a cD-like galaxy and correspondingly deeper gravitational potential (McHardy 1978). McHardy found, however, that cD-like galaxies in poorer clusters (such as AWM (Albert, White, & Morgan 1977), MKW (Morgan, Kayser, & White 1975), and WP (White 1978) clusters) have a much lower probability of X-ray emission as compared to Bautz-Morgan type *I* Abell clusters. Thus, the L_X/richness dependence would appear to be stronger based on these arguments. To complicate matters further, DFJ99 found that the L_X-richness correlation primarily pertains to **late** BM type clusters, and L_X-richness are in fact uncorrelated in early BM type clusters. Their study, however, was limited to the richest (RC$\geq$2) Abell clusters.

We have looked for correlations in the detection statistics of L_X with optical cluster morphology quantified by the RS and BM classifications. We show these results in Table 3. First, we have examined the L_X-richness relationship for the BM and RS cluster types individually. We find that each of the individual classes has a significant L_X-richness correlation (at $>$ than 99.99% probability), surprisingly with the exception of the BM *I-II* and RS *B*-type clusters. For these two classes, the probabilities are 13% and 6% based on Spearman-ρ and 23% and 4% from Kendall-τ for BM and RS types respectively, that L_X and richness are uncorrelated. However, it is unclear if this is actually significant since both of these classes have 100% detection rates in our sample and also have the lowest number statistics of any class. The Spearman-ρ test in particular is known to return questionable results for $N < 30$ data points (Feigelson & Nelson 1985). When we divide the sample into early/late-type bins (early type = RS *cD,B,C,L* and BM *I,I-II*; DFJ99) we find that L_X and richness are correlated at $\approx$ equal significance for both early and late-type clusters, in contrast to the results of DFJ99. Recall, the DFJ99 sample only includes RC$\geq$2 clusters while our sample includes all richness classes.

In the third and fourth columns of Table 3 we list the average L_X and richness of each of the morphological classes. From simple inspection, it is clear that early cluster types appear to have higher L_X than late-types by a fairly large factor. There is a trend for the late-type clusters to have lower richness. To quantify these results in a more robust way, we have applied a number of two-sample statistical tests in order to estimate the probabilities that L_X and richness for the different BM and RS classes are derived from the same parent sample. In this way, we can separate the possible mutual dependence of L_X on richness and morphology to determine which is more important.

For cluster richness, we find marginal evidence that the early/late-type BM or RS clusters are culled from different parent populations (probabilities $< 5\%$ for BM and $< 2\%$ for RS), while for L_X we find that the probability of early/late-type clusters having the same L_X distribution is $< 1 - 2 \times 10^{-4}$. Thus, the statistical results suggest that the cluster morphology is in fact **more** important than the richness in determing L_X for a given cluster, contrary to some other findings (DFJ99 suggest at least equal importance). As a consistency check, assuming $L_X \propto R^{1.7}$, the difference in richness over the range of cluster types would predict a factor of 1.3 increase in L_X from late to early BM or RS types, while we see an increase of $\approx$ a factor of 4.

The presence of a cooling flow can also perturb the scaling relations for clusters. Fabian et al. (1994) showed that clusters with cooling flows have either a lower temperature or a higher luminosity than those without; the offset from the mean L_x/T_x scaling relation being proportional to $\dot{M}$. As cooling flow clusters are thought to tend towards early type morphologies (Edge & Stewart 1991) and the fraction of cooling flow clusters is measured to be $\geq 70\%$ (Peres et al. 1998), the effects we are seeing may be directly related to cooling flows. The percentage increase in L_X resulting from a cooling flow is expected to be of order $< 30\%$, similar to the factor of 1.3 we expect from differences in richness from late to early type clusters. In Figure 10 we show the distribution of RS and BM types for cooling flow and non-cooling flow clusters. While based on similar criteria, it is clear that the RS and BM classifications do not exactly parallel one another for the same clusters. With regard to RS type, 76% of the cooling flow clusters are in early-type (cD (50%) or C) clusters. The cooling flow/non cooling flow RS distributions are different at the 97% level. Surprisingly, however, 39% of the cooling flows are in BM type III clusters (corresonding to mostly C,F RS types). The BM distributions are not statistically different between the two samples.

Because the optical morphological classifications are based on the spatial distribution of the brightest galaxies, the effects of fore-/background contamination can produce a bias with redshift. We have checked the redshift distributions of the RS classes separately and grouped into the early/late-type categories given above. A KS-test shows that the two categories are consistent with having been drawn from the same redshift distribution.

Based on our results from the X-ray properties, we would argue for a modification to the traditional binning of early and late type clusters. For the BM classes, BM types *I*, *I-II*, and *II* have very similar X-ray properties, and the BM *II-III* and *III* classes have nearly identical (and lower) L_X and X-ray detection rates. For the RS classes, the *cD* and *B* types clearly stand out as having higher L_X, whereas the *C*, *L*, *F*, and *I* group all have lower but essentially the same L_X. As the X-ray emission is a better tracer of the underlying gravitational potential and cluster mass, we would argue for this binning scheme over previous, optically based early/late type bins.

The interpretation of these results must be related to both the presence of cooling flows and to the expected evolution in L_x as the cluster becomes more and more centrally concentrated over time and with successive mergers (Bryan et al. 1998). Approximately 40% of all Abell clusters show evidence of recent mergers based on X-ray and optical substructure Jones & Forman (1999), Kolokotronis et al. (2001), and McNamara et al. (2001). Cluster merger simulations predict significant changes in L_X as the gravitational potential is initially weakened in strength early on and later is enhanced over the pre-merger value after a few crossing times (Ricker & Sarazin 2001; Roettiger, Loken, & Burns 1997; Roettiger, Burns, & Loken 1996). These predictions are therefore consistent with our findings, assuming that *early*-type clusters are in fact the most evolved systems and *late*-type systems the least.

6. Conclusions

We report an X-ray analysis of a complete sample of 288 nearby ($z \leq 0.09$) Abell clusters from the *ROSAT* All-Sky Survey. We find a detection rate of 83% at greater than 3σ confidence and tabulate fluxes and luminosities, or upper limits for the entire sample. For each cluster we have identified the most likely X-ray peak and position which should be identified with the cluster emission. We have checked X-ray/optical overlays with the Palomar Digitized Sky Survey to attempt to confirm the association with the clusters. All X-ray peaks within a $2 \times 2 h_{75}^{-1}$ Mpc box centered on

Abell's position have also been catalogued. Additionally, we have made optical/X-ray overlays of all cluster fields available over the WWW at http://put.the.rightaddress.here.

We have looked for correlations between the X-ray and optical cluster properties. We find significant correlations between the cluster richness, optical morphology and L_x. Early cluster types (BM types I,I-II and RS types cD, B) have systematically higher X-ray luminosities than later types. Our results suggest a slight revision of the early/late-type morphological separation into these bins. The results can be explained by the large fraction of cooling flows in clusters ($\geq 70\%$) and a preference for clusters with early-type optical morphology.

The measured X-ray flux ratio (f_{500}) for clusters with and without cooling flows are statistically different. Coupled with an early RS morphological type, f_{500} is potentially useful in identifying cooling flow candidates,

Papers already published using this sample include an analysis of the X-ray luminosity function and comparison to cosmological models (Ledlow et al. 1999), and a computation of the two-point spatial correlation function (Miller, Ledlow, & Batuski 1999).

We thank the referee, Alastair Edge, for his comments which greatly improved the presentation in this paper. This work was supported in part by NASA grants NAG5-6739, NAG5-10516 to ML, NAGW-3152 to JB and FO, and NSF grants AST-9317596 and AST-9896039 to JB The ROSAT Project is supported by the Bundesministerium für Bildung und Forschung (BMBF/DLR) and the Max-Planck-Gesellschaft (MPG). This research was supported by the Gemini Observatory, which is operated by the Association of Universities for Research in Astronomy, Inc., on behalf of the international Gemini parthership of Argentina, Australia, Brazil, Canada, Chile, the United Kingdom and the United States of America. We acknowledge use of the NASA/IPAC Extragalactic Database (NED), which is operated by the Jet Propulsion Laboratory, California Institute of Technology, under contract with NASA.

REFERENCES

Abell, G.O., Corwin, H.G., & Olowin, R.P. 1989, ApJS, 70, 1

Abell, G.O. 1958, ApJS, 3, 211

Albert, C.E., White, R.A., & Morgan, W.W. 1977, ApJ, 211, 309

Arnaud, K.A. 1988, in *Cooling Flows in Galaxies and Clusters*, (ed. A. Fabian), (Dordrecht: Kluwer), p. 31

Aschenbach, B. 1988, *Appl. Optics*, 27, 1404

Bahcall, N.A. 1977, ApJ, 217, L77

Bekki, K. 2001, *Ap&SS*, 276, 1033

Bird, C. 1994, AJ, 107, 1637

Blakeslee, J.P., Metzger, M.R., Kuntschner, H, & Côté, P. 2001, AJ, 121, 1

Bliton, M., Rizza, E., Burns, J.O., Owen, F.N., & Ledlow, M. 1998, MNRAS, 301, 609

Böhringer, H., Schuecker, P., Guzzo, L., Collins, C.A., Voges, W., Schindler, S., Neumann, D.M., Cruddace, R.G., De Grandi S, Chincarini, G., Edge, A.C., MacGillivray, H.T., & Shaver, P. 2001, A&A, 369, 826

Briel, U.G. & Henry, J.P. 1993, A&A, 278, 379

Briel, U.G. 1996, MNRAS, 281, 799

Bryan, G.L. & Norman, M.L. 1998, ApJ, 495, 80

Bryan, G., Klypin, A., Loken, C., Norman, M., & Burns, J.O. 1994, ApJ, 437, L5

Burns, J.O. 1998, *Science*, 280, 400

Burns, J.O., Roettiger, K., Ledlow, M., & Klypin, A. 1994, ApJ, 427, L87

Burns, J.O. 1996, in *Energy Transport in Radio Galaxies & Quasars*, (eds. P. Hardee, A. Bridle, & A. Zensus), ASP Conf. Ser. 100, p. 341

Burstein, D. & Heiles, C. 1982, AJ, 87, 1165

Chambers, S.W., Melott, A.L., & Miller, C.J. 2000, ApJ, 544, 104

Crawford, C.S., Edge, A.C., Fabian, A.C., Allen, S.W., Böhringer, H., Ebeling, H., McMahon, R.G., & Voges, W.V. 1995, MNRAS, 274, 75

Cen, R. & Ostriker, J. 1994, ApJ, 429, 4

Cruddace, R., Voges, W., Böhringer, H., Collins, C.A., Romer, A.K., MacGillivray, H., Yentis, D., Schuecker, P., Ebeling, H., & DeGrandi, S. 2002, ApJS, 140, 239

Dahle, H, Kaiser, N. Irgens, R.J., Lilje, P.B., & Maddox, S.J. 2002, ApJS, 139, 313

David, L.P., Forman, W., & Jones, C. 1999, ApJ, in press (astro-ph/9902129)

de Grandi, S., Böhringer, H., Guzzo, L., Molendi, S., Chincarini, G., Collins, C., Cruddace, R., Neumann, D., Schindler, S., Schuecker, P., & Voges, W. 1999, ApJ, 514, 148

Dickey, J.M. & Lockman, F.J. 1995, *The HI Sky*, NCSA Astronomy Digital Image Library.

Ebeling, H., Edge, A.C., & Henry, J.P. 2001, ApJ, 553, 668

Ebeling, H., Edge, A.C., Allen, S.W., Crawford, C.S., Fabian, A.C., & Huchra, J.P. 2000, MNRAS, 318, 333

Ebeling, H., Edge, A.C., Böhringer, H., Allen, S.W., Crawford, C.S., Fabian, A.C., Voges, W., & Huchra, J.P. 1998, MNRAS, 301, 881

Ebeling, H., Voges, W., Böhringer, H., Edge, A.C., Huchra, J.P., & Briel, U.G. 1996, MNRAS, 281, 799

Ebeling, H., Voges, W., Böhringer, H., & Edge, A.C. 1993, A&A, 275, 360

Edge, A.C. 2003, astro-ph/0307150

Edge, A.C., 1997, in *Galactic Cluster Cooling Flows*, (ed. N. Soker), ASP Conf. Ser. 115, p. 59

Edge, A.C., Stewart, G.C., & Fabian, A.C. 1992, MNRAS, 258, 177

Edge, A.C. & Stewart, G.C. 1991, MNRAS, 252, 428

Evrard, A., Mohr, J., Fabricant, D., & Geller, M. 1993, ApJ, 419, L9

Fabian, A.C., Crawford, C.S., Edge, A.C., & Mushotzky, R.F. 1994, MNRAS, 267, 779

Feigelson, E.D. & Nelson, P.I. 1985, ApJ, 293, 192

Gioia, I.M., Henry, J.P., Mullis, C.R., Voges, W., Briel, U.G., Böhringer, H., & Huchra, J.P. 2001, ApJ, 553, L105

Giovannini, G. & Feretti, L. 2000, *New Astronomy*, 5, 335

Gómez, P.L., Pinkney, J., Burns, J.O., Wang, Q., Owen, F.N. & Voges, W. 1997, ApJ, 474, 580

Johnson, M.W., Cruddace, R.G., Ulmer, M.P., Kowalski, M.P., & Wood, K.S. 1983, ApJ, 266, 425

Jones, C. & Forman, W. 1999, ApJ, 511, 65

Jones, C. & Forman, W. 1992, in *Clusters and Superclusters of Galaxies*, ed. A. Fabian (Dordrecht: Kluwer), p. 49

Jones, C. & Forman, W. 1978, ApJ, 224, 1

Kolokotronis, V, Basilakos, S., Plionis, M.,& Georgactopoulos, I 2001, MNRAS, 320, 49

Ledlow, M.J., Loken, C., Burns, J.O., Owen, F.N., & Voges, W. 1999, ApJ, 516, L53

Ledlow, M.J. & Owen, F.N. 1995a, AJ, 109, 853

Ledlow, M.J. & Owen, F.N. 1995b, AJ, 110, 1959

Ledlow, M.J. & Owen, F.N. 1996, AJ, 112, 9

Lockman, F.J. & Dickey, J.M. 1990, ARA&A, 28, 215

Loken, C., Roettiger, K., Burns, J.O., & Norman, M. 1995, ApJ, 445, 80

Mazure, A. et al. 1996, A&A, 310, 31

McHardy, I. 1978, MNRAS, 184, 783

McNamara, B.R., Vikhlinin, A., Hornstrup, A., Quintana, H., Whitman, K., Forman, W., & Jones, C. 2001, ApJ, 558, 590

Miller, C.J., Ledlow, M.J., & Batuski, D.J. 1999, submitted to MNRAS(astro-ph/9906423)

Mohr, J., Fabricant, D., & Geller, M. 1993, ApJ, 413, 492

Morgan, W.W., Kayser, S., & White, R.A. 19 75, ApJ, 199, 545

Navarro, J. & White, S.D.M. 1994, MNRAS, 267, 401

Owen, F.N. & Ledlow, M.J. 1997, ApJS, 108, 41

Owen, F.N., Ledlow, M.J., & Keel, W.C. 1995, AJ, 109, 14

Owen, F.N., White, R.A., & Burns, J.O. 1992, ApJS, 80, 501

Owen, F.N., White, R.A., & Ge, J.-P. 1993, ApJS, 87, 135

Peres, C.B., Fabian, A.C., Edge, A.C., Allen, S.W., Johnstone, R.M., & White, D.A. 1998, MNRAS, 298, 416

Pinkney, J. Roettiger, K., Burns, J.O., & Bird, C. 1996, ApJS, 104, 1

Pfeffermann, E., Briel, U.G., Hippmann, H., et al. 1988, *Proc. SPIE*, 733, 519

Reiprich, T. & Böhringer, H. 2002, ApJ, 567, 716

Ricker, M., & Sarazin, C. 2001, ApJ, 561, 621

Roettiger, K., Loken, C., & Burns, J.O. 1997, ApJS, 109, 307

Roettiger, K., Burns, J.O., & Loken, C. 1996, ApJ, 473, 651

Sanders, J.S., Fabian, A.C., & Allen, S.W. 2000, MNRAS, 318, 733

Struble, M.F. & Rood, H.J. 1999, ApJ, 125, 35

Trümper, J. 1983, *Adv. Space Res.*, 27, 1404

Voges, W., Aschenbach, B., Boller, T., et al. 1999, accepted for publication in A&A

Watanabe, M., Yamashita, K., Furuzawa, A., Kunieda, H, Tawara, Y, & Honda, H. 1999, ApJ, 527, 80

White, D.A., Jones, C., & Forman, W. 1997, MNRAS, 292, 419

White, S.D.M., Briel, U.G., & Henry, J.P. 1993, MNRAS, 261, L8

White, R.A. 1978, ApJ, 226, 591

Yee, H.K.C. & Ellingson, E. 2003, ApJ, 585, 215

Zhao, J.-H., Burns, J.O., & Owen, F.N. 1989, AJ, 98, 64

This 2-column preprint was prepared with the AAS LaTeX macros v5.0.

FIGURE CAPTIONS

Fig. 1.— (A) The derived selection function for our Abell cluster sample. The aitoff grid is show in Galactic coordinates. The solid-line is the $\delta = -27^\circ$ cutoff of Abell's northern catalog. We estimate a sky-coverage of 34% for our sample. (B) The distribution of all Abell clusters in the sample on the same grid for comparison

Fig. 2.— X-ray/optical overlays from a representative group of 6 clusters from the sample with average L_X. We will make these overlays for all clusters available over the WWW. In Fig. 2a we show overlays for A193 and A602 (top-bottom), Fig. 2b: A1035 and A1541, and Fig 2c: A1650 and A2124.

Fig. 3.— We plot the flux-ratios f_{250} vs. f_{500} for a sample of isolated pointsources. In the lower panel is plotted f_{500} vs. redshift. We conservatively set $f_{250} \leq 2$ and $f_{500} \leq 4$ as the range of values consistent with an unresolved peak.

Fig. 4.— Histogram of the X-ray luminosity of our cluster detections (solid) and upper-limits (dashed).

Fig. 5.— Comparison of total cluster X-ray flux from the BCS, eBCS, and XBACS surveys to those in this paper. See the text for an explanation of the correction factors (and uncertainties) applied to compare the fluxes on a similar scale.

Fig. 6.— Histogram of the flux-ratios for all cluster X-ray detections. The solid-line is for f_{500} as defined in the text. The dashed line is for f_{250}.

Fig. 7.— (a) Histogram of f_{500} for cooling flow clusters, (b) clusters without cooling flows, and (c) clusters from our sample with no deprojection analysis in the literature.

Fig. 8.— f_{500} vs redshift. The different symbols are cooling flow clusters (C), non cooling flow clusters (N), and all other cluster detections.

Fig. 9.— L_X plotted versus Abell richness. Filled circles are detections, the open-symbols are upper-limits. The solid-line is a weighted least-squares fit to the data (excluding the non-detections). The dashed-line is a linear-regression fit which includes the censored data points. At the top of the plot, the range for Abell Richness classes 0-3 are given.

Fig. 10.— Histograms of Rood Sastry (RS; solid line) and Bautz-Morgan (BM; dashed line) morphological types for cooling flow and non cooling flow clusters.